A Coronally-Clutching Ankle to Improve Amputee Balance on Coronally-Uneven and Unpredictable Terrain

Kyle Harris Yeates

A thesis submitted in partial fulfillment of the
requirements for the degree of

Master of Science in Mechanical Engineering

University of Washington

2016

Committee:

Glenn Klute

Katherine Steele

Brian Fabien

Program Authorized to Offer Degree:
Mechanical Engineering

University of Washington

Abstract

A Coronally-Clutching Ankle to Improve Amputee Balance on Coronally-Uneven and Unpredictable Terrain

Kyle Yeates

Chair of the Supervisory Committee:

Glenn Klute

Mechanical Engineering

To improve amputee balance on coronally-uneven and unpredictable terrain, a coronally-clutching ankle (CCA) prosthesis was developed and tested using amputee participants. In its adapting mode, the CCA device enabled free coronal rotation of the prosthetic foot of up to ±15° from horizontal, and approximately 100 ms after heal strike, would cease further rotation. The CCA was tested on three healthy amputee participants that stood still on, and walked across, an instrumented disturbance device that was capable of producing unpredictable inversions and eversions of 15°. Participants' balance during gait over the coronally-uneven and unpredictable terrain was evaluated using the range of coronal angular momentum. This metric exhibited no significant pairwise differences between participants' as prescribed prosthesis and the CCA in its adapting mode, suggesting the CCA did not improve gait balance on coronally-uneven and unpredictable terrain. Lateral sway of participant's center of pressure measured their balance as they stood still on the coronally-uneven terrain. Again, no significant pairwise differences were

observed between prosthesis conditions; however, it appeared the CCA in its adapting mode may have slightly improved participant balance, especially in inversion. During walking trials, the CCA in adapting mode was able to match the coronal angle of the foot to that of the terrain. However, evaluation of the moment about the CCA pivot revealed that its distance from the bottom of the prosthetic foot prevented the CCA from reducing the disturbance moment produced when amputees stepped on the coronally-uneven and unpredictable terrain. Furthermore, when the CCA was adapting to coronally-uneven and unpredictable terrain, large oscillations of the disturbed limb's hip moment were observed, suggesting participants required additional recovery strategies to compensate for the CCA's adaption. Thus, while the CCA in this study was able to adapt the coronal foot angle to coronally-uneven and unpredictable terrain, a clear benefit to gait balance was not observed. A possible benefit to standing balance was observed, but was not statistically significant. Future iterations of the CCA device will incorporate the learnings of this study to improve the balance outcomes of amputees on coronally-uneven and unpredictable terrain.

Table of Contents

List of Figures iv

List of Tables vi

List of Equations vi

List of Abbreviations vi

Acknowledgements vii

Chapter I: Introduction 1

1.1 Motivation 1

1.2 Inversion and Eversion in the Human Ankle 1

1.3 Existing Devices 2

1.4 Purpose 3

1.5 Balance Performance Metrics 4

1.6 Recovery Mechanism Performance Metrics 5

1.7 Device Performance Metrics 6

1.8 Hypotheses 8

1.8a Hypothesis 1 - Balance 8

1.8b Hypothesis 2 – Recovery Mechanisms 9

Chapter II: Methods 11

2.1 Design Inspiration 11

2.2 Coronally-Clutching Ankle Performance Goals 13

2.2a Goals for Participant Testing Outcomes 13

2.2b Goals for Device Design 14

2.3 Mechanical Description of Coronally-Clutching Ankle 17

2.4 Electrical Description of Coronally-Clutching Ankle 25

2.5 Controller and Software Description 29
2.6 Finite Element Analysis 33
2.7 Coronally-Clutching Ankle Bench Testing 35
2.7a Bench Testing Instrumentation 35
2.7b Bench Testing Procedure 36
2.7c Bench Testing Results 38
2.8 Human Participant Testing 44
2.8a Human Participants 44
2.8b Human Participant Test Instrumentation 44
2.8c Human Participant Test Procedure 45
2.8d Data Processing 48
2.8e Whole Body Modeling 48
2.8f Statistics 50
Chapter III: Results 51
3.1 Coronal Angular Momentum 52
3.2 Standing Balance Lateral Sway 54
3.3 Foot Coronal Angle With Respect to Pylon 55
3.4 Coronal Moment About CCA Pivot 57
3.5 Coronal Hip Moment 59
3.6 Recovery Step Lateral Foot Placement 61
3.7 Foot Mount Coronal Angle 62
3.8 Descriptive Statistics of Performance Metrics 63
3.10 Temporal Measurements 65
Chapter IV: Discussion 66
4.1 Interpretation 66

4.1a Hypothesis 1 – Balance 66
4.1b Hypothesis 2 - Recovery Mechanisms 68
4.2 Implications 73
4.3 Limitations 74
4.4 Future Work 75
Appendix A: Results - Individual Participant Means 76
A.1 Coronal Angular Momentum - Individual Participant Means 76
A.2 Standing Balance Lateral Sway - Individual Participant Means 77
A.3 Foot Coronal Angle With Respect to Pylon - Individual Participant Means 78
A.4 Coronal Moment About CCA Pivot - Individual Participant Means 79
A.5 Coronal Hip Moment - Individual Participant Means 80
A.6 Recovery Step Lateral Foot Placement - Individual Participant Means 81
A.7 Foot Mount Coronal Angle - Individual Participant Means 82
References 83

List of Figures:

Figure 1: Plot of Coronal Ankle Angle of Non-Amputees on Coronally-Uneven Terrain 12
Figure 2: Images and Computer Model of Coronally-Clutching Ankle. 17
Figure 3: Computer Model of Coronally-Clutching Ankle Exhibiting Full Range of Motion.... 18
Figure 4: Exploded View of Coronally-Clutching Ankle. 19
Figure 5: Exploded View of Coronally-Clutching Ankle Clutching Mechanism 21
Figure 6: Section View of Coronally-Clutching Ankle Clutching Mechanism..... 22
Figure 7: Images of Clutching Mechanism in Locked and Adapting States 23
Figure 8: Image of Coronally-Clutching Ankle Microprocessor Unit. 26
Figure 9: Image of All Coronally-Clutching Ankle Electronics..... 27
Figure 10: Servo Response Time Plot From Free to Locked Angle. 31
Figure 11: Servo Response Time Plot From Locked to Free Angle. 32
Figure 12: Finite Element Analysis Results of Ratchet Pawl. 34
Figure 13: Finite Element Analysis Results of Ratchet Gear 34
Figure 14: Finite Element Analysis Results of Rigid Pylon Assembly 35
Figure 15: Image of Force Testing Setup of the Coronally-Clutching Ankle. 36
Figure 16: Plot of Foot Mount and Spool Angular Displacements For A 500 N Load..... 40
Figure 17: Plot of Foot Mount and Spool Angular Displacements For A 1000 N Load..... 41
Figure 18: Plot of Foot Mount and Spool Angular Displacements During Neutralization 43
Figure 19: Images of the Coronally-Uneven and Unpredictable Terrain Test Setup. 45
Figure 20: Images of a Participant With the Coronally-Clutching Ankle 47
Figure 21: Images of the Whole Body Model Used. 50
Figure 22: Plots of Coronal Angular Momentum Results 52
Figure 23: Plot of Standing Balance Lateral Sway Results 54
Figure 24: Plots of the Foot Coronal Angle Results 55
Figure 25: Plots of the Coronal Moment About the Coronally-Clutching Ankle Pivot Results. 57
Figure 26: Plots of the Coronal Hip Moment Results 59
Figure 27: Plot of the Recovery Step Lateral Foot Placement Results..... 61
Figure 28: Plot of Coronally-Clutcing Ankle Foot Mount Angle Results..... 62
Figure 29: Visual Analysis of the Coronally-Clutching Ankle at Early Stance 71

Figure 30: Plots of Coronal Angular Momentum – Individual Mean Results..... 76
Figure 31: Plot of Standing Balance Lateral Sway – Individual Mean Results 77
Figure 32: Plots of the Foot Coronal Angle – Individual Mean Results 78
Figure 33: Plots of Coronal Moment About the Coronally-Clutching Ankle Pivot - Individual Mean Results..... 79
Figure 34: Plots of the Coronal Hip Moment – Individual Mean Results..... 80
Figure 35: Plot of the Recovery Step Lateral Foot Placement – Individual Mean Results 81
Figure 36: Plot of Coronally-Clutcing Ankle Foot Mount Angle - Individual Mean Results..... 82

List of Tables:

Table 1: Clutch Performance Characteristics For the 500 N Load 40
Table 2: Clutch Performance Characteristics for the 1000 N Load. 41
Table 3: Descriptive Statistics of All Performance Metrics 63
Table 4: Statistical Test Results of All Performance Metrics 64
Table 5: Descriptive Statistics of All Temporal Measurements 65

List of Equations:

Equation 1: Equation for Whole Body Angular Momentum 4
Equation 2: Control Algorithm for Servo Motor 30

List of Abbreviations:

3D ..... Three-Dimensional

CCA ..... Coronally-Clutching Ankle

COM ..... Center of Mass

COP ..... Center of Pressure

FEA ..... Finite Element Analysis

LED ..... Light-Emitting Diode

LFP ..... Lateral Foot Placement

RCAM ..... Range of Coronal Angular Momentum

RGB ..... Red Green Blue

WRT ..... With Respect To

YS ..... Yield Strength

Acknowledgements:

I would like to thank Glenn Klute for his guidance and for the opportunity to work on meaningful and fascinating research. I would also like to thank Ava Segal for her invaluable support in all aspects of this project, from experimental design to data interpretation. This work could not have been completed without the outstanding human participants and data processing work of Krista Sanchez. Janice Pecoraro coordinated all human participants recruitment and scheduling. Wesley Edmundson handled financing for the entire project. Finally, the excellent machining for this project was donated by Drew Johnson at MDI-CO, without which this project would not have been possible.

This research was supported by the Department of Veterans Affairs, Rehabilitation Research and Development Service, grant A9243C.

Chapter I: Introduction

1.1 Motivation:

Amputees often suffer from a lower quality of life that is associated with a reduction in mobility when compared to similar non-amputee populations [1]. Associated with amputees' reduction in mobility is a fear of falling and an increased prevalence of falls [2]. Extrinsic factors, such as uneven terrain, are a major cause of amputee falls [3]. In environments, such as the outdoors, where extrinsic factors are present, nearly 25% of falls in non-amputees occur in the mediolateral direction [4]. The motivation for this project was to improve amputee quality of life by improving their mobility outdoors, which often involves traversing coronally-uneven and unpredictable terrain.

While there exist technologies that actively adapt prosthetic ankle joint properties in the sagittal plane to improve balance on uneven terrain (see section 1.3), current prosthetic ankles only offer passive mechanical properties in the coronal plane. Coronally passive ankle joints put amputees at a distinct disadvantage when attempting to balance on or traverse coronally-uneven and unpredictable terrain, as their lack of musculature in the calf makes it more difficult for them to regulate their angular momentum [5]. The ankle moment strategy enables non-amputees to actively adapt the moment about their ankle joint in order to maintain their gait stability [6]. The device created in this study is a coronally-clutching ankle (CCA) that actively adapts the coronal plane properties of a prosthetic ankle joint to improve transtibial amputee balance on coronally-uneven and unpredictable terrain.

1.2 Inversion and Eversion in the Human Ankle:

The ankle joint complex is a complex, tri-planar, joint that is composed of two main anatomical joints. The first joint is the tibiotalar joint, a synovial joint which is located between the tibia and talus, and is mainly responsible for dorsiflexion and plantarflexion of the foot. The second joint is the subtalar joint, a synovial joint which is located between the talus and the calcaneus, and is mainly responsible for inversion and eversion of the foot [7]. In the ankle joint, motions in all three anatomical planes are linked with one another. Inversion of the foot is

associated with plantarflexion and internal rotation, and eversion of the foot is associated with dorsiflexion and external rotation [8]. Typical range of motion in inversion is approximately 20°, and in eversion is approximately 10° [9,10].

Motion of the ankle is controlled by bone on bone contact forces, ligament forces, and muscular forces. Bone on bone forces and ligament forces are passive and mainly limit the range of motion of the ankle. There exist two main ligament groups that limit ankle rotation in the coronal plane: the medial (deltoid) ligament, which is composed of four smaller ligaments and acts to resist excessive eversion, and the lateral ligament which is composed of three smaller ligaments and acts to resist excessive inversion [7]. Active control of the ankle joint comes from muscles. The tibialis posterior is the main muscle responsible for producing inversion moments about the ankle, and the peroneus longus and peroneus brevis are the main muscles responsible for producing eversion moments about the ankle [7,11].

1.3 Existing Devices:

There exist a wide variety of prosthetic feet that have coronal compliance; however, none of these devices offer active adaption to their environment in the coronal plane. Instead, they generally offer settings, or interchangeable components, which when chosen ahead of time alter the coronal plane properties of the device. Currently, the two main categories of coronal adaptation in prosthetic foot/ankle systems are the elastomer bushing ankle and the split keel foot. The elastomer bushing design has different implementations, but the general concept is demonstrated by the Earthwalk™ Ankle (WillowWood, Mt. Sterling, USA). The elastomer bushing ankle acts as a flexible linkage between the pylon and foot, and by altering its geometry, material, and supporting structure, its mechanical properties are changed in the sagittal, coronal, and transverse plane. Stiffness in both planes remains constant. The split keel foot design is demonstrated by the Elite2™ (Endolite, Miamisburg, USA). This type of foot divides the keel of the foot along the sagittal plane, allowing the lateral and medial sides of the foot to dorsiflex and plantar flex independently of one another. By doing so, the coronal plane stiffness of the foot is reduced, while the sagittal plane stiffness remains relatively similar to that of a non-split keel foot. Stiffness in both planes remains constant. Finally, some products, such as the Trustep™ (College Park, Warren, USA) implement both categories of coronal adaptation into one product. However, while this foot has elastomer bushings that can be interchanged to create varying

coronal plane properties, this must be done ahead of time, and cannot be done while walking. The inherent weakness in the aforementioned products is they all have static coronal plane properties, which is not the case in the non-amputee ankle [12], whose active adaption is likely important for balance over coronally-uneven and unpredictable terrain.

There also exist devices which adapt the sagittal ankle angle to the surrounding terrain. The more advanced devices in this category adapt to uneven terrain in the sagittal plane using series-elastic actuators and adjustable resistance hydraulic valves. Currently the BioM™ (BionX Medical Technologies, Bedford, USA) is the one of the leading propulsive devices and uses a series-elastic actuator to provide propulsive forces and adaptive capabilities to the device. Other products, such as the Kinterra™ (Freedom Innovations, Irvine, USA), offer set levels of hydraulic damping in the sagittal plane that can be set ahead of time for different activities. Finally, the Magellan™ (Orthocare, Mountlake Terrace, USA) offers dynamic hydraulic damping, allowing it to actively adapt to different types of uneven terrain in the sagittal plane, but it does not provide any propulsive force. These devices, some of which have active adaptation in the sagittal plane, again only offer static mechanical properties in the coronal plane.

1.4 Purpose:

The purpose of this study was to improve amputee balance when walking over coronally-uneven and unpredictable terrain by developing a prosthetic ankle capable of actively adapting its mechanical properties in coronal plane rotation. This adaptation was achieved using a clutching mechanism, which enabled and disabled free rotation of the foot in the coronal plane during key periods of the gait cycle.

The design and evaluation of the CCA was based on kinetic and kinematic data collected from participant testing on an experimental setup capable of producing coronally-uneven and unpredictable terrain with 15° inversions and eversions (see section 2.9b). The initial design parameters of the CCA were based on a set of performance metrics measured from non-amputees walking over this experimental setup [12]. To test the effectiveness of the CCA, a control study was conducted in which amputee participants were asked to walk over coronally-uneven and unpredictable terrain with the CCA in an adapting and in a locked mode, as well as with their as

prescribed prosthesis. By comparing standing and gait balance metrics between these two devices, the efficacy of the CCA was determined.

1.5 Balance Performance Metrics:

Balance During Gait:

The range of whole-body coronal angular momentum (RCAM) of the participants was used as the test metric for balance during gait (***see Equation 1***) [5]. This metric was chosen because it has been linked with the outcomes of clinical balance tests [13], and can also be mathematically related to certain recovery strategies, such as lateral foot placement (LFP) [14]. Whole body coronal angular momentum was derived from a whole body model of the participants (see section 2.9e), and was the sum of the coronal angular momentum of each segment in the model calculated about the center of mass of the body (see ***Equation 1***). Orientation of the sagittal axis was static relative to the lab coordinate system, and was parallel with the average path of travel of the amputees. The range was calculated from the mid-stance of the step prior to disturbed step to the mid-stance of the recovery step. This range is referred to as the disturbance gait period, and was used to capture entire range of the coronal angular momentum induced by the disturbance.

$$\overrightarrow{L_{COM}} = \sum_{i=1}^{n} \left[\left(\overrightarrow{r_i^{COM}} - \overrightarrow{r_{body}^{COM}} \right) \times m_i \left(\overrightarrow{v_i^{COM}} - \overrightarrow{v_{body}^{COM}} \right) + I_i \overrightarrow{\omega_i} \right]$$

Equation 1: $\overrightarrow{L_{COM}}$ is the three dimensional (3D) vector representing the angular momentum of the whole body model calculated about its COM. The position, velocity, and angular 3D vector quantities of the i[th] segment's COM are represented by: $\overrightarrow{r_i^{COM}}$, $\overrightarrow{v_i^{COM}}$, and $\overrightarrow{\omega_i}$, respectively. The position and velocity vectors of the whole body's COM are represented by: $\overrightarrow{r_{body}^{COM}}$ and $\overrightarrow{v_{body}^{COM}}$, respectively. The mass and moment inertia about the COM of the i[th] segment are represented by: m_i and I_i, respectively [5]. Seventeen segments were used in the whole body model, which included the CCA and supporting prosthetic components (see section 2.8e).

Standing Balance:

Lateral sway during eyes-closed, two-footed, standing balance trials was used to assess standing balance of participants. There exists evidence to support that individuals with greater range of lateral sway, as measured by their range of center of pressure (COP), during standing balance trials are less stable [15].

1.6 Recovery Mechanism Performance Metrics:

Lateral Foot Placement

The stepping strategy is a primary strategy used by humans to recover from gait disturbances [16]. By locating the foot in a particular location, an individual is able to alter their COP relative to their center of mass (COM), thereby affecting the external forces and moments acting on their body which influence their gait stability. In this study, the stepping strategy was measured by LFP, which was the distance between the participant's whole body COM, and their ankle joint center (midpoint between the medial and lateral malleoli) upon heel strike.

Joint Angles

Joint angles were model based (see section 2.8e for model details) and were calculated in Visual 3D (C-Motion, Germantown, USA). Coronal angles corresponds to the Y component of the XYZ Euler angle between the distal and proximal limb's coordinate system, and were reported relative to the proximal limb's coordinate system.

Joint Moments

Joint moments were model based (see section 2.8e for model details) and were calculated in Visual 3D using inverse dynamics. Joint moments are reported relative to the coordinate system of the proximal segment. The exact moment calculation methodology is available on the Visual 3D website [17], and is based on biomechanics principles that have been well established [18, 19]. The basic principle of inverse dynamics is that joint reaction forces and moments can be calculated from the most distal segment of the body to the most proximal segments by using Newton's laws of motion. External forces recorded from force plates as well as kinematic data from motion tracking of each segment are used when determining the joint forces and moments required to balance the forces and moments of each segment. The inverse dynamics calculations

assumed each segment of the model was rigid, joint moments and forces between segments were equal and opposite, small amounts of translation existed between the joint surfaces of abutting segments, and gravity was acting on all segments.

1.7 Device Performance Metrics:

Response Times:

Two response times were important for the correct function of the device (see section 2.3 for device performance goals). The first response time was “free to locked” which was the amount of time it took for the device to switch from a state in which the foot could rotate freely, to a state in which it could not. The beginning of this time period was defined as the point at which the microprocessor sent the initiation command to the actuator, and the end of this time period was defined as the point at which the clutching mechanism effectively stopped the rotation of the foot. The second response time was “locked to free” which was the amount of time it took for the device to switch from a state in which the foot could not rotate freely, to a state in which it could. The beginning of this time period was defined as the point in time at which the microprocessor sent the initiation command to the actuator, and the end was defined as the point at which the clutching mechanism effectively allowed the foot to rotate freely.

Angles:

Two separate angles were measured on the CCA device. The first angle will be referred to as the “foot mount angle”, and is the angle between the rigid pylon of the CCA, and the rigid foot mount of the CCA (see section 2.4 for mechanical details of the CCA). The second angle will be referred to as the “foot angle”, and was the angle between the rigid pylon of the CCA, and the prosthetic foot, which was rigidly connected to the foot mount, but was itself not a rigid member. Reported angles were based on the same measurement technique used for other joint angles previously mentioned. In addition, the “clutch angle” was also measured and recorded onboard the device; however, these measurements were used for control of the CCA and bench testing, but were not reported for the human participant testing.

Moments:

The coronal moment about the pivot of the CCA was calculated the same way as other joint moments previously mentioned. In the case of the as prescribed prosthesis, the coronal moment was calculated about an axis which allowed for comparison to the CCA moment. This axis had the same orientation as that of the CCA pivot, was located in the middle of the as prescribed pylon, and was at the same height (relative to the bottom of the prosthetic foot) as the CCA pivot.

Normalization:

Certain metrics were normalized in order to reduce variability amongst different body types, and to allow for meaningful comparison with existing studies. RCAM was normalized to walking speed, body height, and body mass. LFP was normalized to body height. The joint angles and joint moments of left amputee participants were negated to make all measures relative to those of right amputee participants. Joint moments were also normalized to body mass. Finally, the coronal angle of the foot was demeaned by subject in order to account for offsets between subjects neutral foot angle.

1.8 Hypotheses:

1.8a Hypothesis 1 - Balance:

Amputee gait and standing balance on coronally-uneven and unpredictable terrain will be improved by the clutching feature of the CCA.

Based on hypothesis 1 the following statements were statistically tested, with the expected outcomes being highlighted in bold:

Participants' RCAM during gait over coronally-uneven and unpredictable will exhibit:

H0a = No main effect based on the prosthesis condition
H0b = No interaction effect based on the prosthesis and terrain condition
H0c = No pairwise differences between prosthesis conditions within a terrain condition
H1.1a = A significant main effect based on the prosthesis condition
H1.1b = A significant interaction effect based on the prosthesis and terrain condition
H1.1c = Significant pairwise differences between prosthesis conditions within a terrain condition

In quiet stance, participants' lateral sway (COP lateral range) on coronally-uneven terrain will exhibit:

H0a = No main effect based on the prosthesis condition
H0b = No interaction effect based on the prosthesis and terrain condition
H0c = No pairwise differences between prosthesis conditions within a terrain condition
H1.2a = A significant main effect based on the prosthesis condition
H1.2b = A significant interaction effect based on the prosthesis and terrain condition
H1.2c = Significant pairwise differences between prosthesis conditions within a terrain condition

1.8b Hypothesis 2 – Recovery Mechanisms:

When stepping on coronally-uneven and unpredictable terrain, the clutching feature of the CCA will allow the prosthetic foot to adapt to the terrain angle, thereby reducing the disturbance moment produced about the coronal pivot of the CCA. The reduced disturbance moment about this joint will lessen the need for amputees to use the hip moment strategy of the disturbed limb, as well as reduce the need for the stepping strategy of the recovery limb.

Based on hypothesis 2 the following statements were statistically tested, with the expected outcomes being highlighted in bold:

The coronal angle of the disturbed limb's prosthetic foot relative to the pylon at early stance on the coronally-uneven and unpredictable terrain will exhibit:

H0a = No main effect based on the prosthesis condition
H0b = No interaction effect based on the prosthesis and terrain condition
H0c = No pairwise differences between prosthesis conditions within a terrain condition
H2.1a = A significant main effect based on the prosthesis condition
H2.1b = A significant interaction effect based on the prosthesis and terrain condition
H2.1c = Significant pairwise differences between prosthesis conditions within a terrain condition

The integral of the disturbed limb's moment about the CCA pivot (or equivalent thereof in the case of the as prescribed prosthesis) during stance on coronally-uneven and unpredictable terrain will exhibit:

H0a = No main effect based on the prosthesis condition
H0b = No interaction effect based on the prosthesis and terrain condition
H0c = No pairwise differences between prosthesis conditions within a terrain condition
H2.2a = A significant main effect based on the prosthesis condition
H2.2b = A significant interaction effect based on the prosthesis and terrain condition
H2.2c = Significant pairwise differences between prosthesis conditions within a terrain condition

The integral of the disturbed limb's hip coronal moment during stance on coronally-uneven and unpredictable terrain will exhibit:

H0a = No main effect based on the prosthesis condition
H0b = No interaction effect based on the prosthesis and terrain condition
H0c = No pairwise differences between prosthesis conditions within a terrain condition
H2.3a = A significant main effect based on the prosthesis condition
H2.3b = A significant interaction effect based on the prosthesis and terrain condition
H2.3c = Significant pairwise differences between prosthesis conditions within a terrain condition

After the disturbed limb steps on coronally-uneven and unpredictable terrain, the recovery limb's LFP will exhibit:

H0a = No main effect based on the prosthesis condition
H0b = No interaction effect based on the prosthesis and terrain condition
H0c = No pairwise differences between prosthesis conditions within a terrain condition
H2.4a = A significant main effect based on the prosthesis condition
H2.4b = A significant interaction effect based on the prosthesis and terrain condition
H2.4c = Significant pairwise differences between prosthesis conditions within a terrain condition

Chapter II: Methods

2.1 Design Inspiration:

The motivation for creating the CCA came from analysis of a control group of ten participants walking on the coronally-uneven and unpredictable terrain experimental setup [12]. It was observed that non-amputees' coronal ankle angle rapidly adapted to the terrain conditions in the early phase of stance (see ***Figure 1***). In the later phases of gait, the coronal ankle angle appeared to have experienced slower, and more subtle angular changes.

A metric called the clutch point was developed to measure the speed of the aforementioned coronal ankle adaptation, and was defined as the time between heel strike, and the instant at which the ankle reached 90% of its maximum coronal angle (see ***Figure 1***). Median values of both the ankle angle, as well as the clutch point were reported due to their non-normal distribution. The clutch point for the unblinded flush (considered the control condition), blinded inversion, and blinded eversion conditions were relatively close to one another. The median clutch points for unblinded flush, blinded inversion, and blinded eversion conditions occurred at 133ms, 133ms, and 108ms, respectively, with IQRs of 142ms, 33ms, and 33ms, respectively. Furthermore, it appeared that at the clutch point, differences between the median coronal ankle angles approached a 15° difference, which matched that of the terrain conditions. The difference between the median of the unblinded flush clutch point angle, and the blinded inversion clutch point angle was 12.5°; and the difference between the median of the unblinded flush clutch point angle, and the blinded eversion clutch point angle was 10.3°.

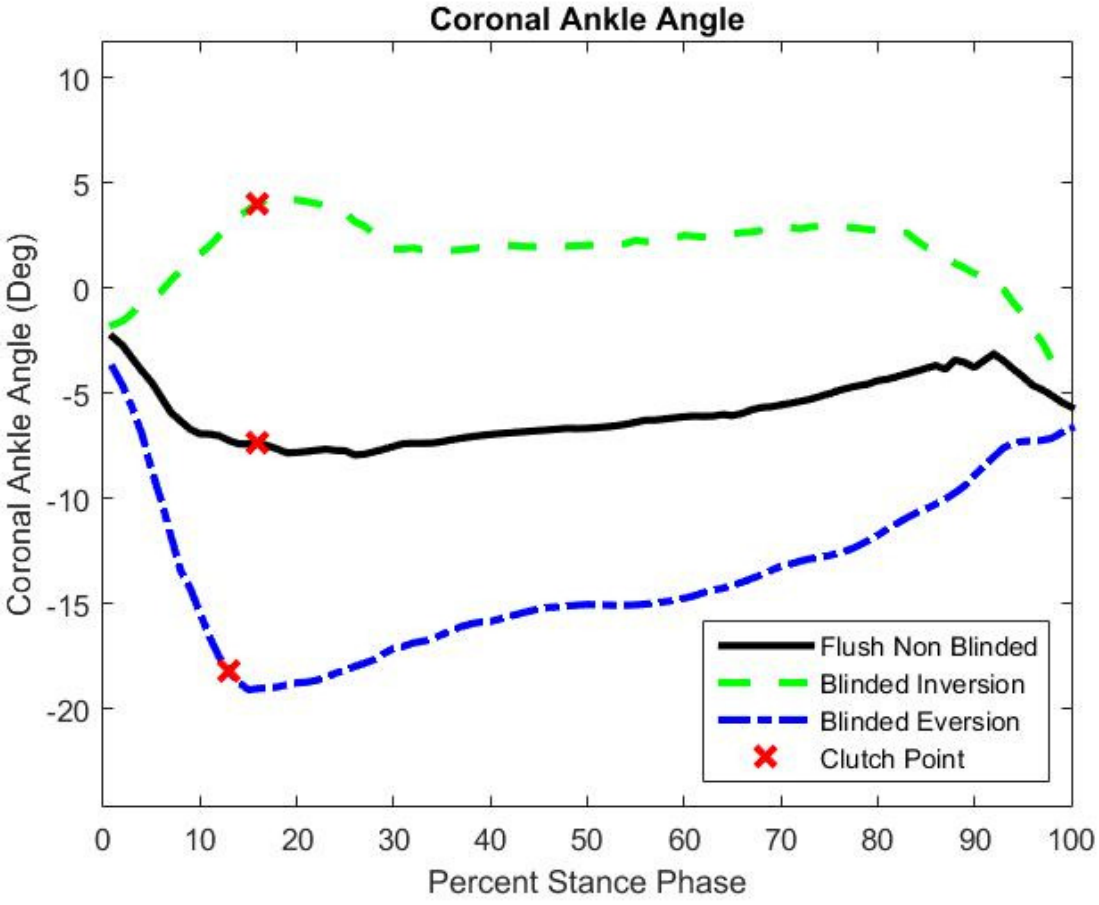

Figure 1: Plot of median coronal ankle angle of non-amputees walking on coronally-uneven and unpredictable terrain. Conditions shown for flush unblinded (control), blinded 15° inversion, and blinded 15° eversion. Mean clutch points, at which participants reached 90% of their maximum angular displacement for a given condition, are shown for all conditions.

The ankle behavior in the blinded inversion condition was targeted when designing the CCA device. This condition was targeted because in the control study, participants were more stable on the inverted terrain when compared to the everted terrain, as measured by their RCAM [12]. It was hypothesized that the ankle's ability to conform early to the inverted terrain, and to remain inverted, may have been partially responsible for the participant's greater stability on inverted terrain. This behavior can be seen in ***Figure 1***, in which the coronal ankle angle appears to have a larger degree of adaption at the clutch point for inversion, and also appears to remain closer to this angle for a longer period of time, when compared to eversion.

Based on these observations, the CCA was designed to control the coronal rotation of exiting prosthetic feet (see ***Figure 2***). The CCA would allow free coronal rotation of the prosthetic foot for a set period time after heel strike. This period of time was similar to that of the adaption period previously observed in control groups (see ***Figure 1***) between heel strike and the clutch point. After this period, the CCA would then cease further free rotation. At this point, the flexible keel of the mounted prosthetic foot could still deform if further adaption to the terrain was required. The intention of the CCA was to reduce the deformation of the prosthetic foot when stepping on coronally uneven terrain. It was reasoned that this would reduce the disturbance moment about the ankle equivalent (the CCA pivot) of the device when stepping on coronally-uneven and unpredictable terrain.

The concept of improving gait balance of participants by reducing the coronal ankle moment (or equivalent thereof) perturbation caused by uneven terrain was supported by previous work. The RCAM, a measure gait balance, was shown to be influenced by the external coronal moment imparted by the disturbed limb on the whole body [5]. Contributing to the external coronal moment of the disturbed limb were the coronal moments of all the joints in the dynamic chain of that limb, which included that of the ankle joint. It was reasoned that by reducing a disturbance's effect on the equivalent of the coronal ankle moment of the CCA, the disturbance's effect would also be reduced on the external coronal moment, and thus on the RCAM.

2.2 Coronally-Clutching Ankle Performance Goals:

2.2a Goals for Participant Testing Outcomes:

The CCA was designed to improve the gait and standing balance of amputees on coronally-uneven and unpredictable terrain. The primary metric used to analyze the gait balance improvements of amputees using the CCA was the RCAM. For a given disturbance, the performance goal of the CCA when it adapted to the terrain was to reduce the RCAM of amputee participants to below that of their RCAM when using their as prescribed prosthesis.

The secondary metric used to analyze the effectiveness of the CCA was the lateral sway (range) of participants' center of pressure (COP) during standing balance trials. For a given terrain condition, the participants' lateral sway was expected to be reduced when the CCA adapted to the terrain, as opposed to when participants used their as prescribed prosthesis.

2.2b Goals for Device Design:

Based on control data previously collected on coronally-uneven and unpredictable terrain [12], as well as existing literature, a set of performance requirements were created to focus the design effort for the CCA. The following criteria were established:

Load:

Based on non-amputee data from the coronally-uneven and unpredictable terrain peak forces transferred through the ankle to the distal end of the tibia were approximately 1000 N in the superior direction, 300 N in the posterior direction, and 150 in the lateral direction, relative to the tibia. The CCA design goal was to withstand all of these loads with a safety factor of 2.

Response Time:

Based non-amputee data from the coronally-uneven and unpredictable trials, it was determined that the CCA would need to have a clutch point which occurred in 133 ms or sooner after heel strike. In addition, during the swing phase following a disturbed step in which the CCA adapted, it would have to neutralize the ankle angle, and prepare for the following step (be it one in which the CCA was to be locked, or was to adapt). From non-amputee studies, the mean swing phase after a recovery step was 439 ms, with a standard deviation of 32 ms [12]. Thus the recovery time goal for the CCA was set to 375 ms, which would allow the foot to recover successfully 98% of the time. This was deemed an acceptable recovery rate, as the stepping on the CCA in a non-neutral state on the recovery step would not pose additional risk to participants.

Mass:

Mass of the device was to be kept at a minimum. The goal was for the device to have a mass of no more than 1.7kg more than a standard transtibial prosthesis. It has been reported that this addition of mass does not significantly affect amputees self-selected walking speed or economy [20].

Prosthetic Component Compatibility:

The CCA was required to be compatible with standard prosthetic sockets and low profile feet. This required that it was equipped with a female adapter at its socket interface, and a female adapter at its foot interface. In addition, its height was kept to a minimum, to allow for use by individuals with varying residual limb lengths.

Controlled Stiffness Ankle Compatibility:

The CCA was required to be an add-on to an existing device capable of adjusting the coronal plane stiffness of an ankle [21]. In doing so, it was possible to not only adjust the neutral angle of the ankle with the CCA, but adjust the angular stiffness about the CCA pivot when the CCA is in the locked mode. This feature was not used during this study, and the CCA pivot was not allowed to rotate once the CCA was locked.

Range of Motion:

Based on the terrain which the CCA would be tested on, it was determined that a ±15° range of motion in the coronal plane would be sufficient. This would allow the device to fully adapt to both the inversion and eversion conditions of the experiment (see ***Figure 3***).

Resolution:

Data from non-amputee participants in the coronally-uneven and unpredictable terrain study showed the ankle joint coronal angle at the clutch point occurred at a variety of angles [12]. Based on this, it was determined that the CCA would need to be able to be locked at a variety of angles. Thus the resolution requirement was set at 1°.

Backlash:

Based on the resolution requirement, it was determined that the backlash from the mechanism should be no more than 0.5°. This would ensure that the range of possible angles at each of the clutching mechanisms locked positions would not overlap with one another.

Other:

The device was also required to be untethered so as to not interfere with participant gait during testing. This required that all sensors, actuators, computers, and power supplies were able to be mounted on to the device itself, or on to the socket of the residual limb without over burdening the amputees.

2.3 Mechanical Description of Coronally-Clutching Ankle:

Based on the performance requirements, multiple concepts for the CCA were evaluated, iterated upon, and narrowed down, and the final design chosen is shown in ***Figure 2*** and ***Figure 3***, with an exploded view of all major components in ***Figure 4.***

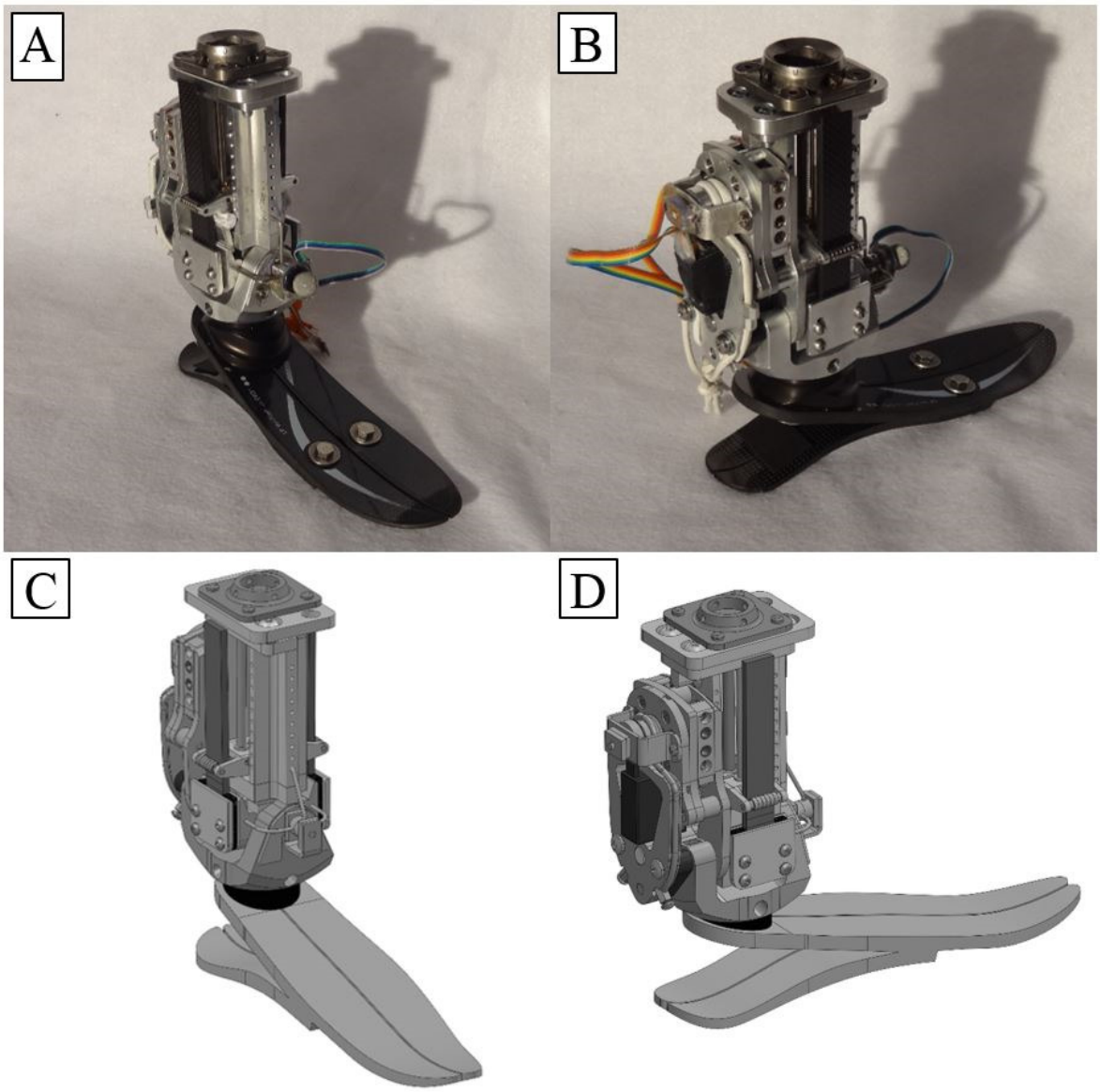

Figure 2: (A,B) Anterior and posterior isometric pictures of the CCA device with a low profile prosthetic foot. (B,C) Anterior and posterior CAD drawing of the CCA device equipped with a low profile foot.

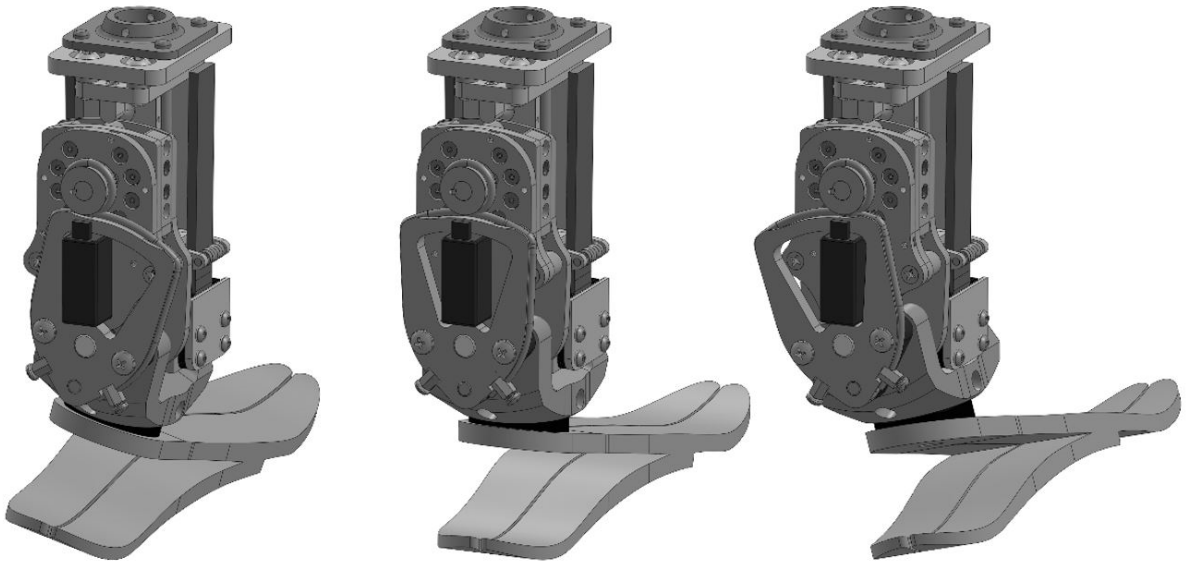

Figure 3: Posterior isometric views of the CCA device exhibiting the full range of coronal motion (±15°) that the clutching mechanism enables between the prosthetic foot and the rigid pylon assembly.

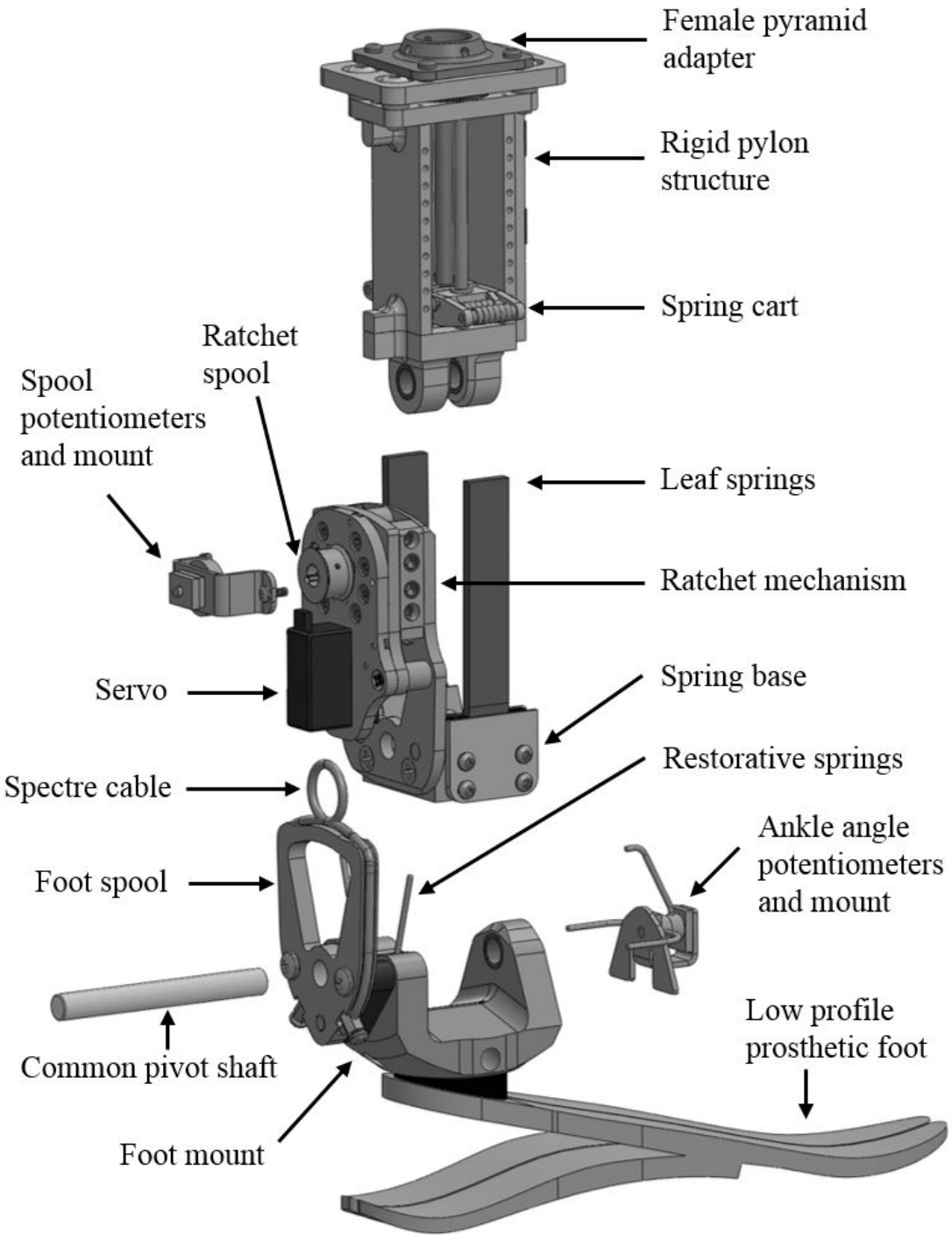

Figure 4: Exploded view of CCA device with all major components. Note that rotation between rigid pylon, and spring base (and attached ratchet mechanism), while possible, was eliminated for the purposes of this study.

The CCA was an update to an existing prosthetic device, the coronal stiffness ankle [21]. The coronal stiffness ankle device was comprised of the female pyramid adapter, the rigid pylon, the spring base, and the leaf springs shown above. The prosthetic foot was attached to the bottom of the spring base and the rotational stiffness between these two bodies could be adjusted by moving the cart position in the rigid pylon to adjust the effective length of the leaf springs. The CCA updated the coronal stiffness ankle by adding a third rotating component, which will be called the foot mount. In addition, the CCA update added a clutching mechanism that enabled or disabled free rotation between the adjustable stiffness spring base and the foot mount. For the purpose of this investigation, rotation between the rigid pylon and the spring base was locked out by a set of wedges. This allowed the investigation to focus purely on the effects of clutching the angle of prosthetic foot.

The CCA clutching design enabled the foot mount to rotate with minimal resistance in the coronal plane until the clutch was engaged. Once the clutch engaged, the only coronal motion of the foot came from the deformation of the foot itself. It should be noted that if the spring base was allowed to rotate relative to the rigid pylon, the leaf springs would also be engaged once the clutch was engaged and would work in series with the stiffness of the foot. However, this functionality is beyond the scope of this project.

The actual clutching mechanism of the CCA was a ratchet and pawl mechanism and can be seen in ***Figure 5-Figure 7***. The body of the ratchet mechanism was rigidly mounted to the spring base, as seen in ***Figure 4***. The pawls were designed to resist motion in both directions of ratchet rotation, were spring loaded by thin music wire to engage the ratchet, and could be disengaged by upwards motion of the pawl release arm. The pawls were organized into two opposing groups of four, each group resisting an opposite direction of rotation of the ratchet gear. The four pawls were positioned on either side of the ratchet in such a way as to decrease the rotation of the ratchet gear required to engage a pawl. The result was that once the pawls were engaged, the ratchet gear had a maximum range of motion of 3.75° before its rotation in both directions was stopped by a pair of opposing pawls. At this point, large rotation of the ratchet gear was disabled, and its range of motion would be limited to 1.5° of backlash. The ratchet gear had a 22 mm major diameter, a 20 mm minor diameter, 24 teeth spaced 15° apart

from one another, each with a 90° inner angle which was oriented symmetrically about the radius of the gear. The contact area between a ratchet tooth and a pawl face when engaged was 17.7mm^2, over which a forces of up to 1000 N were transferred. Due to the high stress imparted on these components they were machined from AISI 4140 annealed steel (yield strength: 415 MPa [22]).

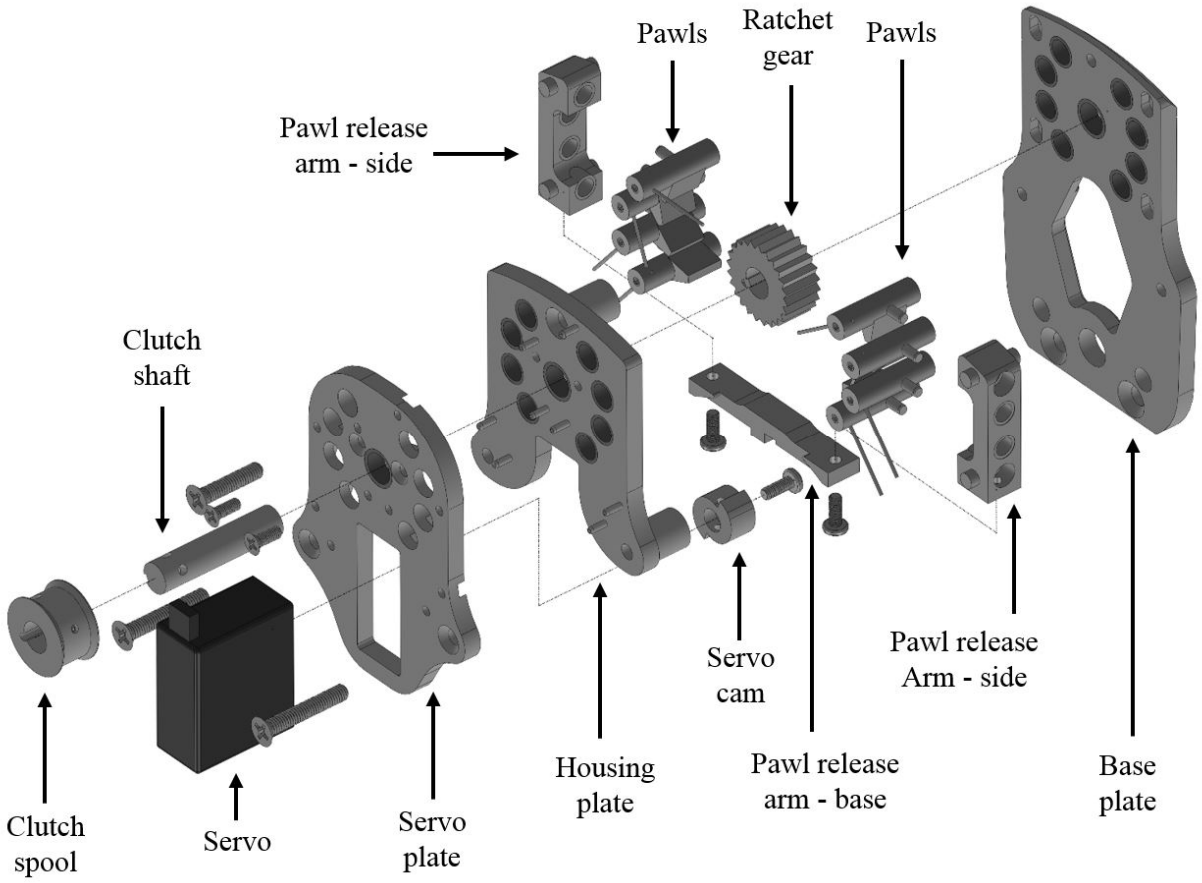

Figure 5: Exploded view of clutch mechanism in CCA device.

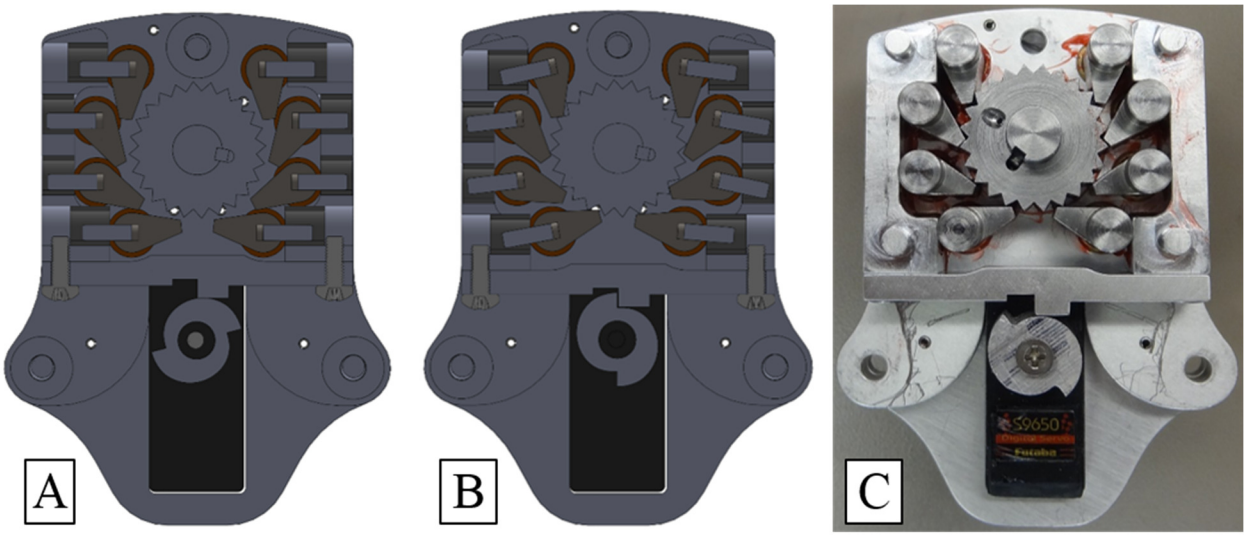

Figure 6: Section view of clutch mechanism (A) Cross section through pawl release arm assembly in the free position. Note how the interaction of the servo cam, pawl release arm, pawls, and ratchet gear allow the ratchet gear to spin freely. (B) Cross section through pawl release arm assembly in in the locked state. Note how the pawl release arm position is lower than in (A), and how the pawls are engaged with the ratchet gear. (C) Manufactured clutch mechanism shown in the locked position.

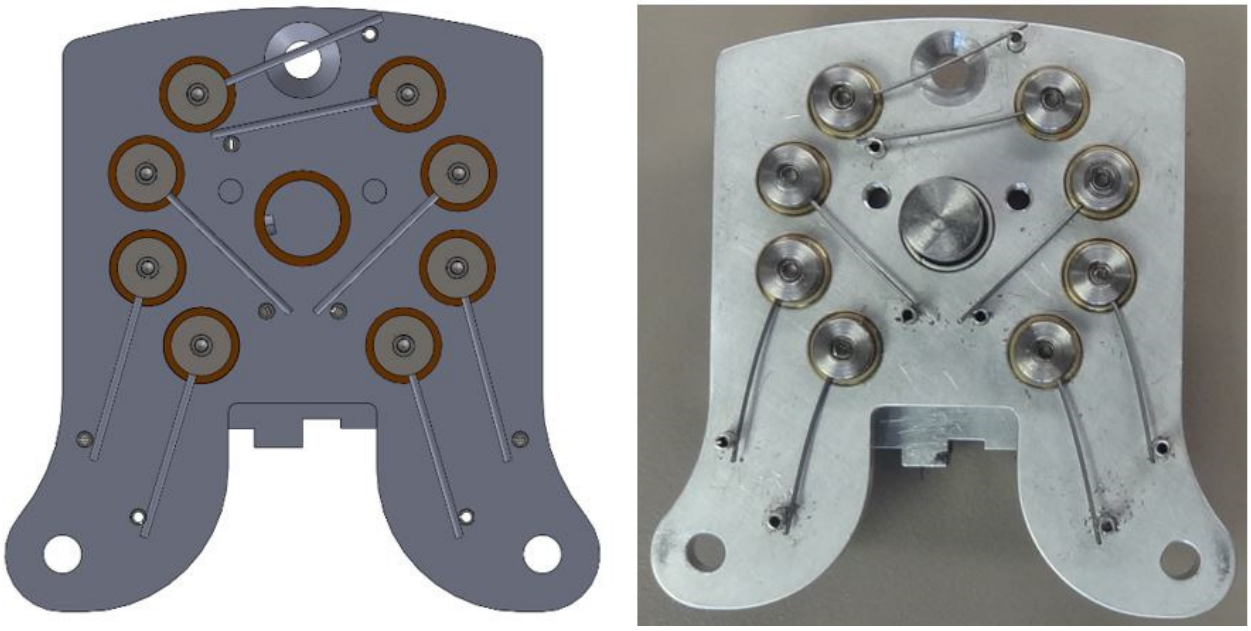

Figure 7: View of CAD (left) and manufactured CCA ratchet mechanism (right) showing the music wire springs used to provide a moment about each of the eight pawls. When the ratchet mechanism was in a locked state, the pawls were engaged with the ratchet gear, the pawl release arm was in a down position, and the springs were not deformed and were providing no moments. When the ratchet mechanism was in a free state, the servo lifted the pawl release arm into an up position, which rotated the pawls away from the ratchet gear (allowing it to spin freely) and also deformed each of the springs. Because each pawl was spring loaded to engage the ratchet gear, transition from the free to locked state occured quickly (see ***Table 2***).

The pawl release arm motion was driven by a cam that was attached to the output shaft of a servo motor (see ***Figure 6***). The cam was an aluminum body shaped to convert the rotational movement of the servo motor into translational displacement of the pawl release arm. Over the course of 160° of cam rotation, the radius of the cam increased from 4.5 mm to 7 mm, which led to +2.5 mm of pawl release arm displacement. Between 160° and 180° of cam rotation the radius remained at 7 mm, and the pawl release arm displacement remained at +2.5 mm, which corresponded to the pawls being disengaged from the ratchet. At 180° of rotation, the cam's radius stepped back down to 4.5 mm, and the pawl release arm returned to its original position, which corresponded to the pawls being engaged with the ratchet. This geometry was repeated once more in the cam. The step in the cam allowed for a quick transition from the adaption mode of the CCA to the locked mode, as this required <10° of cam rotation, which could be

accomplished in <30ms in no load conditions. Transitioning from the locked mode to the adapting mode required approximately 120° of rotation, which could be accomplished in <150ms under no load conditions. See section 2.5 for details on servo performance under load. The servo motor itself was a Futaba S9650 (Futaba, Mobara, JPN) servo that was modified with brass gears and the ability to continuously rotate. It was capable of rotating at 545 degrees/sec with a torque of 0.445 N-m at an operating voltage of 6V.

The ratchet gear of the clutching mechanism was attached to an aluminum spool, which controlled the motion of a Spectra® cable that was attached to the foot mount via a larger diameter partial spool (***Figure 4***). The ratchet spool had an effective diameter of 22 mm, while the foot mount spool, had an effective diameter of 110 mm. Thus, for every 1° of rotation that the foot mount experienced the ratchet spool, and the ratchet gear, experienced 5° of rotation. This gear ratio enabled the 3.75° resolution of the ratchet to be reduced to 0.75°, thus satisfying the <1° resolution requirement. The gear ratio also reduced the 1.5° of backlash in the ratchet mechanism to 0.3° of backlash in the foot mount, satisfying the <0.5° of backlash requirement.

A set of two leaf springs were mounted to the foot mount and used to restore a neutral angle between the foot mount and rigid pylon during the swing phase of gait. Each spring was made of 1095 tempered spring steel with a 1.09 mm thickness, a 4 mm width, and an effective length of 39 mm (***Figure 4***). As the foot mount rotated with respect to the socket mount one of the two springs would be displaced. This displacement created a restorative spring force that when translated into a rotation stiffness of approximately 1.7 N/degree. This restorative moment was sufficient to overcome frictional forces of the system and restore the foot mount from a 15° displacement to a neutral angle within approximately 100 ms (see ***Figure 18***).

Within the foot mount was a permanently fixed titanium female pyramid insert which allowed any low-profile foot mount to be mounted to the CCA. The height between this adapter, and the rotational axis of the CCA was kept to a minimum. Additionally, the overall height of the device between the foot mount pyramid adapter and the socket mount pyramid adapter was minimized to 140 mm. Because standard pyramid adapters were used on both the distal and proximal end of the CCA, prosthetists were able to fully adjust the device, ensuring correct foot alignment for participants in the study.

Keeping device mass a minimum influenced many decisions. All major structural members of the CCA device were machined from 7075-T6 aluminum (Yield Strength: 538 MPa [23]) due to its high strength to mass ratio. In addition, titanium and aluminum prosthetic adapters and components were chosen over those made of steel. In addition to material choice, the mass restriction influenced the clutching mechanism used. The ratchet design was chosen because it required a small servo motor (26g) to operate, and when the ratchet mechanism was not mode switching, its bi-stable nature required no energy from the motor. These two factors meant that a small and light battery could also be used (see section 2.4 for details on electrical design).

For testing purposes, the CCA was designed to operate in an adapting mode and a locked mode. In the adapting mode, the control algorithm would allow the foot to adapt to uneven terrain as described in section 2.5. In the locked mode, rotation of the foot mount relative to the pylon was physically disabled. However, in the locked mode, the same control algorithm was used. This meant that that the CCA made the same servo and ratchet sounds regardless of which mode it was in, preventing participants from distinguishing the configurations based on sound.

2.4 Electrical Description of Coronally-Clutching Ankle:

In order for the CCA to operate untethered, it required a microprocessor, a servo motor, a motor driver, a battery, power regulators, and a number of sensors (see ***Figure 8***, ***Figure 9***). The microprocessor chosen was the Arduino Micro 3.3V (Arduino, Torino, ITA), which had sufficient clock speed, internal memory, and digital and analog inputs and outputs for the required task. In addition, the Arduino Micro was capable of communicating with other devices via numerous communication protocols such as I2C, SPI, serial and PWM. Shown in ***Figure 8*** is the core processing unit, without any protective housing. Multiple breadboards were used and connected with flexible wiring so the electronic package could easily conform the amputee's socket. ***Figure 9*** shows all electronics with a protective housing made of gaffer's tape. Notice the addition of the servo motor, battery, potentiometers, and heel strike sensors.

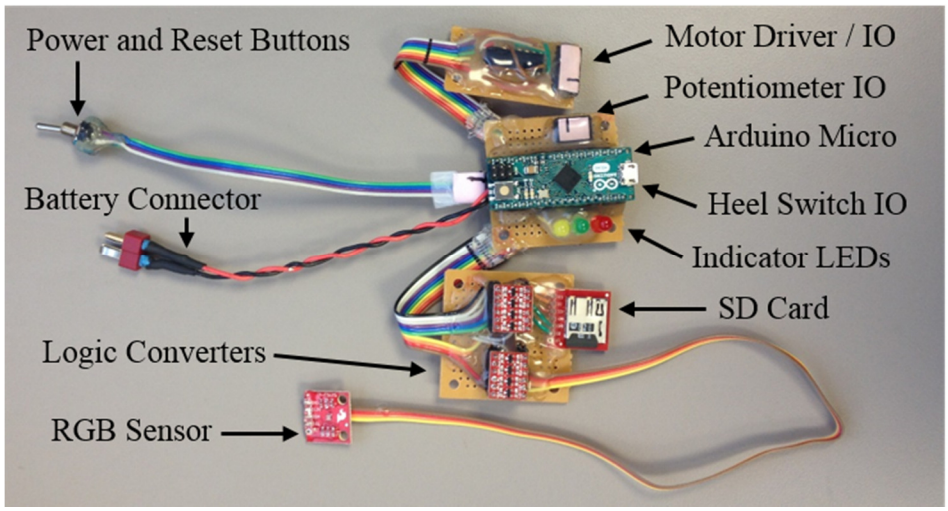

Figure 8: Microprocessor unit shown without any protective housing. Major electronic components labeled.

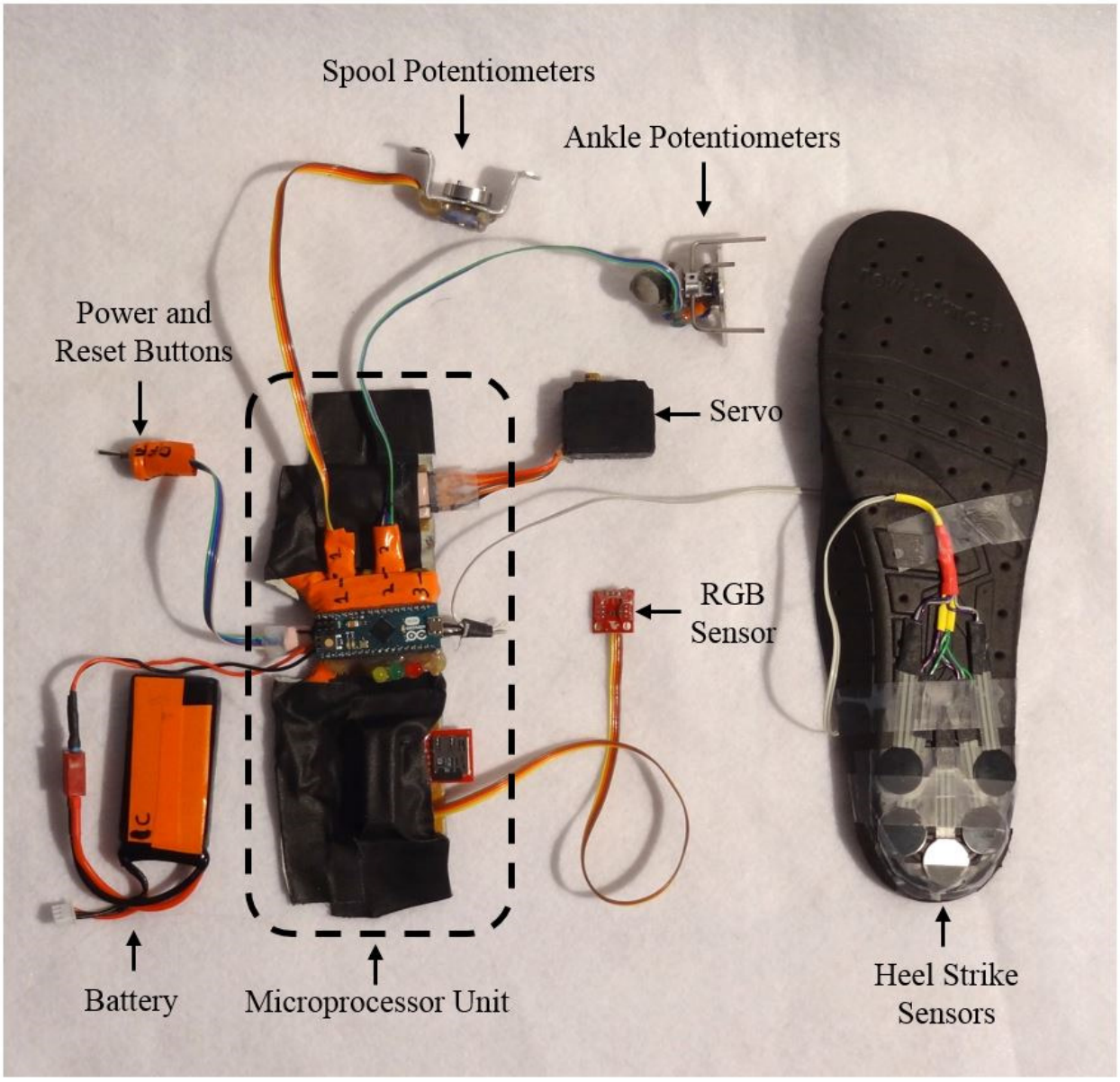

Figure 9: All electronics required for untethered operation of the CCA. Gaffer's tape used to protect electronics from damage. Modular design used for most sensors, motors, and switches in order to make component replacement easy.

The servo motor, which was a Futaba S9650, operated at 6V and thus required a motor driver. The motor driver chosen was a SN754410 (Texas Instruments, Dallas, USA), which was capable of controlling the servo in both directions via two PWM signals. Because the servo was modified to allow for continuous rotation, its original potentiometer had to be replaced by two Murata SV01A103AEA01R00 (Murata, Kyoto, JPN) potentiometers. These were installed on the

drive shaft of the servo in opposing orientations to enable for continuous accurate reading of the shaft position, as each potentiometer had a zone between 330° and 30° in which they were not accurate.

Four identical Murata potentiometers were installed on the device at other locations. There was a potentiometer which measured the rotation between the socket mount and the foot mount, and a potentiometer which measured the rotation between the foot mount and the adjustable stiffness spring base (see ***Figure 9***). Combined, the output from these two potentiometers recorded the angular position of all three rotational bodies of the CCA, relative to one another, about the coronal rotational axis (CCA pivot). The other two potentiometers were mounted, opposed to each other, to record the rotation of the ratchet spool. It was important to record the rotation of the spool and compare it to the rotation of the foot mount in order to know whether there was any play in the cable system that connected the two bodies. In addition, the rotation of the spool was the most direct measure of when the clutch was engaged or disengaged.

Two other sensors were used to help the device detect when to engage and disengage the clutch. The first was an Intersil ISL29125 (Intersil, Milpitas, USA) RGB light sensor which was used to detect where the device was in space (there was a blue light placed 1m before the disturbance). This sensor communicated via I2C to the microprocessor a digital value relating to the intensity of blue light that it observed. Next there were two sets of FSR 402 (Interlink, Camarillo, USA) force sensitive resistors that were placed under the removable insole of the shoe that was worn by the study participant. These sensors enabled the microprocessor to detect heel strike and toe off events.

The data from all sensors mentioned were recorded on to a micro-SD card. This card also recorded the time stamp of the microcontroller. Communication between the SD card and the microcontroller was carried out using SPI communication. Sensor recordings occurred approximately every 4 ms (250 Hz), and every new trial was associated with a unique file name on the SD card. This made it possible in post-processing to sync and compare trial data collected from external measurement systems and trial data collected on the device.

Powering the electronics was a 7.4V 1000mAh lithium ion battery. The battery voltage was chosen based on the highest voltage needed by the system components, which was the 6V servo. The capacity was chosen to allow for data collections of up to four hours, with up to 200

mode transitions from locked to unlocked and back to locked, without needing to switch batteries.

2.5 Controller and Software Description:

The Arduino Micro was programmed to control the CAA using Arduino's native language, which used standard C commands. The software was designed for a specific test procedure which would occur in controlled conditions of a gait lab (see section 2.8 for details on test procedure). The software ran in a continuous main loop, which recorded sensor data, activated the servo motor, and displayed critical information to operators during the test procedure.

The primary objective of the software was to ensure the CAA only adapted during interaction with coronally-uneven and unpredictable terrain, and to ensure the foot returned to a neutral angle prior to the next step. When a trial began, the servo motor was rotated to a locked position. As a participant walked toward the disturbance, their prosthetic limb would pass near a blue LED during its swing phase immediately prior to stepping on the disturbance. The RGB sensor would detect this light and the force sensitive resistors would detect whether the prosthetic foot was in swing phase. When both these conditions were detected, the servo would be rotated to an adapting position, allowing the prosthetic foot to rotate freely. Once in this position, the program would wait for the detection of a heel strike from the force sensitive resistors in the heel of the insole. Upon detecting a heel strike, the controller would again turn the servo to a locked position. On average, during actual trials, it took approximately 47-50 ms between heel strike and clutch engagement (see ***Table 5***). At this point, it was assumed that the foot had conformed to the surface.

After foot conformation, the controller enacted a series of commands to restore the neutral angle of the foot mount. Based on experimental control data, as well as participant gait speed, the controller was programmed to wait for set amount of time after heel strike before sending a release signal to the servo. Typically, this waiting period was 350 ms. Once the servo received the release signal, and reached the free position, which was during the swing phase after the disturbed step, the restorative springs would restore the foot mount to a neutral angle. The time required to neutralize the foot mount angle was typically 200 ms after the release signal was

received. The time required to neutralize the foot mount angle and lock the clutch, was typically 400 ms (see ***Figure 18***).

Control of the servo motor was carried out using a modified proportional controller, whose formula can be seen below in ***Equation 2***.

$$P_{OUT} = \begin{cases} 255 & if \quad 45° < e \\ |K_p e| & if \quad 5° < e \leq 45° \\ 0 & if \quad e \leq 5° \ or \ e \geq 355° \end{cases}$$

Equation 2: Control algorithm of servo motor. P_{OUT} is the PWM duty cycle sent to the motor driver, which has a 100% duty cycle at a value of 255. e is the error, in degrees, between the measured servo rotation and the reference signal. Note that e is always positive, as the servo could only turn in one direction, and is modulo 360°. K_p is the proportional gain, which was 255/45.

The system output was limited in that the asymmetric cam pattern required the servo rotate in a single direction. Thus, a balance was struck between reducing system overshoot as much as possible (as reverse correction was not possible), and maintaining sufficient response times. As the motor spun, the actual servo angle would be reduced, until it reached 0, at which point it would jump back to 359, as it was modulo 360. Due to this, the error value was always calculated as the number of degrees the servo motor would have to spin in order to reach the reference angle, and was always considered to be a positive value between 0 and 359. The motor was commanded to spin at full speed (command signal = 255), until the error was within 45° of the target angle. Then, the command signal to the motor would be proportional to the error. The proportional gain, K_p, was 255/45. Finally, if the motor position was within ±5° of its target, the command signal would be 0. The controller parameters were empirically derived based on bench testing as described in section 2.7.

Figure 10 and ***Figure 11*** show the mean and standard deviation of the servo's step response when switching from locked to free, and from free to locked angles. The data was recorded by the microcontroller, and the servo was installed on the fully assembled CAA that was undergoing test conditions meant to represent actual use (see section 2.7).

In response to a step input from the free to the locked angle, the controller was underdamped, as evidenced by its percent overshoot (mean:10.9% SD: 3.6%), but did not oscillate, due to its ability to only drive in one direction (see ***Figure 10***). The overshoot is most likely due to the servo cam being assisted by the pawl push arm assembly, which was being pushed down by each of the pawl springs during the transition from the free to locked state. The servo had a mean 10-90% rise time of 118ms, with a standard deviation of 9ms. This was the rise time between the servo in its free and locked angles; however, the angle at which the cam step passed over the ledge in the pawl assembly arm (see ***Figure 6***), was somewhere in between the two angles shown in ***Figure 10*** . As a result, the ratchet mechanism actually switched from free to locked in a shorter amount of time, and this is further is discussed in section 2.7c.

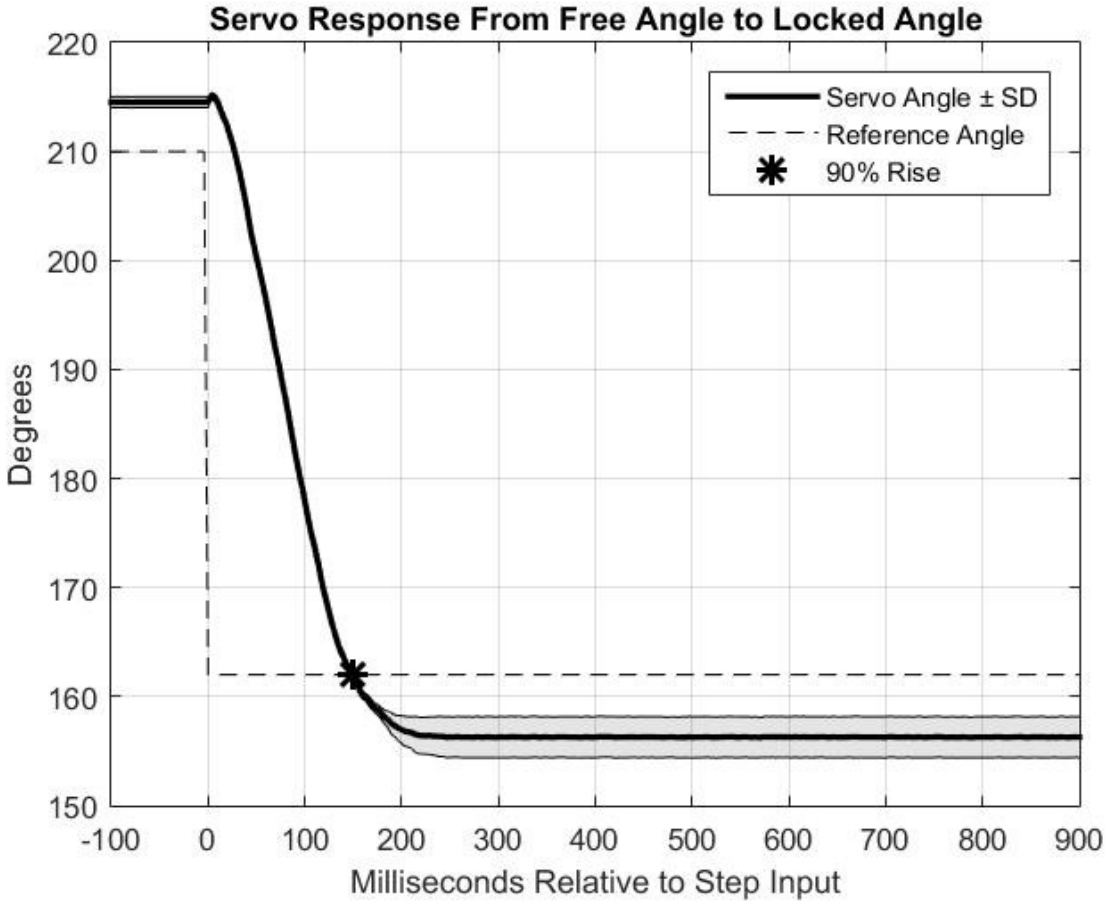

Figure 10: Servo response from free to locked angle for 20 trials simulating actual use.

In response to a step input from the locked to the free angle, the controller appears to be overdamped, as evidenced by its undershoot (mean: 3.6% SD: 0.5%) (see ***Figure 11***). The overdamping and undershoot are most likely due to the servo rotation being resisted by each of the pawl springs as the servo cam pushes the pawl release arm assembly upward into the free position. The servo had a mean 10-90% rise time of 288ms, with a standard deviation of 13ms. However, the angle at which the cam was able to lift the pawl release arm assembly high enough to free the ratchet gear (see ***Figure 6***), was somewhere in between the two angles shown in ***Figure 11***. As a result, the ratchet mechanism actually switched from locked to free in a shorter amount of time, and this is further is discussed in section 2.7c.

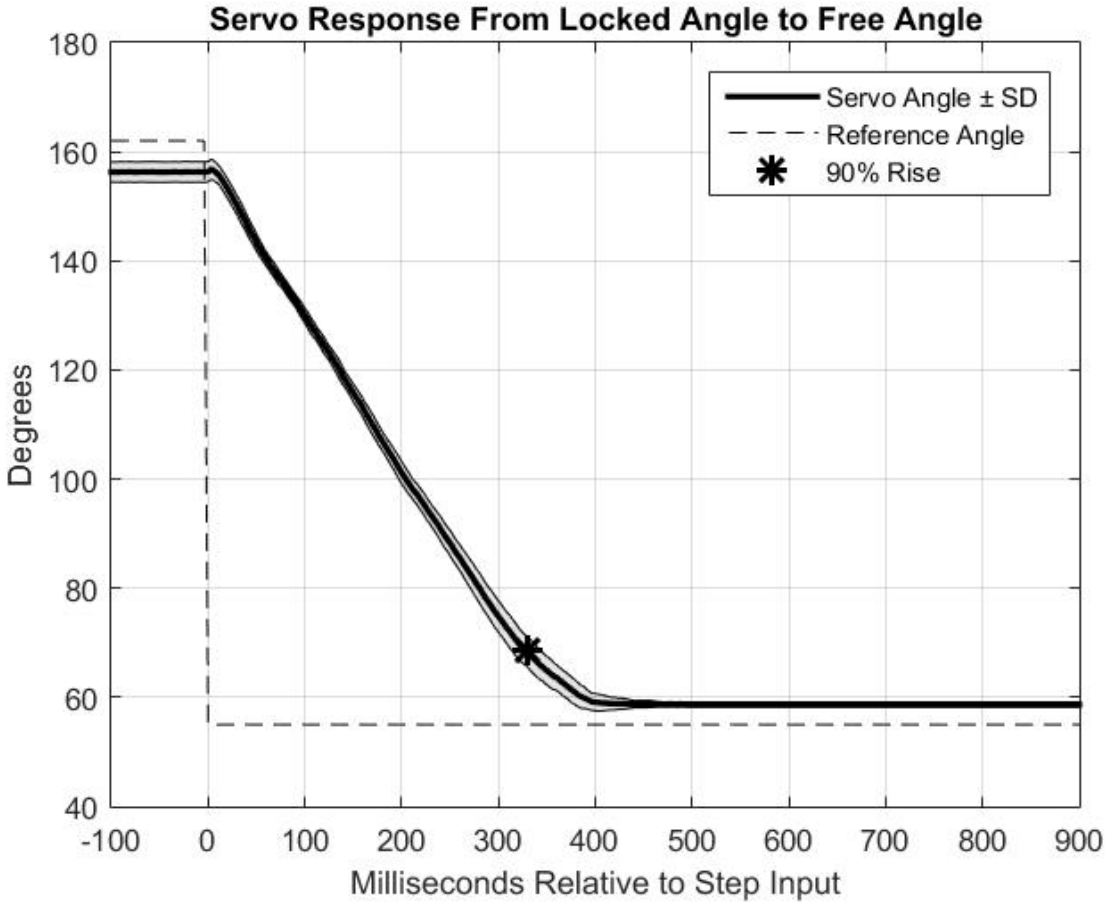

Figure 11: Servo response from locked to free angle for 20 trials simulating actual use.

2.6 Finite Element Analysis:

Finite element analysis (FEA) was performed on all major load bearing components of the CAA prior to fabrication to ensure structural integrity of the device. FEA was carried out using ANSYS Mechanical (Ansys, Canonsburg, USA), and was performed on both the component and sub-assembly levels. The loading parameters used for analysis were based on joint forces and moments calculated from a study on non-amputees on coronally-uneven and unexpected terrain [12], which used the same disturbance that the CAA would be tested on (see section 2.8b). A factor of safety of 2 was achieved for all components whose structural failure could lead to a catastrophic failure of the device.

The components which benefitted most from the use of FEA were the pawls, ratchet gear, and rigid pylon assembly. In the case of the ratchet and pawls, FEA helped minimize the size of the ratchet teeth and pawl geometry. The results of the pawl and gear analysis are displayed in ***Figure 12***, and ***Figure 13***, respectively. The 1500 N normal force magnitude used in these two simulations was 50% greater than the maximum normal force that was calculated based on the maximum ankle moment of the control subjects in the coronally-uneven and unpredictable experiment. The pawl experienced a maximum Von-Mises stress of 99MPa, which gave it a factor of safety of 4.15 for the given load, based on the yield strength of the AISI 4140 steel used (Yield Strength (YS): 415MPa). The gear experienced a maximum Von-Mises stress of 147MPa, which gave it a factor of safety of 2.82 for the given load, based on the yield strength of the AISI 4140 steel used (YS: 415MPa). In the case of the rigid pylon assembly, FEA was used to understand if material from the original parts could be removed in order to make clearance for new assembly parts. A 2123N force, which was twice that of the average maximum load transferred through in control subjects' tibias in the coronally-uneven and unpredictable terrain experiment, was applied to the face of the assembly that interacted with the socket. The surfaces of the assembly which interacted with the common pivot shaft were fixed. The results, shown in Figure 14 showed that even with minor material removal, the maximum Von-Mises stress was 138MPa. With the given load, this still provided a factor of safety of 3.89, based on the yield strength of 7075 T6 Aluminum (YS: 538 MPa). These results were considered grounds for accepting the mechanical design, and building the first prototype.

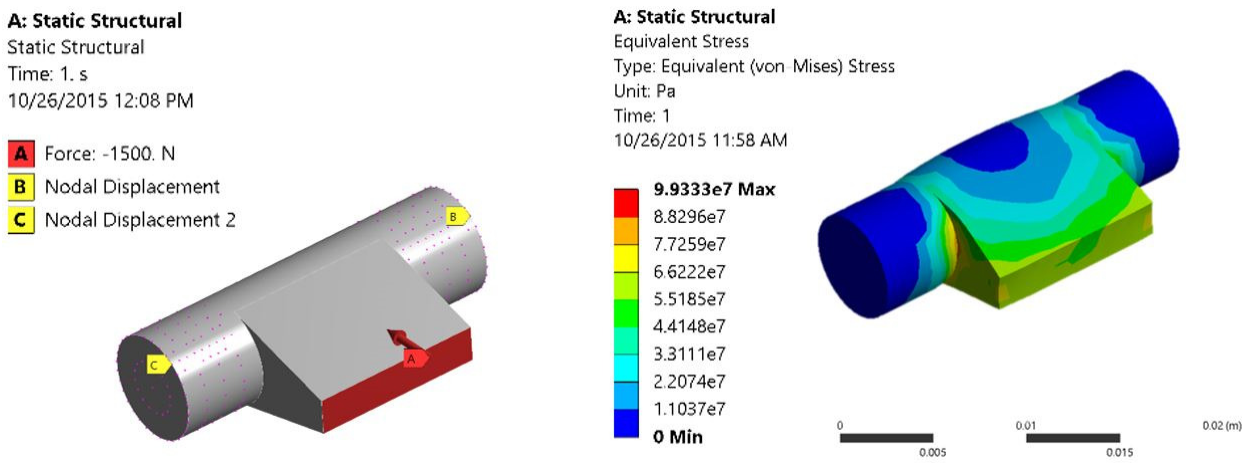

Figure 12: Ansys results from FEA analysis of ratchet pawl. Right: A 1500 N normal force was applied to the face of the pawl which interacted with the gear, and the displacement of the end surfaces of the pawl were constrained. Left: Stress contours of the pawl show the max von Mises stress (99 MPa) are well below the yield stress of the material (AISI 4140 Steel YS: 415 MPa).

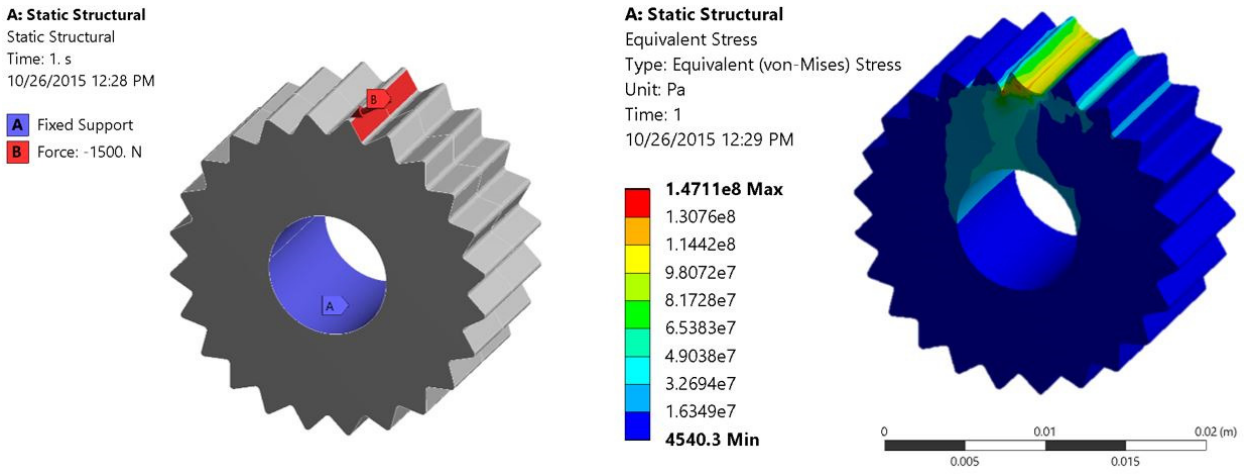

Figure 13: Ansys results from FEA analysis of ratchet gear. Right: A 1500 N normal force was applied to the face of the gear which interacted with the pawl, and the displacement of the surface of the inner diameter was constrained. Left: Stress contours of the gear show the max von Mises stress (147 MPa) are well below the yield stress of the material (AISI 4140 Steel YS: 415 MPa).

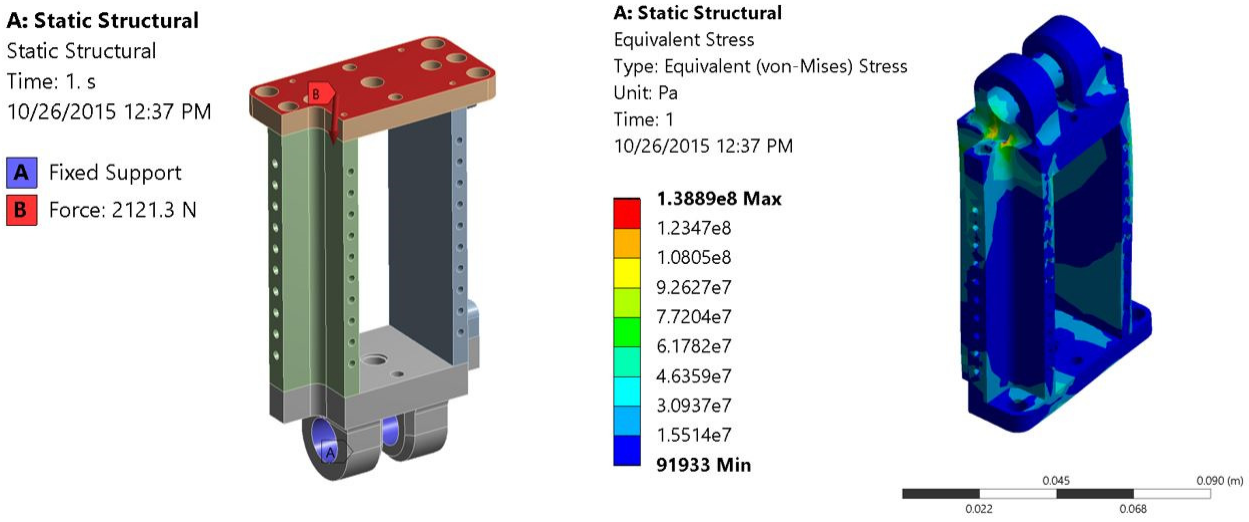

Figure 14: Ansys results from FEA analysis of rigid pylon assembly. Right: A 2121N magnitude force was applied to the face of the assembly which interacted with the female socket adapter. The common pivot bearing surfaces were fixed, and all contact faces were assumed to be bonded. Left: Stress contours of the assembly show the max Von-Mises stress (138 MPa) is well below the yield stress of the material (7075 T6 Aluminum YS: 538 MPa). Orientation flipped show area of maximum stress.

2.7 Coronally-Clutching Ankle Bench Testing:

After the CCA was constructed, a series of bench tests were executed to understand the CCA's performance characteristics. The bench tests focused on characterizing the CCA's adaptation response time, recovery response time, ability to support a full body load, and ability to stop ankle rotation under load.

2.7a Bench Testing Instrumentation:

An 858 Mini Bionix II testing system (MTS, Eden Prairie, USA) was used to provide the load required for bench testing. A custom built test base was used to simulate the conditions the CCA would experience when stepping on inverted or everted terrain [21]. The test base consisted of a 15° coronally inclined surface which was mounted on a set of linear bearings that allowed the inclined surface to freely translate in the mediolateral direction (see ***Figure 15***). This additional degree of freedom was added as to not over constrain the system during loading of the

foot, and has been used in similar test procedures [24]. In addition, a flat test base was used which did not invert or evert the foot. The CCA was mounted to the head of the tester, and the test base was mounted to the base of the tester for all testing. A Low Profile Vari-Flex (Ossur, Reykjavik, ICL) foot with parameters representing that of a typical amputee participant (size: 27, category: 4) was mounted to the CCA with a cosmetic shell and a New Balance M577 (New Balance, Boston, USA) walking shoe. These were the same types of feet and shoes that were used in the human participant test procedure (see section 2.7b).

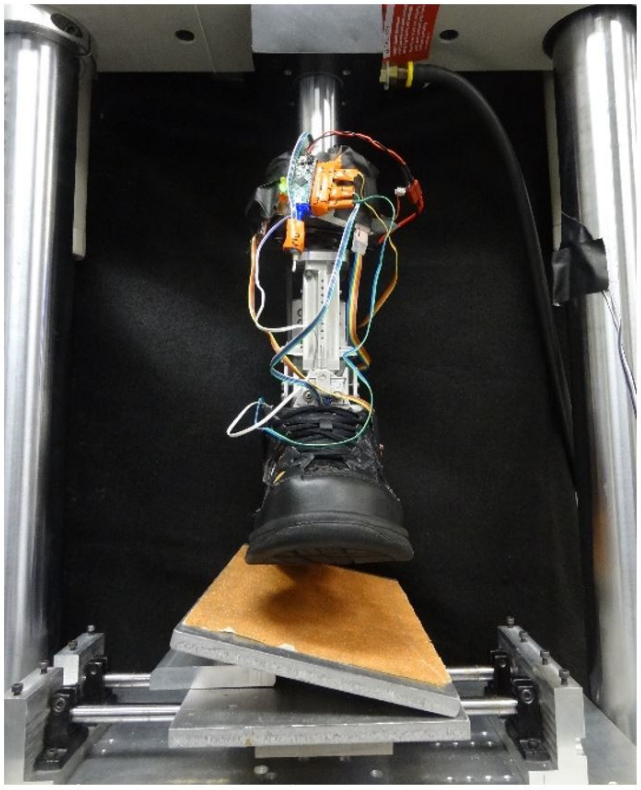

Figure 15: Anterior view of the test hardware configuration for an inversion trial with a left foot. CCA with electronics shown mounted to the head of tester, with the sliding test base beneath.

2.7b Bench Testing Procedure:

To test the load bearing capabilities of the CCA, the test head was displaced at a rate of 50 mm/sec with a load limit of 1000 N, which was sustained for 1 second during a dwell period, after which, the head was positioned at a speed of 100 mm/sec back to its original position. From

previous control studies, 1000 N was determined to be an average maximum axial load through the tibia encountered during walking, and the loading rate was approximately 25% that of which was observed during walking. This was the fastest speed at which the 1000 N limit could be consistently achieved. This test was performed 10 times with the base in a position which inverted the foot, 10 times with a base position which everted the foot, and 10 times with the flat base. For all trials, the foot was initially positioned neutrally in all three planes of rotation. Data from the test machine was recorded at 120 Hz, and data from all the CCA's sensors were recorded at 250 Hz.

To test the adaptation response time of the CCA, the tester was displaced at a rate of 100 mm/sec with a load limit of 500 N, which was sustained for 1 second during a dwell period, after which the head was positioned at a speed of 100 mm/sec back to its original position. From previous control studies, 500 N was determined to be half of the average maximum tibial axial load during walking, and the loading rate was approximately 50% that of which was observed during walking. Given the test setup, this load rate was the fastest speed at which the MTS could be driven without irregular behavior. This test was performed 10 times with the base in a position which everted the foot, 10 times with a base position which inverted the foot, and 10 times with the flat base. For all trials, the foot was initially positioned neutrally in all three planes of rotation. Data from the MTS was recorded at 120 Hz, and data from all the CCA's sensors were recorded at 250 Hz.

To determine whether the clutching mechanism could stop ankle rotation during rotation under load the CCA control software had to be modified. The modification accommodated for the fact that the feed rate of the MTS was much slower than the striking velocity of the foot during human walking. In this modified control software, for the inversion and eversion cases, the foot of the CCA was able to rotate freely until the CCA detected not only a heel strike, but also ankle joint rotation. Once these were both detected, a signal was sent to the servo of the ratchet mechanism to engage the pawls and cease rotation of the ankle joint. Without the addition of the ankle rotation detection, it was observed that the clutch would engage prematurely and be locked before any significant ankle rotation had occurred. For the flat condition, the control software relied only on heel strike detection to trigger the clutch.

Finally, the recovery times were tested by measuring ankle and servo angles as the CCA neutralized the ankle angle from being fully adapted in both inversion and eversion positions. 10 recovery trials were conducted for each position, in which the foot was fully adapted in the corresponding direction, and then lifted from the terrain and allowed to recover as it would during the swing phase of gait. The first recovery time, which will be referred to as the neutralization time, was the time from which a release signal was sent to the ratchet mechanism servo until the ankle was within 10% of its steady state neutral position. The second recovery time, which will be referred to as the locked time, was the time from which the release signal was sent until the time at which the ankle was neutralized, and the ratchet mechanism was locked. As locking had no effect on the ankle angle, the servo position was used as a surrogate measure, as it was known which servo angle (44°) corresponded to the ratchet mechanism being locked after the neutralization process.

2.7c Bench Testing Results:

No plastic deformation was observed after all loading condition and position trials were completed. For both loading conditions, the ratchet mechanism was able to successfully stop the rotation of the ratchet gear while it was in motion. This is supported by the fact that the foot mount to pylon angle never reached 15° of rotation (see ***Figure 16*** and ***Figure 17***), which it would have done if the ratchet mechanism was unable to stop the ratchet gear during rotation.

Two separate adaptation clutch times were calculated from the loading trials. The first clutch time, which will be referred to as the spool clutch time, measured the time from which the heel strike was detected, to the time at which the spool reached 90% of its final angular position during the dwell period. The second clutch time, which will be referred to as the foot mount clutch time, measured the time from which heel strike was detected, to the time at which the foot mount angle reached 90% of its final angular position during the dwell period. ***Figure 16*** shows the spool and foot mount angle for the 500 N load, and ***Figure 17*** shows the spool and foot mount angles for the 1000 N load. The clutch times and their associated angular clutch displacements can be seen in ***Table 1*** and ***Table 2***.

For both the 500 N and 1000 N loading conditions, the spool clutch time came close to meeting the 40ms response time target (see ***Table 1*** and ***Table 2***). However, the foot mount clutch times were considerably larger than the 40ms response time target. It can be seen that

once the spool clutch time was reached, there was additional rotation of the foot mount for both loading conditions, but particularly for the 1000 N condition (see ***Figure 16*** and ***Figure 17***). This additional rotation can be attributed to stretching of the Spectra® cable under the loading force. In the case of the 1000 N condition, there was approximately an additional 3° of foot mount rotation after the spool clutch stopped rotating. This additional rotation was a large contribution to the overall range of motion of the foot mount for the 1000 N condition, and it was only during this time, when the Spectra® cable was being stretched, that the ankle angle reached 90% of its overall range of motion.

The foot mount angle graphs for both the 1000 N and 500 N conditions show that at the spool clutch time there appears to be a reduction in the angular velocity of the ankle. This suggests that while the clutch did not immediately stop the foot mount rotation, it did effectively split the ankle behavior into two modes. The first, pre-clutch, mode was the adapting mode, characterized by relatively fast angular velocity of the foot mount. The second, post-clutch, mode was the locked mode, characterized by relatively slow, or negligible angular velocity of the foot mount.

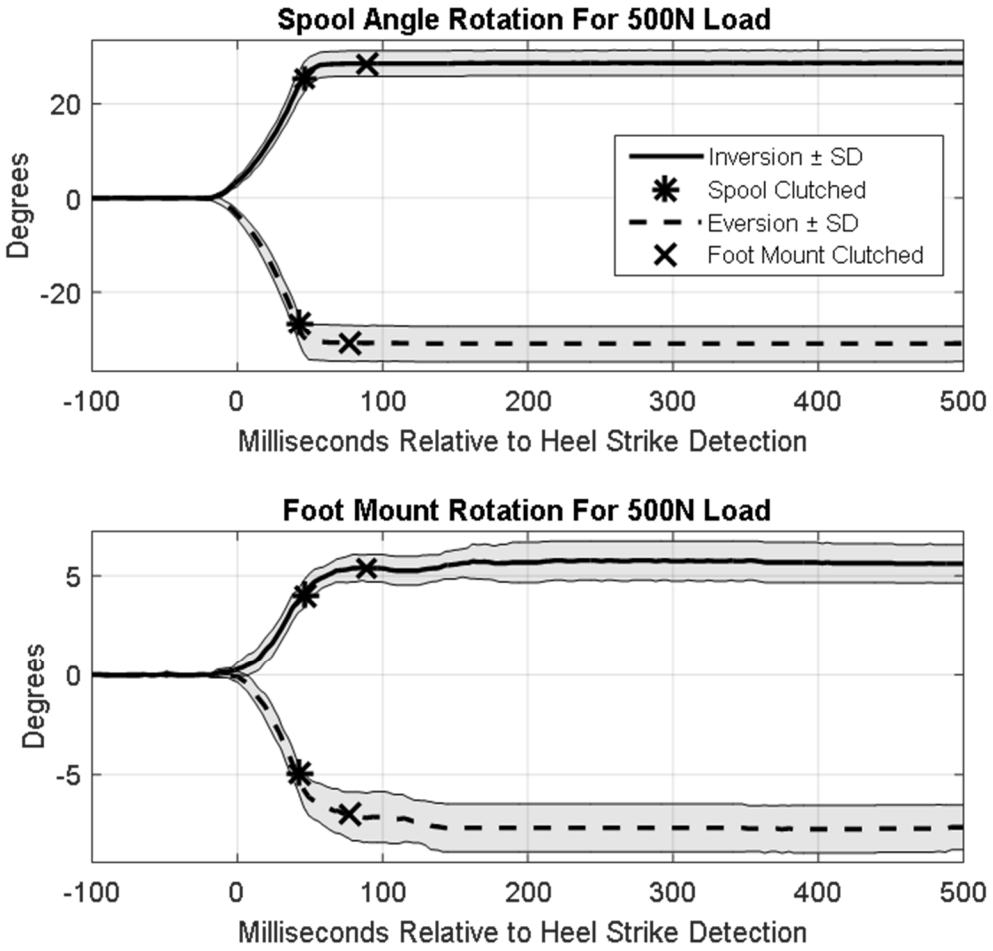

Figure 16: MTS results for a 500 N load with a feed rate of 100 mm/sec. Top: Mean spool angle in degrees from 100 ms before heel strike detection to 500 ms after heel strike detection for both inversion and eversion. Bottom: Mean foot mount angle in degrees from 100ms before heel strike detection to 500ms after heel strike detection for both inversion and eversion. Average spool clutch time and foot mount clutch time shown on both graphs for both conditions.

Table 1: Clutching characteristics for the 500 N load and 100 mm/sec feed rate condition. Mean ± standard deviation values provided for all measures.

Angle	**Spool Angle**		**Foot Mount Angle**	
Metric	**Clutch Time (ms)**	**Clutch Displacement (deg)**	**Clutch Time (ms)**	**Clutch Displacement (deg)**
Inversion	46 ± 4	26.3 ± 2.5	89 ± 42	5.3 ± 0.9
Eversion	42 ± 2	-28.4 ± 3.6	77 ± 22	-7.0 ± 1.1

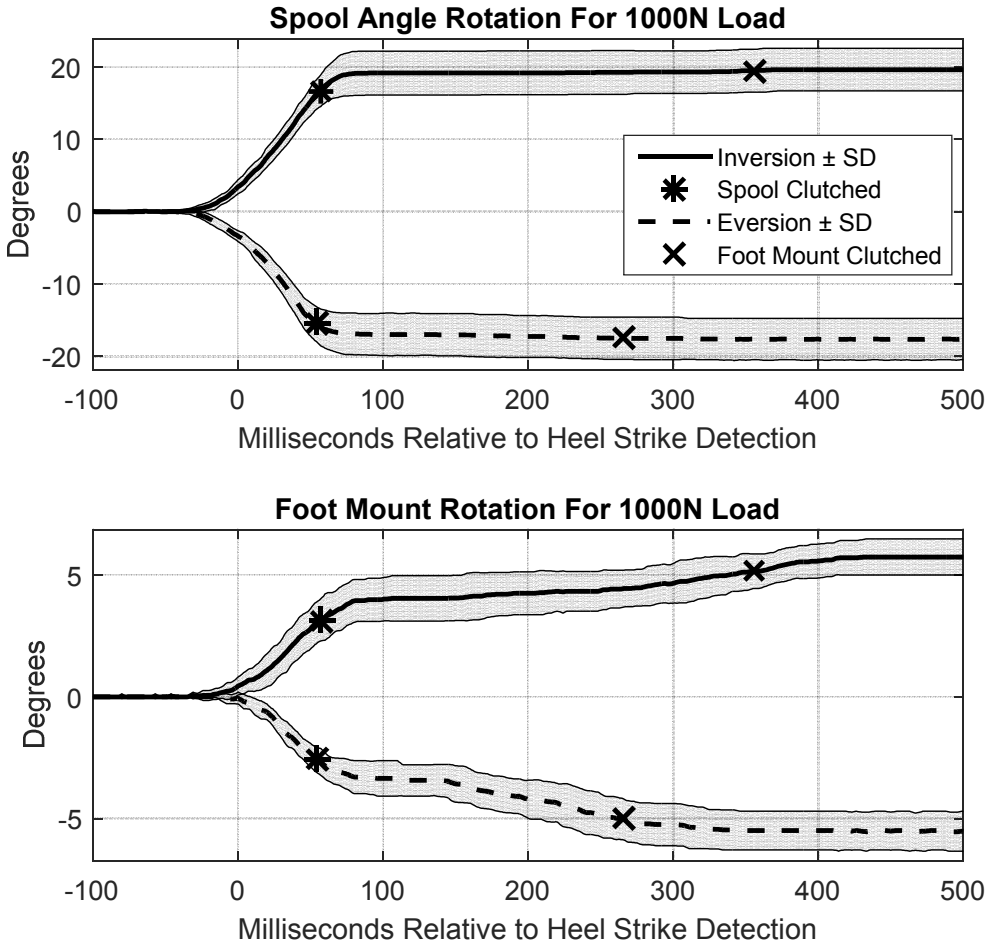

Figure 17: MTS results for a 1000 N load with a feed rate of 50 mm/sec. Top: Mean spool angle in degrees from 100 ms before heel strike detection to 500 ms after heel strike detection for both inversion and eversion. Bottom: Mean foot mount angle in degrees from 100 ms before heel strike detection to 500 ms after heel strike detection for both inversion and eversion. Average spool clutch time and foot mount clutch time shown on both graphs for both conditions.

Table 2: Clutching characteristics for the 1000 N load and 50 mm/sec feed rate condition. Mean values provided with corresponding standard deviations in the parenthesis.

Angle	**Spool Angle**		**Foot Mount Angle**	
Metric	**Clutch Time (ms)**	**Clutch Displacement (deg)**	**Clutch Time (ms)**	**Clutch Displacement (deg)**
Inversion	57 ± 9	17.8 ± 2.7	356 ± 26	5.2 ± 0.7
Eversion	54 ± 6	-16.0 ± 2.6	265 ± 34	-5.0 ± 0.7

The ankle and servo angles used to calculate the recovery times of the CCA are shown in ***Figure 18***. There was no observable difference between inversion and eversion regarding the recovery behavior of the CCA, and thus the results of both sets of trials are combined. The absolute value of the ankle angular displacement from its initial position when the release signal was received was used to determine the neutralization time. The mean neutralization time for all 20 trials was 243 ms with a standard deviation of 11 ms. The locked time was measured by the time from the release signal being sent until the time at which the servo reached 44°, at which point the ratchet mechanism was locked. The mean locked time was 428 ms with a standard deviation of 3 ms. These results, while outside of the initial design specifications, show that if the release signal is sent to the servo right at toe-off, the CCA is able to neutralize the ankle angle, and either be in the adapting mode or the locked mode, before the subsequent heel-strike at a normal walking speed.

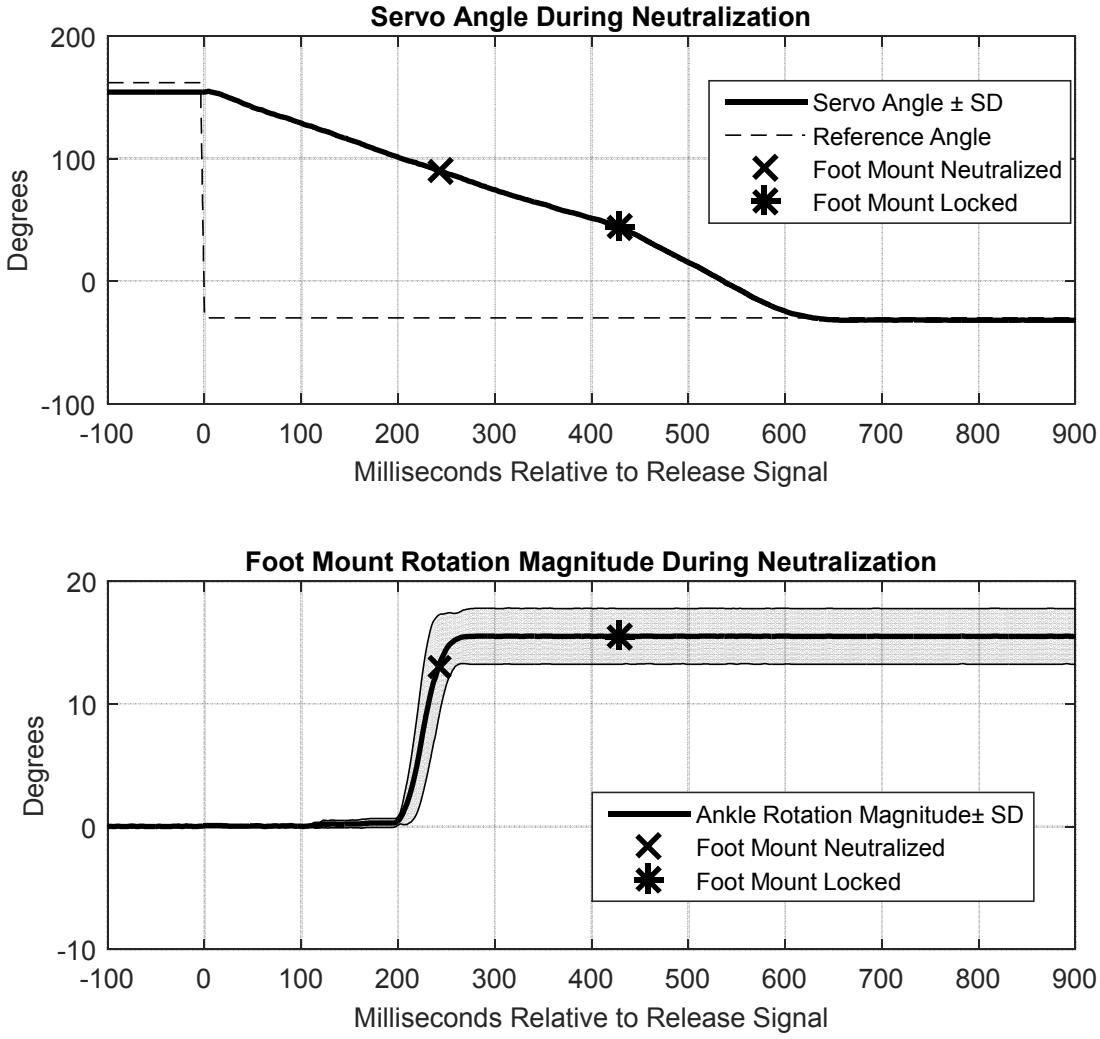

***Figure 18**:* Neutralization behavior of the CCA from fully adapted positions in both inversion and eversion. Top: Servo angle and controller reference angle during neutralization and locking. Modulo 360 units converted to absolute scale for clarity. Bottom: Foot mount rotation magnitude during neutralization. Neutralized time point based on 90% recovery of ankle angle, locked time point based on servo reaching 44° of rotation.

Based on the CCA's structural integrity under the equivalent of full body loads it was considered safe for use in human participant testing. In addition, the CCA was able to perform its main function of stopping, or at least considerably reducing, ankle velocity under full body loads in a period of time that corresponded with that of the early stance phase of gait. Finally, it was

demonstrated that the CCA was able to recover the ankle angle to a neutral position and lock it in time for a subsequent step. Based on these factors, it was concluded that the CCA was suitable for human participant testing.

2.8 Human Participant Testing:

2.8a Human Participants:

Unilateral, transtibial amputee participants were chosen for this study. All participants met the following criteria: 1) were between the ages of 18 - 75 years old, 2) had been fit with and used a prosthesis for over a year, 3) ambulated without aids, 4) were under 200lbs, 5) had enough build height in prosthesis to fit the CCA. Participants were excluded if they: 1) did not have a proper fitting prosthesis and could not be fit with one before the study, 2) had any condition unrelated to amputation that could affect gait, as determined by observation or self-report. No restrictions were placed on the as prescribed prosthesis. All participants were consented in accordance with the requirements of the Institutional Review Boards of the University of Washington, as well as the VA Puget Sound Health Care System.

2.8b Human Participant Test Instrumentation:

Coronally-uneven and unpredictable terrain was reproduced in a gait lab using the coronally-uneven and unpredictable terrain setup [12] (see ***Figure 19***). The setup consisted of a raised walkway (8.0 m x 1.5 m), in the middle of which was a disturbance device made of a Kistler 9286AA force plate (Kistler, Winterthur, CHE) that could be rigidly positioned +15° in the coronal plane, -15° in the coronal plane, or flush with the walkway (see ***Figure 19***). In addition, the position of the disturbance device could be concealed with a removable, opaque, latex membrane that was 0.48 mm thick. On either side of the disturbance device, flush with the walkway, existed two platforms which were rigidly fixed to two separate AMTI BP400600 force plates (AMTI, Watertown, USA). These force plates, when combined with that of the disturbance device, allowed for kinetic data collection of the disturbed step, as well as the two steps before and after it. Kinematics were captured using a 12-camera Vicon MX system (Vicon Motion Systems, Oxford, UK) and reflective markers placed on the participants (see section 2.8e).

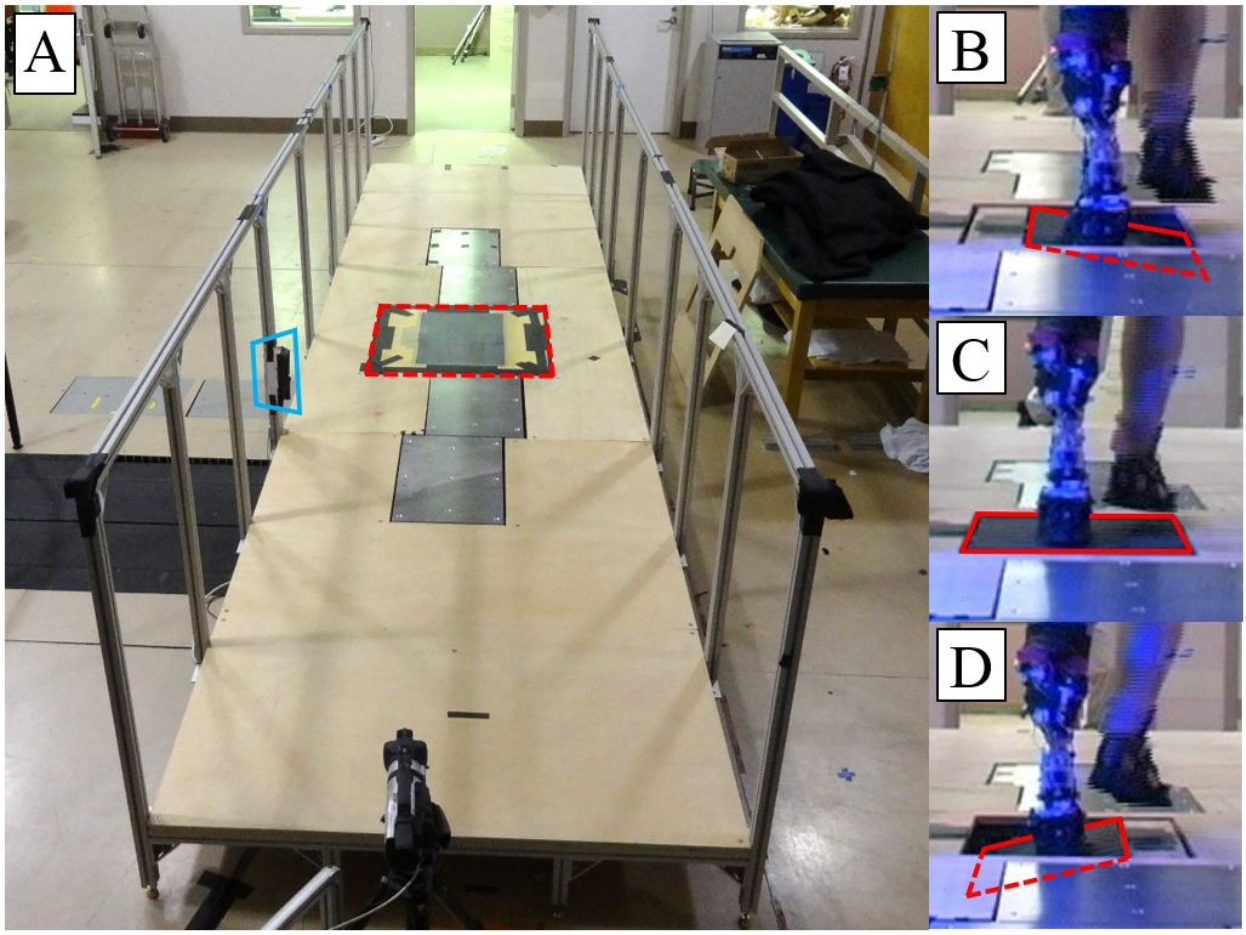

Figure 19: (A) Raised walkway with embedded force plates, handrails, and LED light fixture (blue trapezoid) for communication with CCA. The experimental setup is shown in the blinded condition, in which the disturbance device was concealed beneath a latex membrane (outlined by red dashed line). (B-D) Posterior view of amputee subject with CCA stepping on the disturbance device in the everted (B), flush (C), and inverted (D) positions. (B-D) Experimental setup is shown without the latex membrane installed, and the portable force plate is highlighted with a red line.

2.8c Human Participant Test Procedure:

The test procedure was designed to explore the effect of two independent variables, the prosthetic device and terrain type, on amputees' gait and standing balance. Three different prosthetic devices were tested: the participant's as prescribed prosthesis, the CCA in its adapting mode, and the CCA in its locked mode. In its adapting mode, the CCA operated as described in section 2.5. In its locked mode, all rotation of the CCA foot mount relative to the socket mount

was disabled, yet it still produced the same noises as it would in the adapting mode. Six different terrain conditions were tested: unblinded flush, unblinded inversion, unblinded eversion, and blinded flush, blinded inversion, and blinded eversion.

Due to the large amount of test conditions, testing occurred over two separate days. One of the days was dedicated to participants being tested with their as prescribed prosthesis, while the other day was dedicated to participants being tested with the CCA device in both the adapting and locked modes. The order in which these two days of testing occurred was randomized. In addition, when the CCA device was being tested, the order in which the modes were tested was randomized.

The test procedure for the standing and gait balance trials for all three prosthesis conditions was the same. Participants were equipped with a black spandex outfit, motion tracking markers, and either the CCA or as prescribed prosthesis (see ***Figure 20***). If the CCA was used, a research prosthetist from the VA Puget Sound Health Care System was responsible for aligning the foot prior to any trials. Anthropometric measures such as height, mass, limb length, joint width, and hallway walking speed were recorded for later use in data processing.

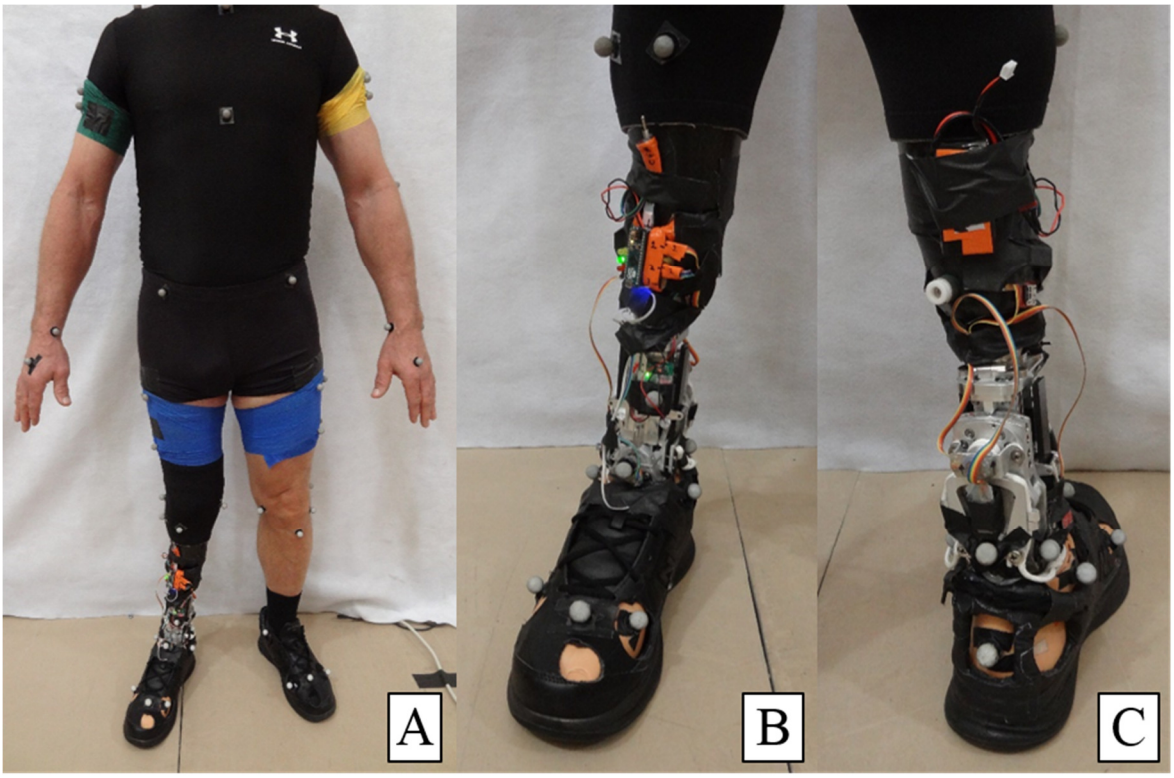

Figure 20: (A) Fully instrumented participant fitted with CCA device, motion capture markers, and walking shoes (B) Anterior view of CCA (C) Posterior view of CCA.

In order to acquaint participants with the types of terrain in the trial, unblinded trials were always conducted prior to blinded trials. In the unblinded trials, three conditions (flush, inverted, everted) were presented to the participants in a block randomized order, with four repeated trials per condition. For each condition, participants were instructed to walk at a self-selected walking speed across the walkway, and strike the disturbance device with their prosthetic foot. Once each terrain condition was complete, a standing balance trial was conducted to evaluate standing balance. In this trial, participants were instructed to place their feet as close together as possible and flat as flat as possible on the plate, to cross their arms, to close their eyes, and to remain as still as possible for 40 seconds.

Once all unblinded trials were completed, a series of blinded trials were conducted. During blinded trials, the disturbance device was either inverted or everted, and the position was presented to participants in a random order, with a total of four trials per position. For all blinded trials an opaque latex membrane was placed over the disturbance device to conceal its position to

participants. Between trials, participants stayed in a separate room behind a closed door to prevent them from seeing or hearing the changing process of the disturbance device and its future position. The instructions given to participants were the same as those in the unblinded trials.

Trials were rejected if participants' feet fell outside the force plates immediately before and after the disturbance device, or did not make full contact with the disturbance device's force plate. Trials were also rejected if participants caught their heel or toe on the walkway while interacting with the disturbance device. In order to maintain a minimum number of repeated trials amongst all the conditions, additional trials were collected to compensate for rejected trials if time permitted. In the case of unblinded trials, additional trials were simply added to the end of a condition. In the case of blinded trials, a series of randomly presented terrain conditions were added until all condition deficits were remedied.

2.8d Data Processing:

Prior to being used as inputs for the whole body model, kinetic and kinematic data from the trials were filtered. Kinetic data from the force plates was first filtered with physical low-pass filters, with the cutoff frequency of the disturbance device force plate at 100 Hz, and that of the flat plates at 1000 Hz. To eliminate the potential for aliasing noise, and to also eliminate the plates' resonance [12], a digital, 25 Hz low-pass, bi-directional, 4^{th} order, Butterworth filter was applied to all force signals. Existing literature regarding the frequency content of standard gait forces supports that this filtering process did not cut-off critical signal frequencies critical for gait analysis [25]. Kinematic data was also filtered with the same digital filter, except with a cutoff frequency of 6 Hz. Again, existing literature supported that this cutoff frequency retains critical kinematic frequency content for standard gait [19].

2.8e Whole Body Modeling:

The filtered data was used as inputs in to a whole body model that was developed in Visual 3D. The model was based on the Plug-In Gait model (Vicon Motion Systems, Oxford, UK), and was slightly modified to improve tracking of coronal rotation of the feet, as well as to accommodate tracking of the CAA. 66 makers were placed on the body, which were used to track 17 segments. Head and left/right hands were modeled as ellipsoids, with all other segments

(abdomen, pelvis, upper arms, forearms, thighs, shank, feet, residual limb/socket, CCA, foot mount) modeled as truncated cones. Besides modeling the CCA and residual limb, the only other major departure from the Plug-In Gait model were the markers used to track the feet. The in-tact foot was tracked by makers on the head of the 1st, 2nd, and 5th metatarsals, as well as on the insertion point of the Achille's tendon on the calcaneus.

The CCA, residual limb, and socket were modeled as accurately as possible (see ***Figure 21***). The residual limb and socket were modeled as a single rigid segment whose mass was the sum of the residual limb mass (proportional to its length relative to the contralateral shank segment), the socket mass, and the mass of the electronics that were mounted to the socket. The rigid pylon assembly, spring base, and ratchet mechanism were modeled as a separate segment that was rigidly attached to the socket / residual limb segment, and had the mass of all the CCA mechanical components except the foot mount and foot spool. The foot mount and spool were modeled as a separate segment, and were tracked by three markers. The prosthetic foot and shoe were modeled as a separate segment so their elasticity did not affect the tracking of the foot mount. The prosthetic foot was tracked with markers located in positions as equivalent as possible to the in-tact foot.

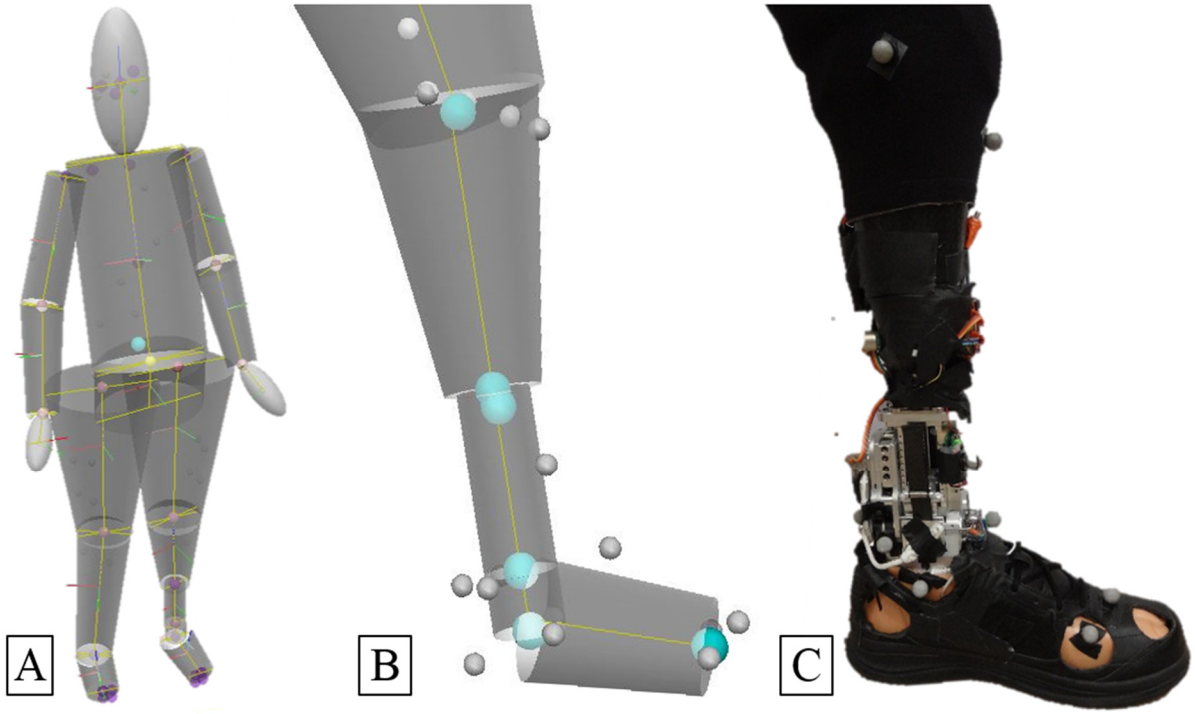

Figure 21: (A) Anterior isometric view of visual 3D whole body model with 17 segments. (B) Medial view of visual 3D model of CCA device, from the top down showing thigh, residual limb and socket, rigid pylon assembly, foot mount, and foot segments. (C) Medial photo of CCA device fitted to a participant shown for reference.

2.8f Statistics:

A three-way, fixed-effects, ANOVA test was used to evaluate the terrain and device effects on participants' performance metrics. ANOVA factors were the prosthesis, terrain, and participants, and were all treated as fixed effects (see section 4.3 for statistical limitations). To ensure the ANOVA test was appropriate for each metric, normal probability plots of the residuals were visually inspected for outliers and departures from normality, and residual vs fitted value plots were inspected for a uniform distribution. Tukey's honestly significant difference test was used to determine the significance of pairwise differences if either of the main effects of the ANOVA test exhibited significance at an alpha level of 0.05.

Chapter III: Results

Three participants successfully completed the procedure (mass: 86.2±3.6 kg, height: 1.80±0.03 m, age: 48.7±17.0 years, 3 male) with no falls or adverse events. All amputations were the result of trauma, and had occurred at least five years prior to the collection date. Each participant completed at least three trials for the unblinded flush, blinded inversion, and blinded eversion conditions that could be used for processing. The statistical implications of the small sample size collected in this study is discussed in section 4.3. In the following results section and discussion, the flush unblinded trials will be referred to as flush, and the blinded inversion and blinded eversion conditions will be referred to as inversion and eversion, respectively. All figures in the results section are averaged data from all repeated trials from all participants Equivalent figures showing individual participants' mean data are presented in Appendix A.

3.1 Coronal Angular Momentum:

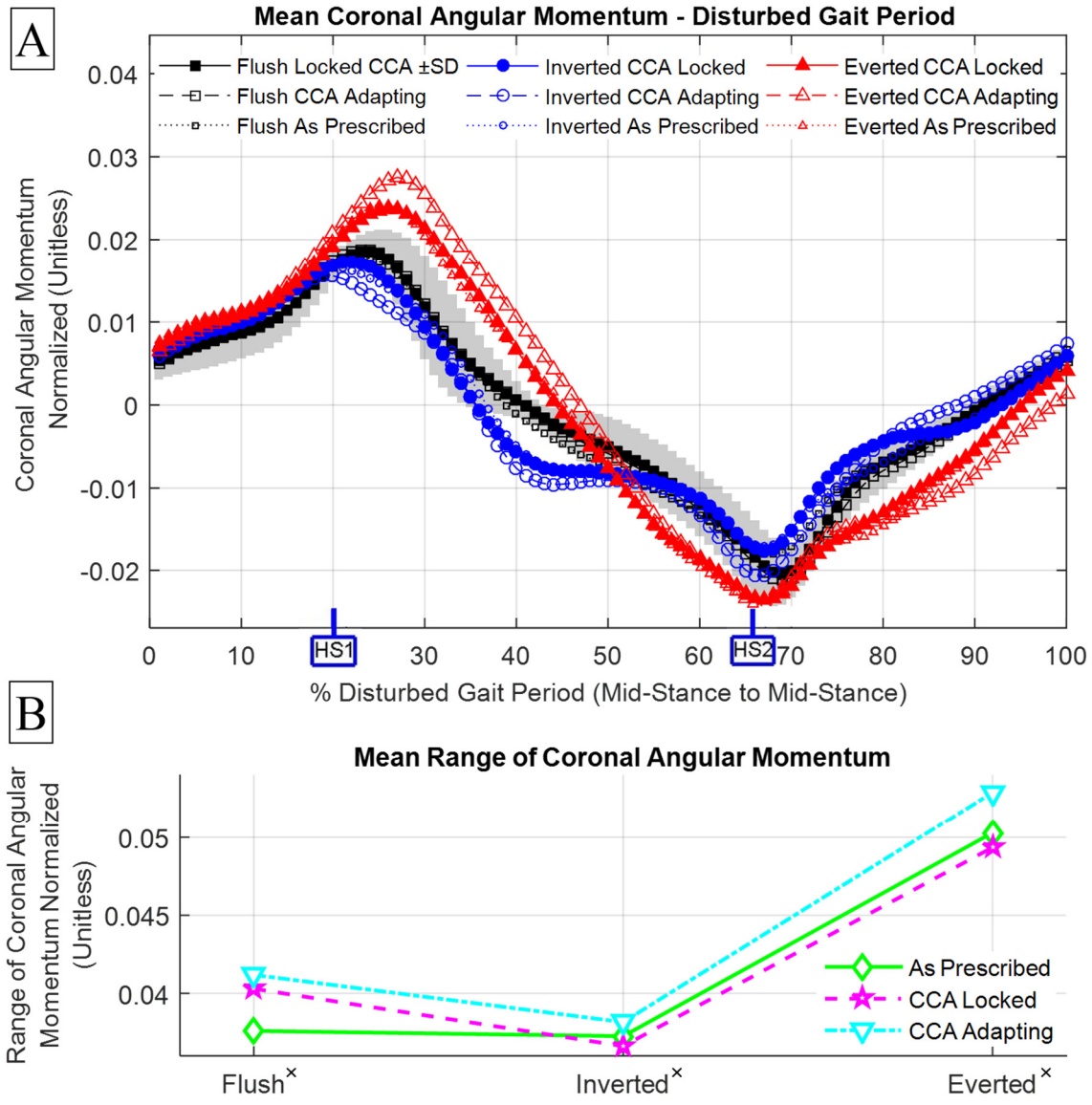

Figure 22: (A) Coronal angular momentum time series for all terrain and prosthesis combinations during the disturbed gait period. HS1 and HS2 signify heel strike of disturbed and recovery step, respectively. (B) Mean range of coronal angular momentum for all terrain and prosthesis combinations. × denotes no significant pairwise differences between prosthesis conditions for a given terrain condition.

The coronal angular momentum curves for each of the prosthesis conditions seem to be grouped together within a given terrain condition (***Figure 22A***). This is also seen in ***Figure 22B***, as the mean RCAMs for each prosthetic condition are grouped together in each of the given terrain conditions. While the prosthesis ($p=0.041$) and terrain ($p<0.001$) conditions both had significant main effects on the RCAM (see ***Table 4***), it appears the terrain had more of an effect on RCAM (***Figure 22B***). It also appears the CCA in adapting mode consistently had higher RCAMs than the other two prosthesis conditions for all terrain conditions; however, no significant pairwise differences between prosthesis conditions were observed (see ***Table 4***).

3.2 Standing Balance Lateral Sway:

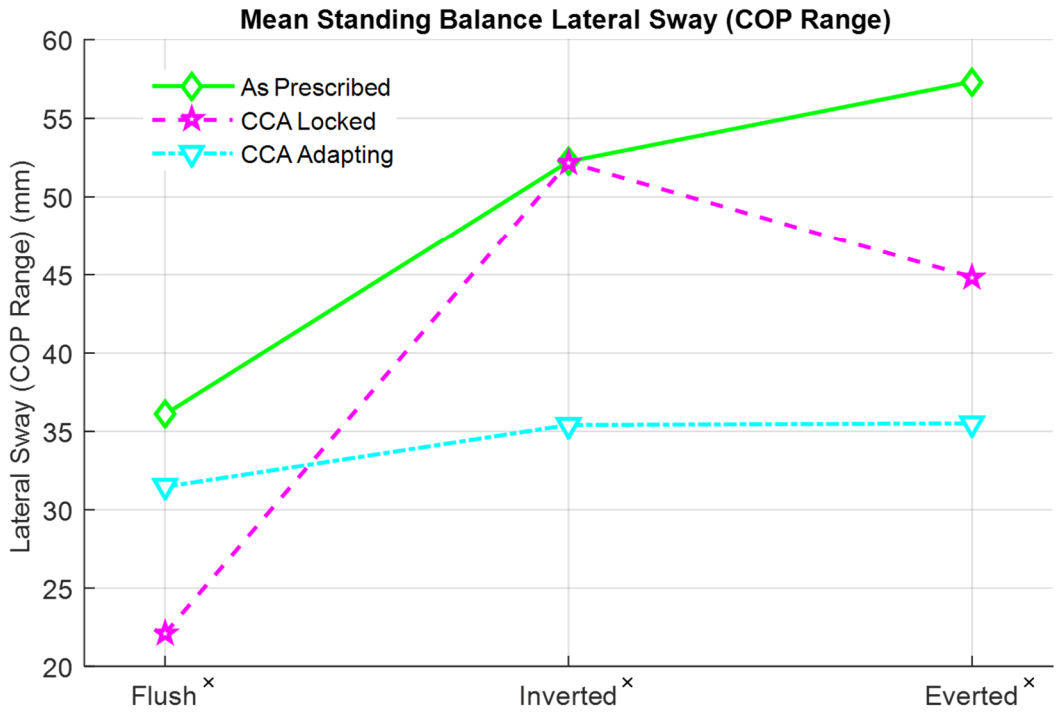

Figure 23: Mean standing balance lateral sway shown for all terrain and prosthesis combinations. × denotes no significant pairwise differences between prosthesis conditions for a given terrain condition. Center of pressure abbreviated to COP.

There are no significant pairwise differences between any of the prosthesis conditions for a given terrain condition (see ***Figure 23*** and ***Table 4***). There are, however, significant prosthesis (p=0.007) and terrain (p=0.001) main effects on the standing balance lateral sway (see ***Table 4***). In ***Figure 23*** it appears the everted terrain produced the largest lateral sway, while the flush terrain produced the smallest. Also, averaged across all the terrain conditions, it appears the as prescribed prosthesis condition produced the largest lateral sway, while the CCA in adapting mode produced the smallest.

3.3 Foot Coronal Angle With Respect to Pylon:

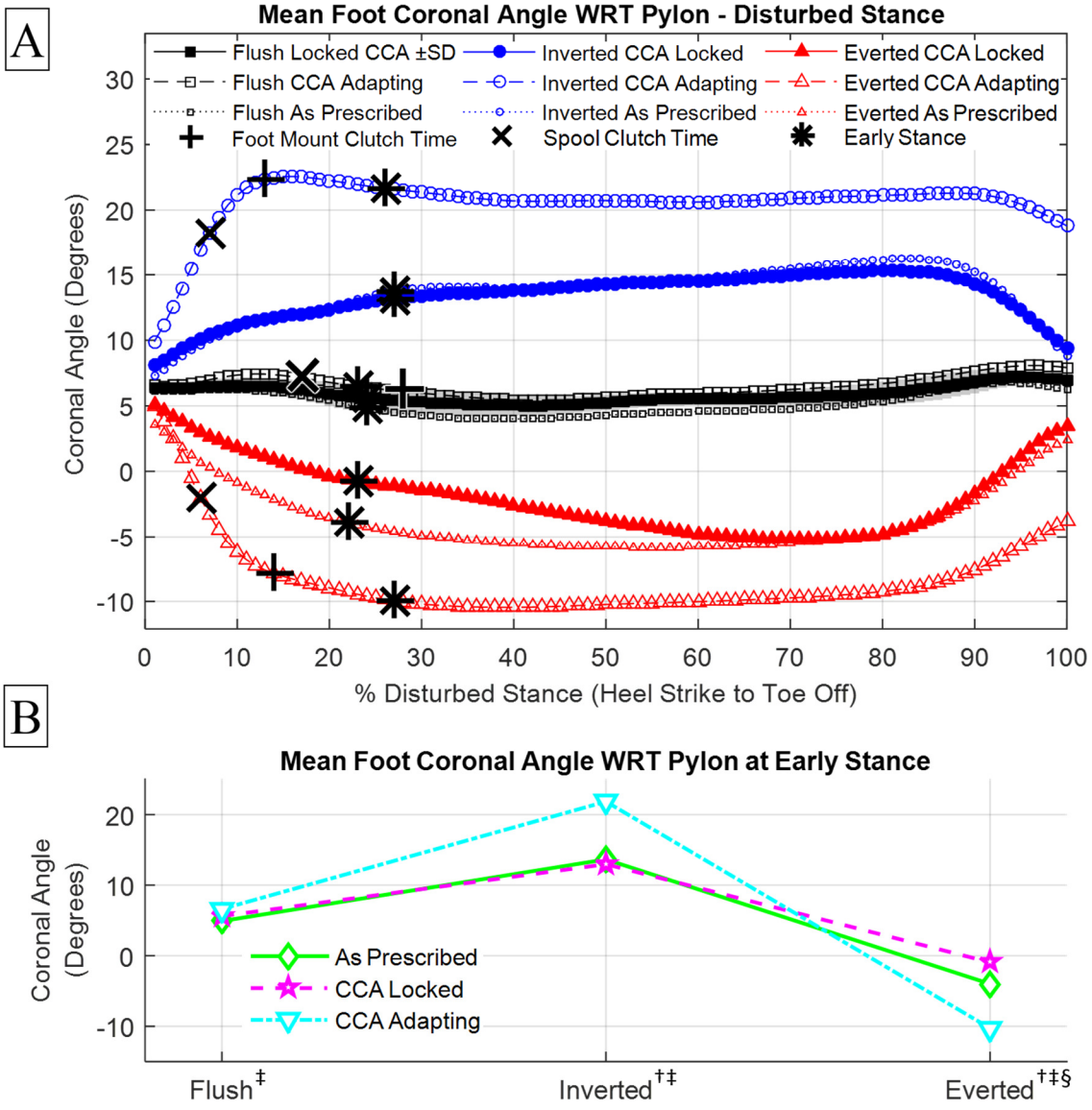

Figure 24: (A) Times series of the mean foot coronal angle with respect to the pylon (WRT) for all terrain and prosthesis combinations during the disturbed stance. Spool clutch time, foot mount clutch time, and early stance are shown for reference. (B) Mean foot coronal angle WRT the pylon at early stance for all terrain and prosthesis combinations. † denotes a significant pairwise difference between CCA adapting and locked prosthesis, ‡ between CCA adapting and as prescribed prosthesis, and § between CCA locked and as prescribed prosthesis. Positive angles represent inversion of the foot, negative angles represent eversion of the foot.

The prosthetic foot has more coronal angle movement with respect to the pylon when compared to the other prosthesis conditions on inverted and everted terrain ($p<0.001$) (see ***Figure 24*** and ***Table 4***). The differences between the prosthesis conditions are less pronounced on the flush terrain. There is no significant main effect of the prosthesis condition, but there is a significant terrain main effect ($p<0.001$), and a significant prosthesis terrain interaction effect ($p<0.001$). This interaction effect can clearly be seen in ***Figure 24B***, as the CCA angle at early stance is significantly ($p<0.001$) greater than other prosthetic conditions in inversion, but is significantly ($p<0.001$) less than other prosthetic conditions in eversion (***Table 4***). Finally, it can be seen that there is considerable of movement in the foot after the foot after the CCA spool has clutched, and after the CCA foot mount has clutched.

3.4 Coronal Moment About CCA Pivot:

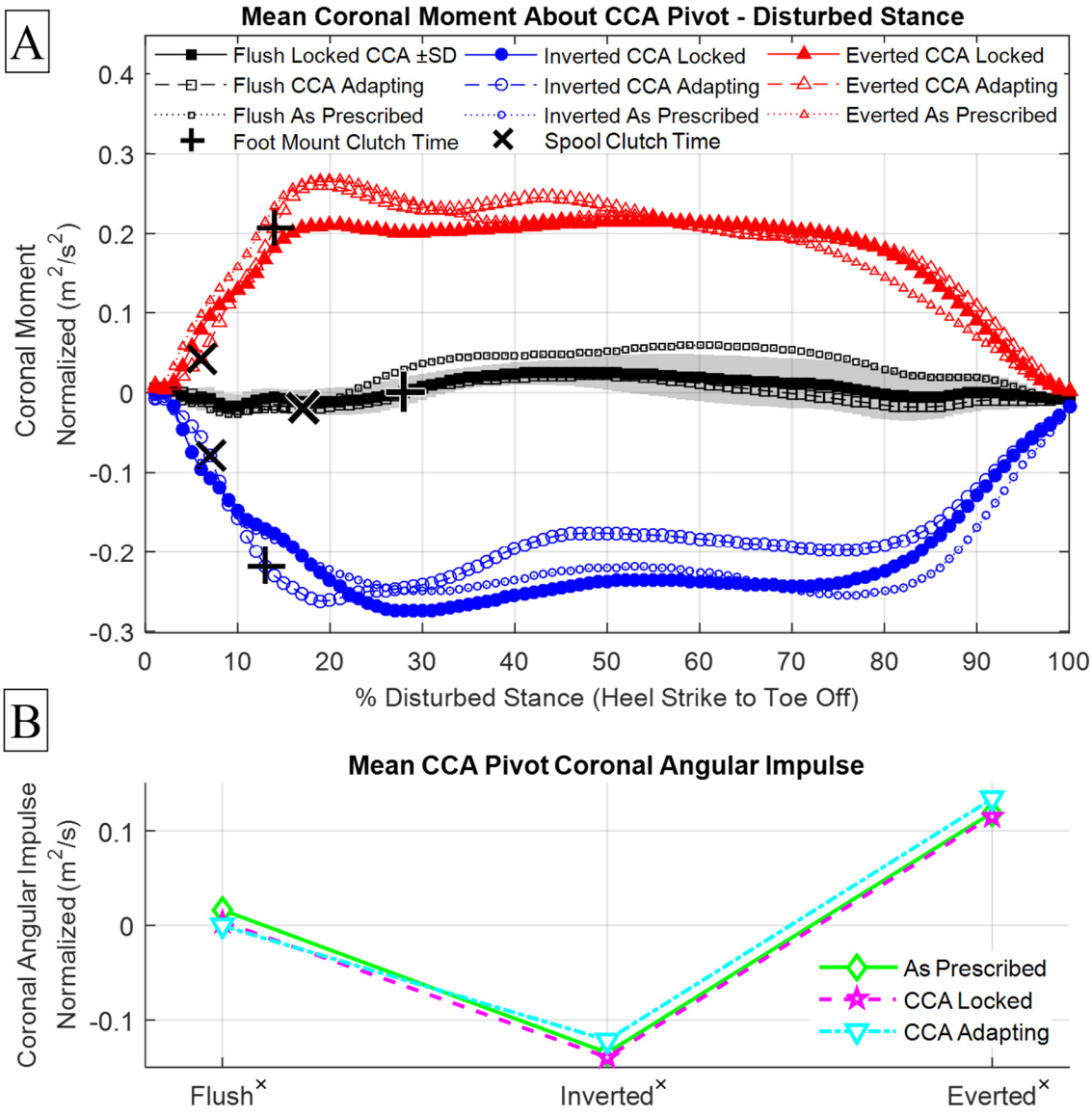

Figure 25: (A) Time series for mean coronal moment about CCA pivot (or equivalent thereof) over the disturbed stance for all prosthesis and terrain combinations. Spool clutch time and foot mount clutch time are shown for reference. (B) Mean CCA pivot coronal angular impulse for all terrain and prosthesis combinations. × denotes no significant pairwise differences between prosthesis conditions for a given terrain condition.

The mean coronal moment curves for each of the prosthesis conditions seem to be grouped together within a given terrain condition (see ***Figure 25A***). This is mirrored in ***Figure 25B***, where the mean CCA pivot CAIs of each prosthesis condition are tightly grouped together for each of the terrain conditions. The terrain conditions had a significant main effect on the CCA pivot CAI ($p<0.001$) (***Table 4***) and this is shown in ***Figure 25B***. For inversion terrain there appears to be a more negative coronal moment, and for eversion terrain there appears to be a more positive coronal moment about the CCA pivot.

3.5 Coronal Hip Moment:

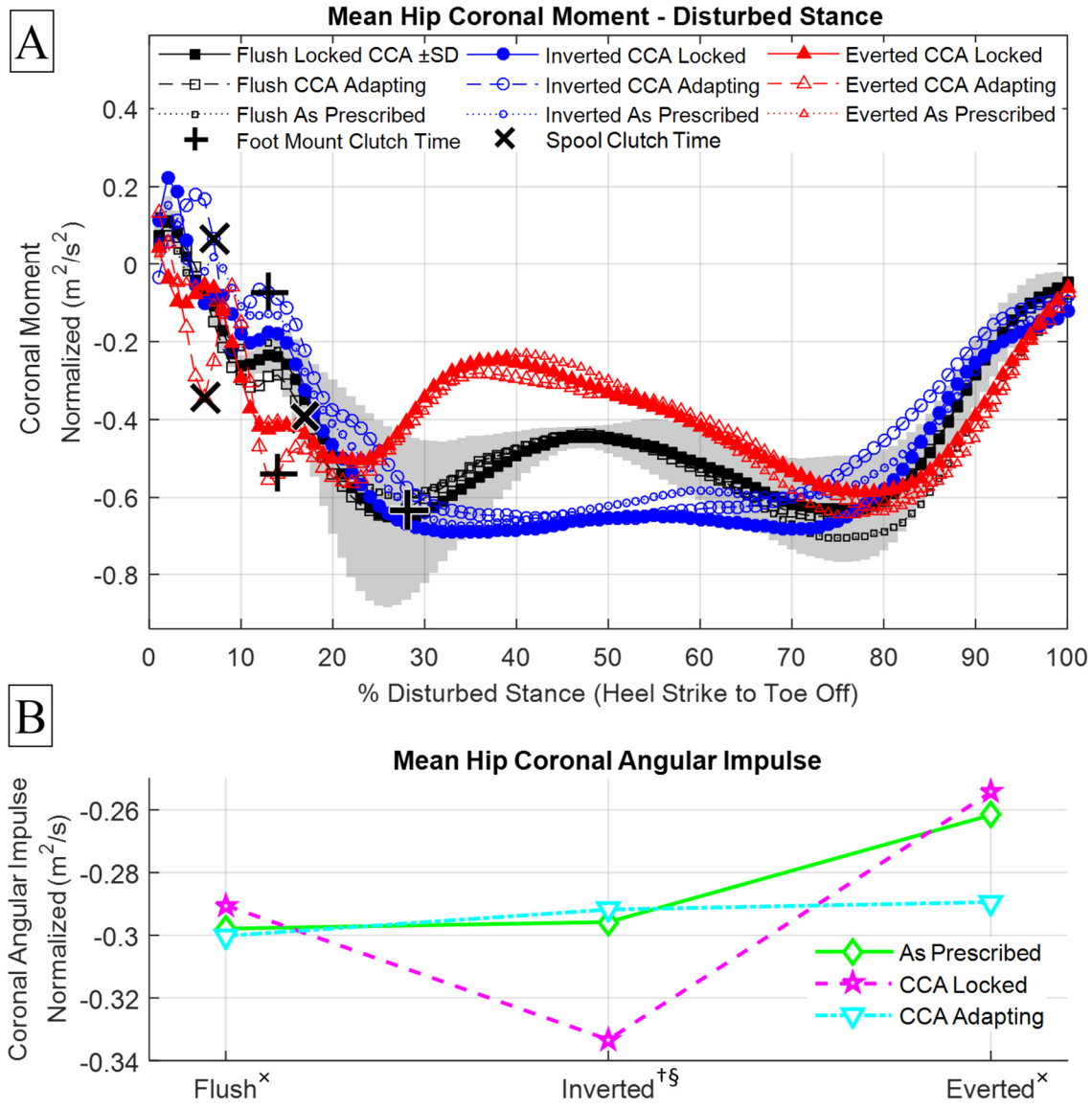

Figure 26: (A) Time series for mean coronal hip moment over the disturbed stance for all prosthesis and terrain combinations. Spool clutch time and foot mount clutch time are shown for reference. (B) Mean coronal hip angular impulse for all terrain and prosthesis combinations. × denotes no significant pairwise differences between prosthesis conditions for a given terrain condition. † denotes a significant pairwise difference between CCA adapting and locked prosthesis, and § between CCA locked and as prescribed prosthesis.

The mean coronal moments about the hip for each of the prosthesis conditions seem to be grouped together within a given terrain condition during mid-stance, as seen in ***Figure 26A***. The terrain condition had a statistically significant main effect ($p<0.001$) (***Table 4***), while the prosthesis condition did not. However, the device-terrain interaction was statistically significant at $p<0.001$, and apparent differences in the moment curves between prosthesis conditions within a given terrain condition can be seen in the first 20% of stance, particularly before the foot mount clutch time. In this first 20%, the hip moments corresponding to the adapting mode of the CCA on inversion and eversion have large oscillations that are not seen in other conditions. The differences between the hip CAI when the CCA was in adapting vs locked mode can be seen in ***Figure 26B***, where the hip CAI was significantly less for the locked mode ($p<0.001$) in inversion, and appears to greater in eversion. Also note the hip CAI for the CCA in adapting mode appears to stay constant throughout all three conditions (***Figure 26B***) when compared to the other two prosthesis conditions.

3.6 Recovery Step Lateral Foot Placement:

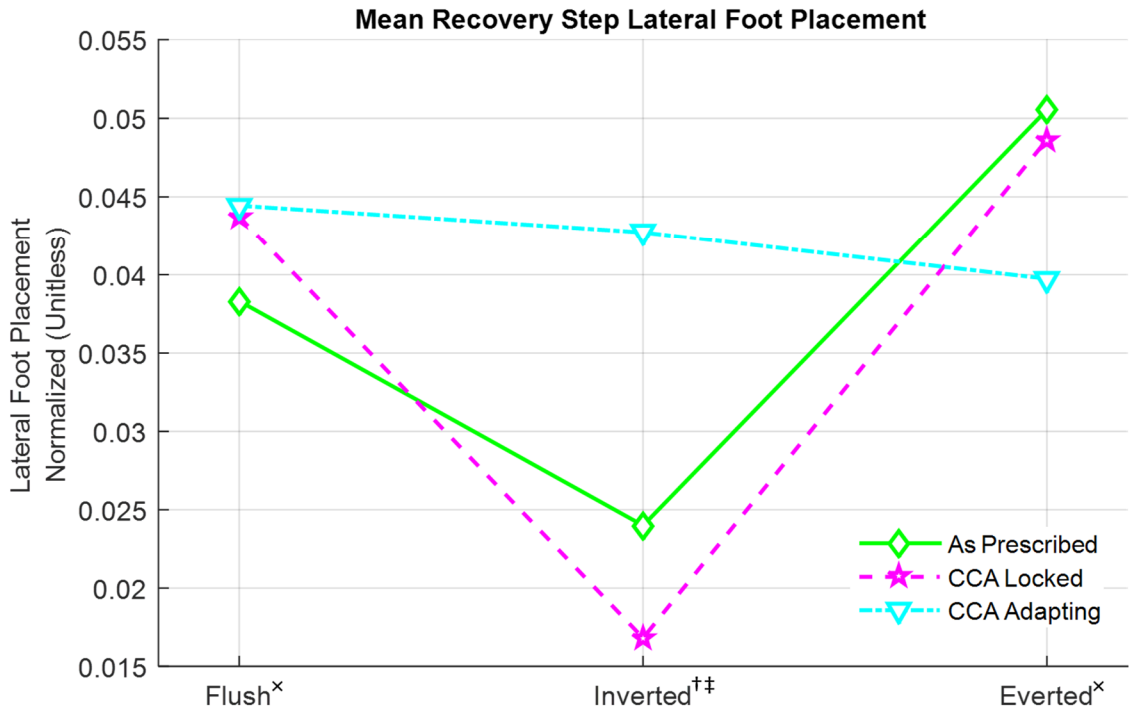

Figure 27: Mean recovery step lateral foot placement for all terrain and prosthesis combinations. × denotes no significant pairwise differences between prosthesis conditions for a given terrain condition. † denotes a significant pairwise difference between CCA adapting and locked prosthesis, and ‡ between CCA adapting and as prescribed prosthesis.

The mean recovery LFP was significantly affected by the device condition ($p=0.037$), the terrain condition ($p<0.001$), and the interaction between the two ($p<0.001$) (***Table 4***). The prosthesis condition had the largest effect in the inverted terrain condition, where the CCA in the locked condition exhibited a significantly larger LFP relative to the other two prosthesis conditions ($p<0.001$) (***Table 4***). An opposite and lesser effect appears to occur in eversion, where the CCA in the adapting position appears to exhibit a smaller LFP compared to the other prosthesis conditions (***Figure 27***). It should be noted that the mean LFP appears to remain relatively constant for the CCA in the adapting mode across all terrain conditions, when compared to the other two prosthesis conditions.

3.7 Foot Mount Coronal Angle:

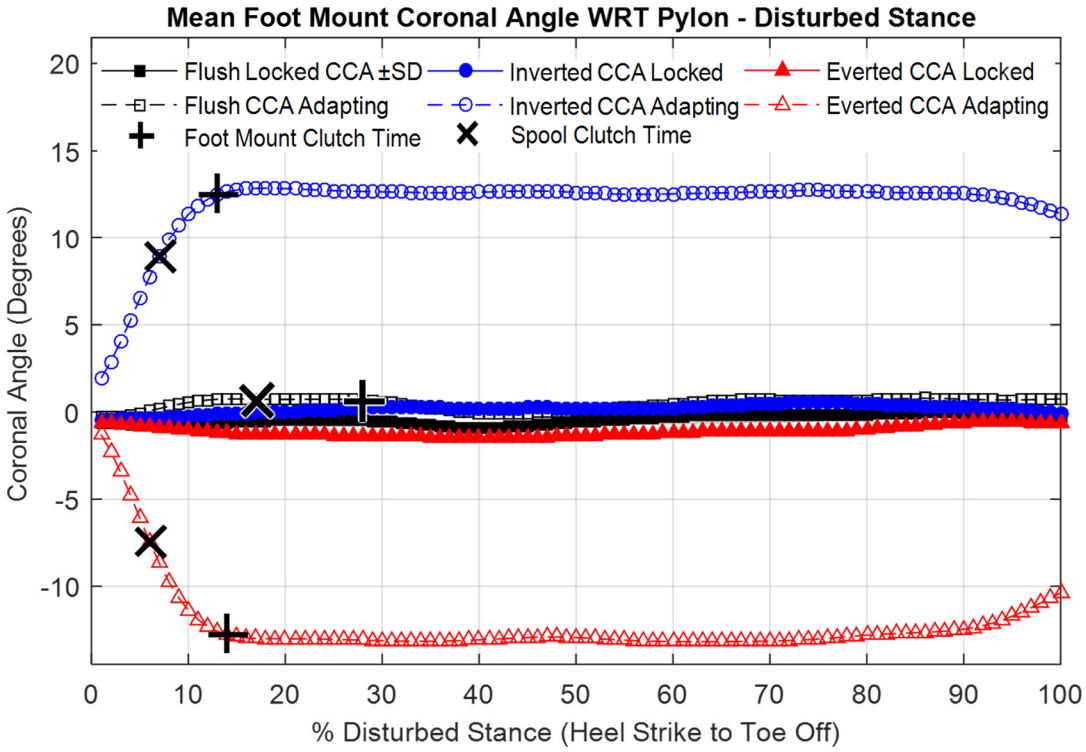

Figure 28: Time series of mean foot mount coronal angle with respect to the CCA pylon over the disturbed stance. Spool clutch time, and foot mount clutch time are shown for reference.

There exists a large amount of adaption in the coronal angle of the CCA foot when the CCA is in its adapting mode on inverted and everted terrain (see ***Figure 28***). For inverted and everted terrain, after the foot mount clutch time, the coronal angle of the CCA foot mount appears to be relatively constant until late stance. Also note the relatively small amount of coronal rotation of the CCA mount shown for the CCA in the locked mode for all terrain conditions. A relatively small amount of coronal rotation is also observed when the CCA is in adapting mode on the flush terrain condition. For all CCA adapting conditions, the spool clutch time occurs before the foot mount clutch time.

3.8 Descriptive Statistics of Performance Metrics:

Table 3: Mean and standard deviations (STD) for all performance metrics on all reported terrain and prosthesis conditions. Abbreviations: Range of coronal angular momentum (RCAM), standing balance (SB), coronal angular impulse (CAI), and lateral foot placement (LFP).

Metric	Flush (Mean±STD)			Inversion (Mean±STD)			Eversion (Mean±STD)		
	As Prescribed	**CCA Locked**	**CCA Adapting**	**As Prescribed**	**CCA Locked**	**CCA Adapting**	**As Prescribed**	**CCA Locked**	**CCA Adapting**
RCAM (unitless)	0.038±0.006	0.040±0.006	0.041±0.009	0.037±0.006	0.037±0.006	0.038±0.005	0.050±0.007	0.049±0.012	0.053±0.008
SB Lateral Sway (mm)	36.1±9.2	22.1±9.9	31.5±8.0	52.5±8.2	52.2±10.6	35.4±3.1	57.3±18.3	44.9±17.8	35.5±7.0
Foot Early Stance Coronal Ang. (deg)	4.9±0.3	5.6±0.3	6.6±2.3	13.7±1.8	13.0±1.4	21.8±2.3	-4.0±1.0	-0.9±2.0	-10.3±1.3
CCA Pivot CAI (m^2/s)	0.016±0.032	0.004±0.010	0.000±0.009	-0.135±0.042	-0.139±0.026	-0.121±0.019	0.119±0.054	0.116±0.017	0.134±0.014
Hip CAI (m^2/s)	-0.298±0.068	-0.290±0.033	-0.300±0.025	-0.296±0.073	-0.333±0.053	-0.292±0.054	-0.262±0.081	-0.254±0.059	-0.289±0.074
Recovery Step LFP (unitless)	0.038±0.012	0.044±0.010	0.044±0.015	0.024±0.014	0.017±0.012	0.043±0.015	0.051±0.011	0.049±0.016	0.040±0.016
Foot Mount Clutch Angle (deg)	N/A	-0.5±0.0	0.5±2.7	N/A	0.1±0.5	12.7±3.8	N/A	-1.2±0.5	-12.9±2.2

Table 3 summarizes the descriptive statistics for all performance metrics analyzed in this study. The means and standard deviations are for all repeated measures for all participants within a given terrain and prosthesis combination. Foot mount clutch angle is provided for reference, and it should be noted that it appears to have a smaller magnitudes than the early stance coronal angle of the foot for all conditions and prosthesis combinations. It should also be noted that the hip CAI appears to have larger magnitudes than the CCA pivot CAI for all terrain and prosthesis combinations.

3.9 Statistical Test Results of Performance Metrics:

Table 4: Results for 3-Way ANOVA tests of all performance metrics. P-values for the main effects of the prosthesis and terrain conditions, as well as the interaction between the two are reported. P-values for pairwise comparisons between prosthetic conditions within a given terrain condition are also reported. Bolded p-values represent significance an alpha level of 0.05. Abbreviations: Range of coronal angular momentum (RCAM), standing balance (SB), coronal angular impulse (CAI), and lateral foot placement (LFP).

Metric	Prosthesis Main Effect P-Value	Terrain Main Effect P-Value	Prosthesis Terrain Interaction P-Value	Pairwise Comparison P-Values								
				Flush			Inversion			Eversion		
				A to L	A to AP	L to AP	A to L	A to AP	L to AP	A to L	A to AP	L to AP
RCAM	**0.041**	**<0.001**	0.374	1.000	0.303	0.569	1.000	1.000	1.000	0.624	0.862	1.000
SB Lateral Sway	**0.007**	**0.001**	0.071	0.758	0.993	0.361	0.202	0.200	1.000	0.761	0.067	0.479
Foot Early Stance Coronal Ang.	0.333	**<0.001**	**<0.001**	0.456	**0.042**	0.942	**<0.001**	**<0.001**	0.139	**<0.001**	**<0.001**	**0.011**
CCA Pivot CAI	0.055	**<0.001**	**0.038**	1.000	0.469	0.727	0.395	0.741	1.000	0.356	0.667	1.000
Hip CAI	0.234	**<0.001**	**<0.001**	0.997	1.000	1.000	**0.007**	1.000	**0.023**	0.097	0.221	1.000
Recovery Step LFP	**0.037**	**<0.001**	**<0.001**	1.000	0.605	0.607	**<0.001**	**<0.001**	0.726	0.240	0.105	1.000

Table 4 shows the terrain condition had a significant main effect on all performance metrics. The prosthesis condition had a significant main effect on the RCAM, SB Lateral Sway, and the Recovery Step; however, neither the RCAM nor the SB Lateral Sway demonstrated any significant pairwise differences between prosthetic conditions within a given terrain condition. In the case of the foot early stance coronal angle, and the hip CAI, where there was no main effect of the prosthesis, but a significant prosthesis terrain interaction was present, pairwise differences were observed between certain prosthesis conditions within a terrain condition. In both inversion and eversion terrain conditions, the foot early stance coronal angle exhibited significant pairwise differences ($p<0.001$)

between the CCA in adapting and locked mode. In inversion, both the Hip CAI and Recovery Step LFP exhibited significant pairwise differences between the CCA in adapting and locked modes.

3.10 Temporal Measurements:

Table 5: Mean and standard deviation (STD) for temporal measurements used in study for visualization and normalization. Clutching parameters not shown for CCA in locked mode and for as prescribed prosthesis.

Metric	Flush (Mean±STD)			Inversion (Mean±STD)			Eversion (Mean±STD)		
	As Prescribed	CCA Locked	CCA Adapting	As Prescribed	CCA Locked	CCA Adapting	As Prescribed	CCA Locked	CCA Adapting
Foot Mount Clutch Time (ms)	N/A	N/A	182±146	N/A	N/A	86±44	N/A	N/A	105±45
Spool Clutch Time (ms)	N/A	N/A	115±146	N/A	N/A	50±6	N/A	N/A	47±4
Disturbed Stance Time (ms)	888±250	905±245	937±250	913±249	897±268	913±245	899±248	885±246	907±248
Disturbed Period Time (ms)	1120±41	1152±56	1168±82	1145±41	1194±51	1198±53	1159±37	1180±63	1226±67
Walking Speed (m/s)	1.257±0.039	1.218±0.046	1.191±0.059	1.229±0.050	1.157±0.040	1.148±0.041	1.187±0.060	1.157±0.051	1.109±0.069
Early Stance Time (ms)	159±17	163±31	157±43	182±28	185±33	181±49	152±37	157±42	205±75

Table 5 shows that for all terrain conditions, the spool clutch time occurred prior to the foot mount clutch time. The clutch times for the flush condition appear to be much larger than those of the inversion and eversion conditions. The disturbed stance time appears to have greater variation between conditions than the disturbed period time. Walking speed shows minor variations across terrain and prosthesis conditions. Early stance time, used to calculated the foot coronal angle at early stance, seems to be largest in the inversion condition, with the exception of the CCA in the adapting mode of eversion, which appears to have an abnormally late early stance time.

Chapter IV: Discussion

4.1 Interpretation:

4.1a Hypothesis 1 – Balance:

It was hypothesized that the coronally-clutching feature of the CCA would improve the gait and standing balance of amputees on coronally-uneven and unpredictable terrain.

The RCAM results (***Figure 22, Table 4***) suggest the CCA in adapting mode did not improve the gait balance of amputees when walking on coronally-uneven and unpredictable terrain. Specifically, the ranges of coronal angular momentum (***Figure 22, Table 4***) exhibited no significant prosthesis main effect, nor any significant pairwise differences between prosthesis conditions on uneven terrain. In addition, it appears the RCAM for the adapting condition is actually slightly larger, but not significantly so, than that of the other prosthesis conditions for any given terrain, hinting that the adapting mode of the CCA may have actually been destabilizing to participants. As previously reported [12], eversion appears to have elicited the largest RCAM, indicating it was the most destabilizing terrain condition. On flush terrain with the as prescribed prosthesis the observed participant RCAM in this study was 0.038±0.009. This was slightly higher than that observed in a previous amputee study, which reported a value of 0.03±0.01 [5] for the walking speed of 1.2 m/s. The small sample size of this study is a likely the explanation for the apparent discrepancy (see section 4.3).

The lack of significantly improved gait balance on coronally-uneven and unpredictable terrain with the CCA in adapting mode is likely due to the fact that the coronal angular impulse about the CCA pivot was not significantly different between the locked and adapting modes of the CCA (**Figure 25*, Table 4***). The goal of the CCA in the adapting mode was to reduce the magnitude of the coronal disturbance moment produced by coronally-uneven and unpredictable terrain about the CCA pivot, which would hypothetically improve gait stability (see section 2.2). However, because the coronal angular impulse about the CCA pivot did not significantly change between prosthesis conditions, it stands to reason that neither did the RCAM. See section 4.2b for further details regarding the moment about the CCA pivot.

The sudden training regime used for the CCA in the adapting mode may have also reduced the benefit of the CCA. It has been suggested that gradual training may improve performance outcomes of amputees using powered prostheses [26]. Had participants been gradually introduced to the capabilities of the device, by slowly increasing the ramp angle over many trials, the balance outcomes of participants using the CCA in its adapting mode may have improved (see section 4.3).

In the case of standing balance, it appears that on coronally-uneven terrain, the CCA in the adapting mode may have been associated with lower lateral sway than the other prosthesis conditions (***Figure 23***). The main effect of the prosthesis condition was statistically significant ($p=0.007$), suggesting the CCA may have improved the lateral sway of participants; however, there were no statistically significant pairwise differences between prosthesis conditions within a given terrain condition. The lateral sway observed in participants on uneven terrain with the CCA in adapting mode was around 35 mm, which is slightly higher than the 31 mm lateral sway that has been observed in elderly Parkinson's patients on flat ground [15]. However, in the as prescribed and CCA locked conditions, participants' lateral sway increased by 10-20 mm on coronally-uneven terrain, which is approximately the difference between the lateral sway of healthy young adults (18 mm) and that of an elderly Parkinson's patients (31 mm) on flat ground. This suggests that the observed difference in the lateral sway, while not statistically significant, was clinically relevant. The notion that an adapting coronal foot angle has the potential to improve the biomechanics of amputees on uneven terrain is further supported by previous studies conveying the benefit of an adapting sagittal foot angle [2, 27, 28].

The CCA may have improved standing balance, and not gait balance, because in the standing balance trials the CCA properties were more predictable to the participants. During gait trials, the CCA would quickly rotate and then lock into a position at early stance, as opposed to the standing balance trials, in which it was at a fixed and adapted angle throughout the entire trial. The static nature of the CCA device in the standing balance trials likely enabled participants to become more familiar with its properties, and use them to their benefit.

4.1b Hypothesis 2 - Recovery Mechanisms:

It was hypothesized that when stepping on coronally-uneven and unpredictable terrain, the ankle clutching feature of the CCA would allow the prosthetic foot to adapt to the terrain angle, thereby reducing the disturbance moment produced about the coronal pivot of the CCA. It was further hypothesized that the reduced disturbance moment about the CCA pivot would lessen the need for amputees to use the hip moment strategy of the disturbed limb, as well as reduce the need for the stepping strategy of the recovery limb.

The CCA device successfully adapted the coronal angle of the foot to the coronally-uneven and unpredictable terrain. This is most clearly seen in ***Figure 24*** and ***Table 3*** which demonstrate that for the early stance coronal foot angle on coronally-uneven and unpredictable terrain there existed significant pairwise differences between the CCA in the locked and adapting mode ($p<0.001$). With the CCA in adapting mode on inverted terrain, the coronal angle of the foot with respect to the pylon had an average early stance angle of 21.8°, which was 15.2° more inverted than on the flush terrain (6.6°). With the CCA in adapting mode on everted terrain, the average early stance angle was -10.3°, which was 16.9° more everted than on the flush terrain (6.6°). That the difference in the foot angle between the CCA in locked and adapting mode is approximately equal to that of the disturbance indicates the CCA successfully accomplished the goal of adapting the foot to the coronally-uneven and unpredictable terrain. The CCA foot mount itself, demonstrated slightly less coronal adaption (approximately 12° in both inversion and eversion (see ***Figure 28*** and ***Table 3***)) indicating the last few degrees of adaption were accomplished by deformation of the prosthetic foot keel and shell.

Deformation of the prosthetic foot keel and shell was also observed with the CCA in locked mode. With the CCA in locked mode on inverted terrain the coronal angle of the foot was 7.4° more inverted than that on the flush terrain, but the CCA foot mount itself was only 0.6° more inverted. In eversion, with the CCA locked, the foot coronal angle was 6.5° more everted than on flush terrain, but the CCA foot mount was only 1.7° more everted. The small amount of movement of the CCA foot mount in the locked mode can be attributed to stretching in the Spectra® cable and some backlash in the ratchet mechanism (see section 2.7).

Temporal information recorded from the CCA device during participant trials confirmed response times observed in bench tests were achieved. The mean spool clutch times observed in

bench tests ranged from 42-57 ms (see ***Table 1***, ***Table 2***), and in the participant trials ranged from 47-50 ms on uneven terrain (***Table 5***). This confirms that the ratchet mechanism performed as expected. The mean foot mount clutch times in the bench tests ranged from 77 ms at 500 N, to 356 ms at 1000 N (see ***Table 1***, ***Table 2***). In participant trials, mean foot mount clutch times on coronally-uneven and unpredictable terrain had means between 86-105 ms (see ***Table 5***). This indicates that stretching of the Spectra® cable, which accounted for the longer clutch times observed at the 1000 N loads during bench testing (see section 2.7), did not have as negative an impact on the response time during participant testing. This may be due to the faster loading rate applied during participant testing, as the 1000 N load was applied at 25% the typical loading rate of a heel strike, thus allowing for more creep.

It should also be noted that the clutch times for the CCA in adapting mode on flush terrain were notably longer than those on uneven terrain. This is because the range of angular motion was relatively small on flush terrain, thus, even after the ratchet mechanism had switched to the locked mode, the spool and foot mount angles did not immediately exceed the amount of motion allowed by the backlash of the system. When the range of motion in the spool and foot mount finally exceeded what was allowed by the backlash of the system, a steady state was achieved. Because reported clutch times were a calculation of how long it took a particular angle to reach within 10% of the steady state angle, the reported clutch times were longer.

The coronally-clutching feature of the CCA device did not have a significant main effect on the coronal angular impulse about the CCA pivot. There were also no pairwise differences in the CAI about the CCA pivot between prosthesis conditions within a given terrain condition (***Figure 25*** and ***Table 4***). There was a significant terrain affect ($p<0.001$), and the CAI of the CCA pivot appears to have a larger eversion moment in the inversion condition, and a larger inversion moment in the eversion condition. This agrees with previous findings exploring coronal ankle moments on coronally-uneven and unpredictable terrain [12].

The lack of pairwise differences in the CAI of the CCA pivot between prosthesis conditions suggests the coronally-clutching feature of the CCA did not achieve its intended purpose. It was supposed to improve amputee balance by reducing the magnitude of the CAI about the CCA pivot that was produced by stepping on coronally-uneven and unpredictable terrain. It can be seen in ***Figure 24*** and ***Figure 25*** that when the CCA was in adapting mode, the

foot angle significantly adapted to the terrain compared to the locked condition, but the moment about the CCA pivot remained nearly identical between the locked and adapting modes. This can be explained by the location of the pivot axis used in the CCA device, which was approximately 120mm superior to the base of support (bottom of the walking shoes) when a low-profile foot and the M577 walking shoes were used. This design parameter was minimized, but not sufficiently so.

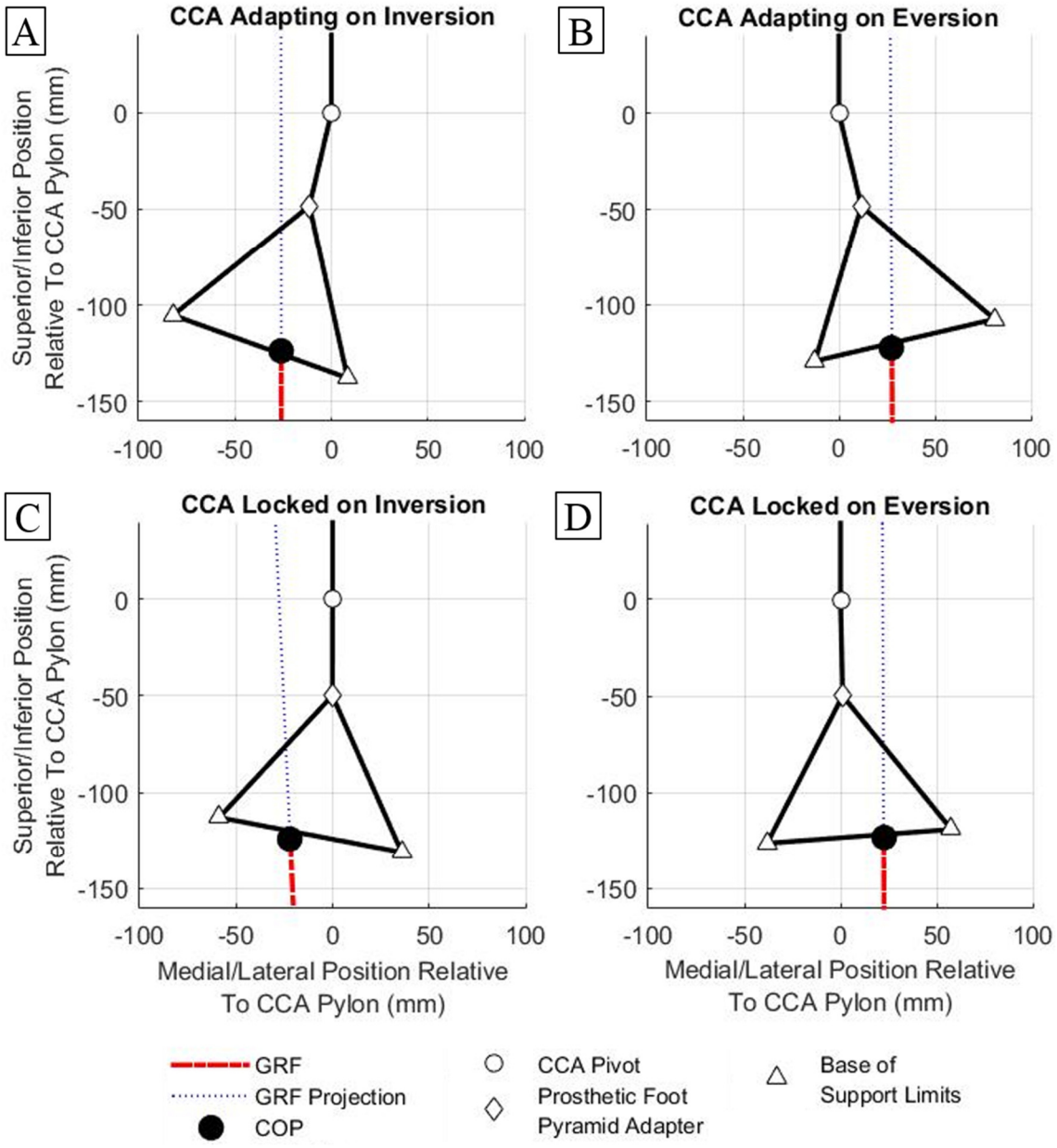

Figure 29: Posterior view of the CCA device, with the center of pressure (COP) and ground reaction force (GRF) during steps on inverted (A,C) and everted (B,D) terrain with the device in adapting (A,B) and locked (C,D) modes. All forces and locations are oriented relative to the rigid pylon of the CCA device. Images represent mean data from all participants at early stance on coronally-uneven and unpredictable terrain. Data normalized to right side amputees, lateral and superior values are positive. Base of support limits are equivalent to the medial and lateral limits of the shoe.

Figure 29 illustrates why the large distance between the CCA pivot and the base of support undermined the effectiveness of the clutching feature of the CCA in reducing the moment about the CCA pivot. ***Figure 29*** shows a graphical representation of the critical components of the CCA, as well as the ground reaction forces and centers of pressure acting on CCA. In comparing ***Figure 29A*** and ***Figure 29C***, it appears that when the CCA was adapting (***Figure 29A***) the COP was more lateral on the base support compared to when the CCA was locked (***Figure 29C***). However, because of the large distance between the base of support and the CCA pivot, when the CCA adapted the angle of the foot to the inverted terrain (***Figure 29A***), the base of support appears to have translated medially relative to the CCA pylon. Thus, while the mode of the CCA may have affected the lateral position of the COP relative to the base of support, it does not seem to have affected the lateral position of the COP relative to the CCA pivot. Therefore, regardless of the CCA mode, the moment arm of the ground reaction force, the corresponding disturbance moment, and the calculated joint reaction moment used to calculate the CAI about the CCA pivot remained relatively constant. An equivalent phenomenon was also observed on everted terrain, and can be seen in in ***Figure 29B*** and ***Figure 29D***. The negative effect of the large distance between the CCA pivot and the base of support may partially explain the relatively short distance between the subtalar joint and the bottom of the natural foot [7].

The hip moments observed on flush terrain ***Figure 26*** mostly matched those previously reported [29]. The late stance and mid stance magnitudes of the hip moments observed in this study are within a standard deviation of those reported by Winter. However, the early stance peak observed in this study has a magnitude which is approximately 40% less than that observed by Winter in non-amputees. It is possible that this discrepancy is due to the population difference; however, frontal plane hip kinematics for transtibial amputees were not available for comparison.

The hip CAI was used to understand if the prosthesis condition on coronally-uneven terrain affected participant reliance on the hip strategy of the disturbed limb. By itself, the level nature of the hip CAI across all terrain types when the CCA was in adapting mode (***Figure 26B***) suggests CCA adaption reduced participant's reliance on the hip strategy during gait on coronally-uneven ground. However, inspection of the coronal hip moment graphs (***Figure 26A***) reveal the level nature of the hip CAI when the CCA was adapting conceals the large oscillations

observed in the coronal hip moment at early stance on coronally-uneven and unpredictable terrain. These oscillations appear only when the CCA was adapting, and continue until shortly after the foot mount clutch time, at which point, they begin to appear more similar to the other prosthesis conditions. The hip oscillations may have been an attempt by the participants to compensate for the relative translation between the CCA pylon and their base of support (see ***Figure 29***), which one amputee reported as a "sideways sliding" sensation. This would align with previous research which has found the hip moment strategy to be used when use of the ankle moment and stepping strategies are insufficient [6, 30]. The hip oscillations also corroborate anecdotal observations of occasional participant arm spreading and verbalizations when the CCA was in the adapting mode, suggesting it may have caught participants off guard.

The lateral foot placement (LFP) of the recovery step was used to evaluate participant reliance on the stepping strategy of the recovery limb. In the flush condition, the recovery step LFPs for all prosthesis conditions were approximately equal to that previously shown for amputees [31], and exhibited no significant differences between the prosthesis conditions. Additionally, the recovery step LFP of the CCA in the adapting mode appears to have been relatively constant across all three terrain conditions (***Figure 27***). This appears to delineate the CCA in the adapting mode from the other two prosthesis conditions, which in inversion were both significantly smaller ($p<0.001$), and in eversion appear to be slightly larger. This implies the adapting mode of the CCA device reduced the need for the stepping strategy to be used on the recovery step after inversions, and possibly eversions. Because the stepping strategy is the primary strategy [30] used when recovering from gait disturbances, it may be possible that the adapting CCA allowed, or mandated, participants to recover from the coronally-uneven and unpredictable terrain within the disturbed stance.

4.2 Implications:

The results of this study are most relevant to the field of prosthetic engineering. It was observed that standing balance on coronally-uneven terrain may have slightly benefited from the angular adaption of the CCA. Thus, interventions which can only adapt to coronally-uneven and unpredictable terrain during quiet stance, and not during gait, may still be able to provide benefit to amputees and should therefore be considered for development. Regarding balance during gait on coronally-uneven and unpredictable terrain, the coronal adaption of the CCA did not provide

significant benefit, likely due to the large distance between CCA pivot relative to the prosthetic foot. If this distance can be significantly reduced, it is possible that a prosthetic device which adapts the coronal foot angle may improve amputee balance while walking over coronally-uneven and unpredictable terrain. Finally, it should be noted that when the CCA was locked, the prosthetic foot still demonstrated approximately ±7° of coronal rotation. This range covers the maximum allowed grade of a sidewalk as recommended by the US department of transportation [32], and highlights the fact that a coronally adapting prosthesis may only be needed for amputees that frequently ambulate outdoors or in less controlled environments.

4.3 Limitations:

A primary limitation was the small sample size (n=3) used, and the use of a less conservative statistical model in which the subject effect was fixed. Because the subject effect was fixed the statistical results acquired only applied to the sample population, and not the general population; in addition, the small sample population may not have represented the entire target population. However, the nature of this study was to determine the efficacy of the CCA, and to inform future work, which was mostly achieved. The small sample size, combined with post hoc pairwise comparisons, also resulted in underpowered pairwise comparisons. For all metrics, there existed significant p-values for the prosthesis main effect and/or the prosthesis terrain interaction effect. However, for the same metrics, there was a noticeable lack of significant p-values in the pairwise comparisons. This suggests the study was sufficiently powered to detect the existence of difference associated with the prosthesis condition, but was not sufficiently powered to determine what those differences were (see ***Table 4***). Unfortunately, due to the time and resource intensive nature of this study, the number of participants were the maximum allowable.

Another limitation of this study was the time available for implementing training with the CCA. As previously mentioned in section 4.1a, the full capabilities of the CCA were suddenly introduced to participants with the full 15° of inversion and eversion. Had more time and resources been available, a gradually increasing series of coronal angles could have been used to slowly introduce participants to the capabilities of the device. This may have improved their familiarity with the device and enabled them to full utilize its capabilities on coronally-uneven and unpredictable terrain [26].

The terrain disturbance itself was also limited in that all conditions were coupled with a slight step down. This step down was minimized, but was necessary to keep the disturbance device below the surface of the walkway, and was 7 mm for the flush condition, and 27 mm for the inverted and everted conditions. It should be noted that there exist real world scenarios in which an inversion or eversion is associated with a slight step down, such as when stepping in a pot hole on the street, or a dip in a grassy field.

Finally, this study was limited in that only coronal plane kinetics and kinematics were analyzed. Biomechanics in the sagittal and transverse planes were likely affected by the prosthesis conditions used, as well as the terrain conditions. For instance, participant walking speeds (a sagittal plane measure) appear to have changed slightly between conditions (***Table 5***). It is also likely that recovery mechanisms acting in the sagittal and transverse planes affected the stability metrics reported.

4.4 Future Work:

Based on the findings of this study, future work will focus on developing a new CCA device to improve upon the current iteration's performance. The first item to be improved is the distance between the CCA pivot and the base of support. By reducing this distance, the ability of the CCA to reduce the disturbance moment produced by coronally-uneven and unpredictable terrain will likely be improved. A relevant goal would be to match the distance between the bottom of the prosthetic foot and the CCA pivot with distance between the subtalar joint and the bottom of a natural foot. Another improvement that will be made to the device is replacement of the Spectra® cable with a different material with less stretch. This will reduce the movement of the CCA foot mount that occurred after the ratchet mechanism was locked (***Figure 17***), and allow for tighter control of the coronal angle of the foot. Finally, anecdotal observations (see section 4.1b) suggest that participants may have been caught off guard by the quick rotational speed of the CCA. These observations, when combined with the use of adjustable damping in sagittal plane adaptive ankles (see section 1.3), suggest future iterations of the CCA may benefit from some level of damping in the coronal plane. Thus, future work may also investigate the possible benefit of adaptive damping in combination with, or as a replacement of, the adaption technology chosen for this study.

Appendix A: Results - Individual Participant Means

A.1 Coronal Angular Momentum - Individual Participant Means:

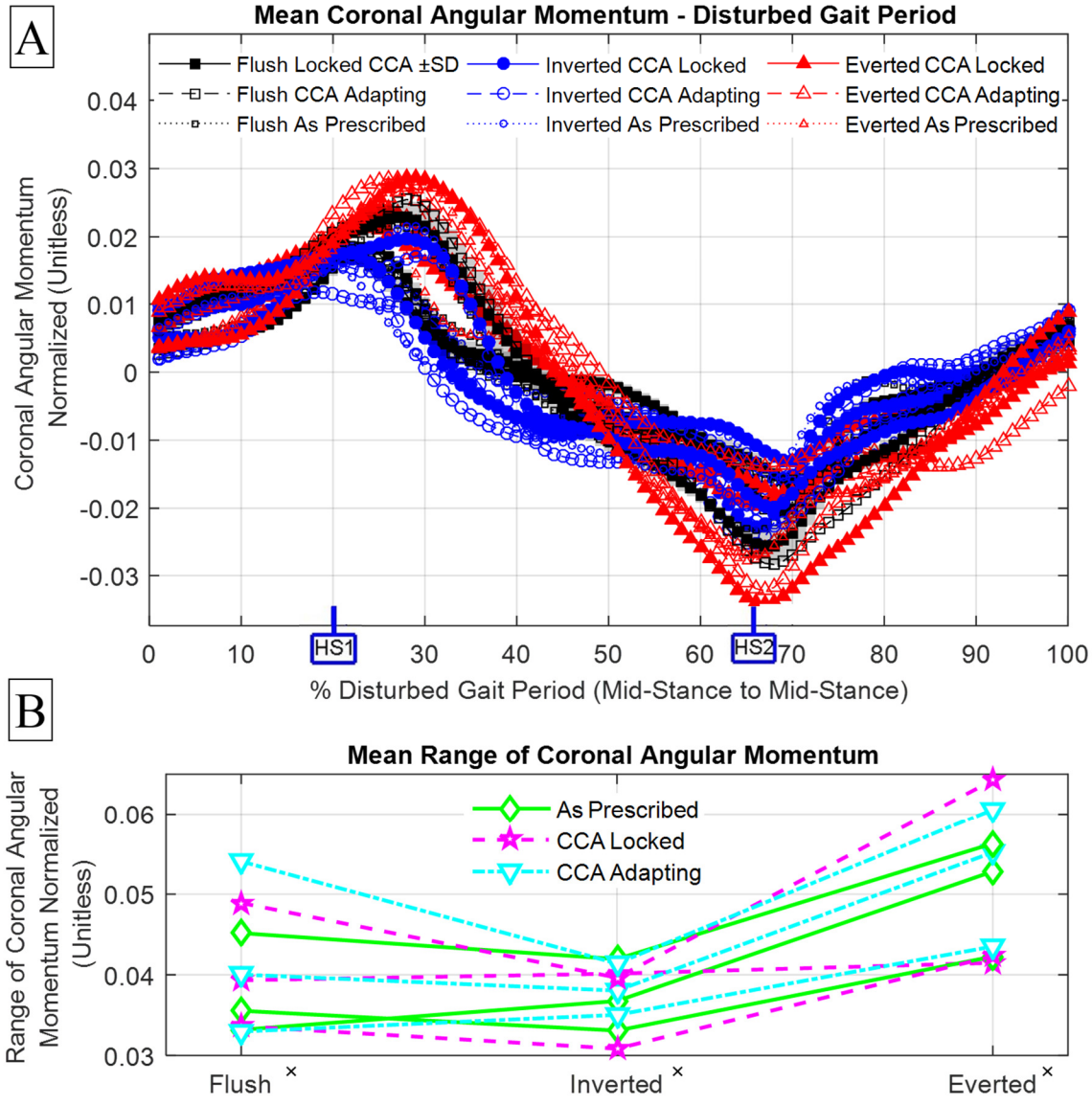

Figure 30: (A) Coronal angular momentum time series for all terrain and prosthesis combinations during the disturbed gait period. HS1 and HS2 signify heel strike of disturbed and recovery step, respectively. (B) Mean range of coronal angular momentum for all terrain and prosthesis combinations. × denotes no significant pairwise differences between prosthesis conditions for a given terrain condition. Means for all repeated trials of each individual participant are shown in both plots.

A.2 Standing Balance Lateral Sway - Individual Participant Means:

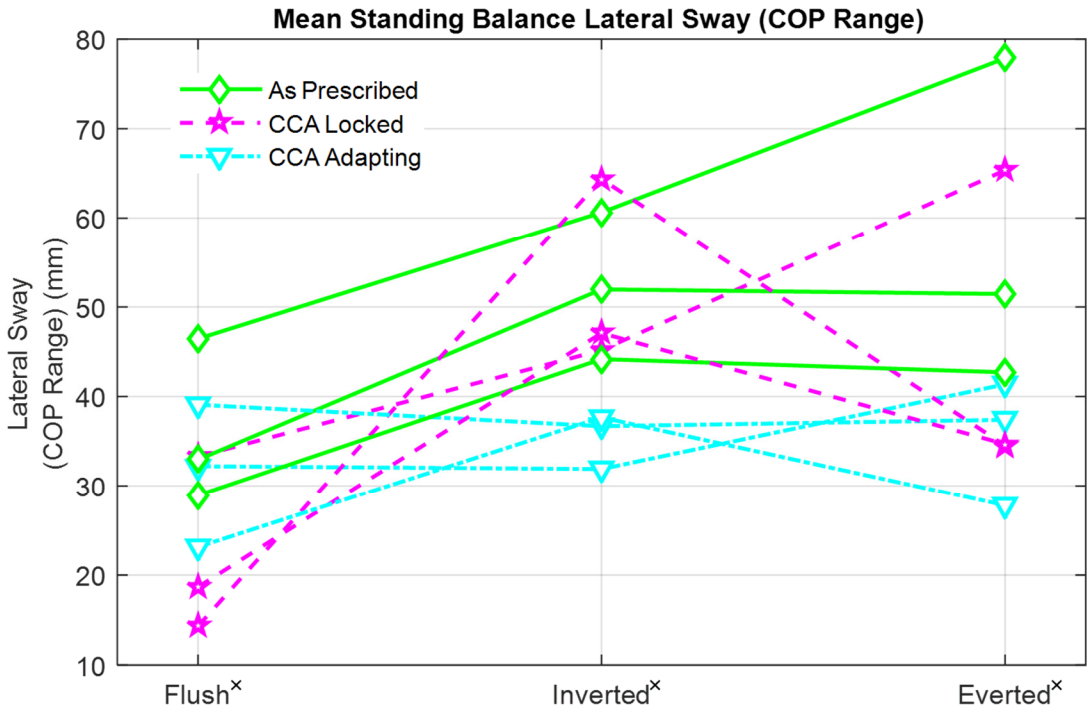

Figure 31: Mean standing balance lateral sway shown for all terrain and prosthesis combinations. × denotes no significant pairwise differences between prosthesis conditions for a given terrain condition. Center of pressure abbreviated to COP. Means for all repeated trials of each individual participant are shown.

A.3 Foot Coronal Angle With Respect to Pylon - Individual Participant Means:

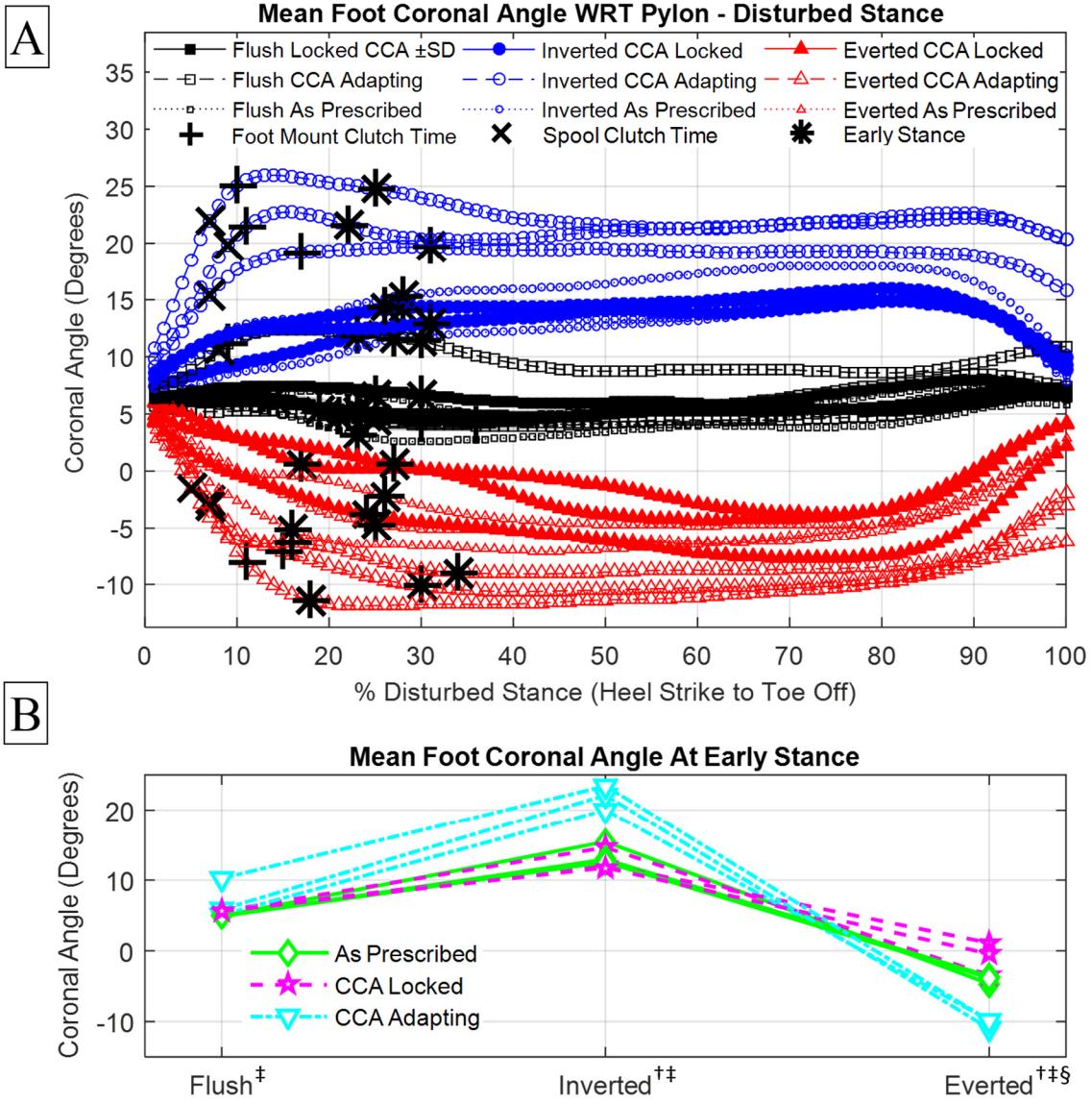

Figure 32: (A) Times series of the mean foot coronal angle with respect to the pylon (WRT) for all terrain and prosthesis combinations during the disturbed stance. Spool clutch time, foot mount clutch time, and early stance are shown for reference. (B) Mean foot coronal angle WRT the pylon at early stance for all terrain and prosthesis combinations. † denotes a significant pairwise difference between CCA adapting and locked prosthesis, ‡ between CCA adapting and as prescribed prosthesis, and § between CCA locked and as prescribed prosthesis. Positive angles represent inversion of the foot, negative angles represent eversion of the foot. Means for all repeated trials of each individual participant are shown in both plots.

A.4 Coronal Moment About CCA Pivot - Individual Participant Means:

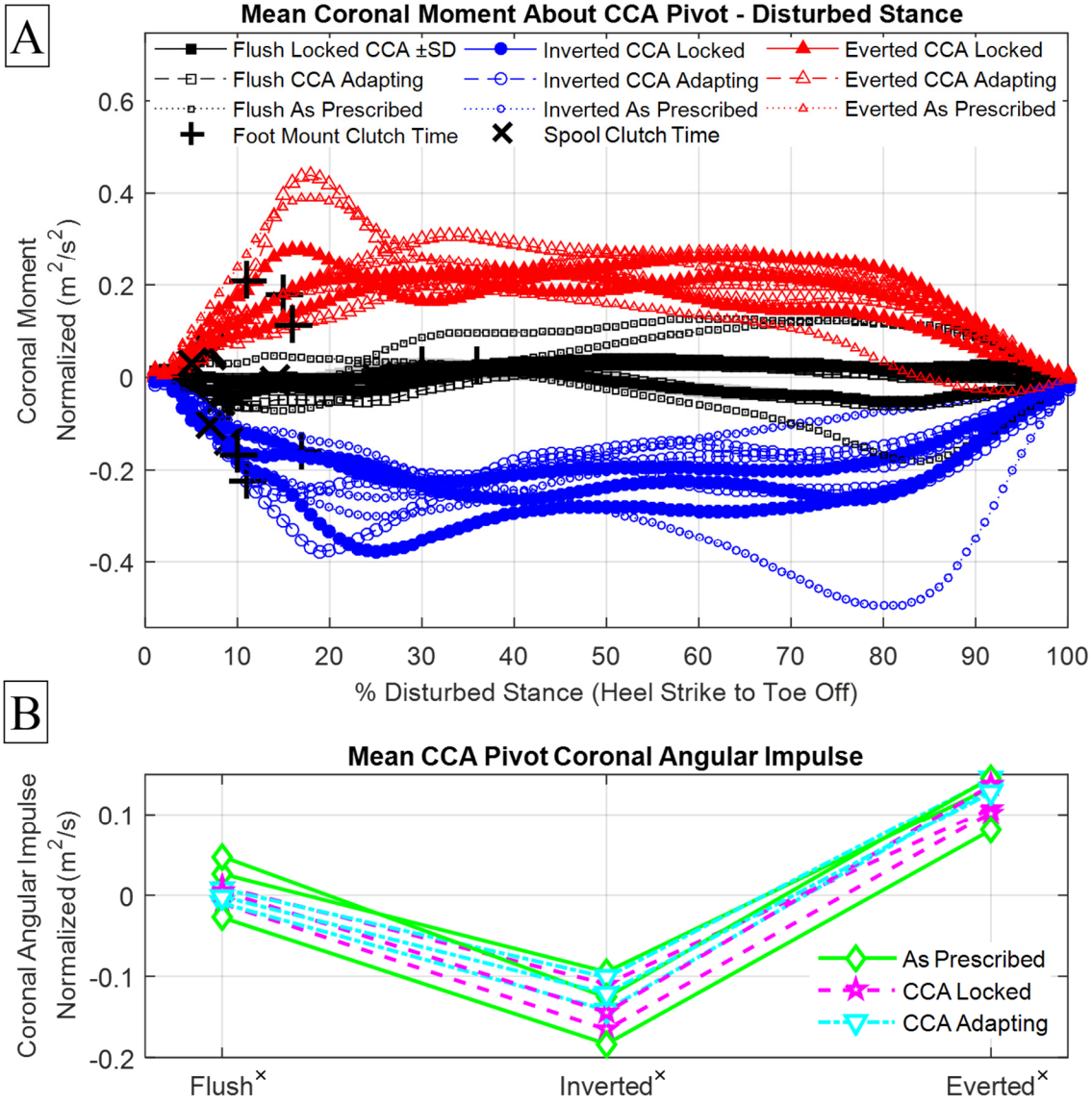

Figure 33: (A) Time series for mean coronal moment about CCA pivot (or equivalent thereof) over the disturbed stance for all prosthesis and terrain combinations. Spool clutch time and foot mount clutch time are shown for reference. (B) Mean CCA pivot coronal angular impulse for all terrain and prosthesis combinations. × denotes no significant pairwise differences between prosthesis conditions for a given terrain condition. Means for all repeated trials of each individual participant are shown in both plots.

A.5 Coronal Hip Moment - Individual Participant Means:

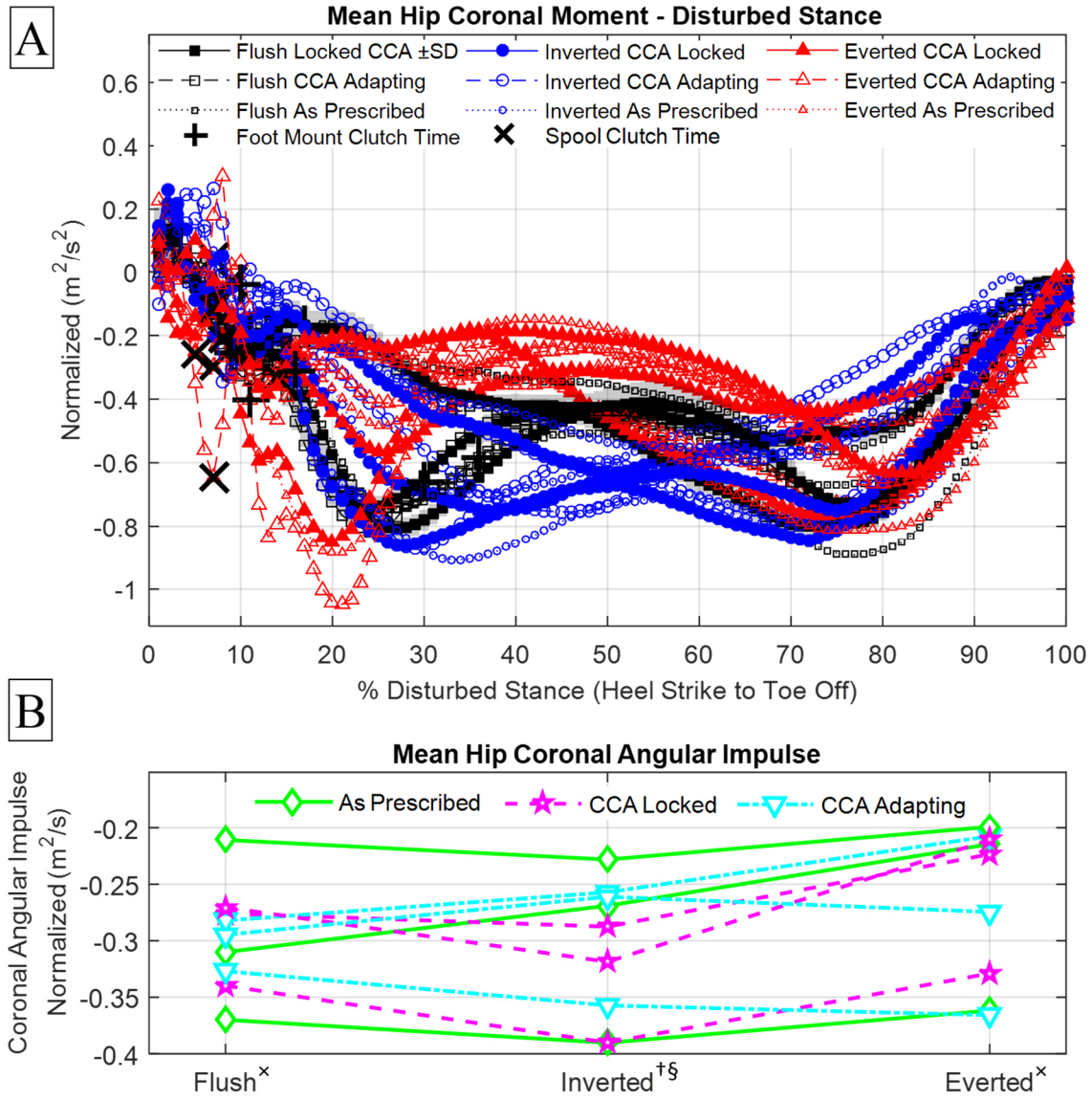

Figure 34: (A) Time series for mean coronal hip moment over the disturbed stance for all prosthesis and terrain combinations. Spool clutch time and foot mount clutch time are shown for reference. (B) Mean coronal hip angular impulse for all terrain and prosthesis combinations. × denotes no significant pairwise differences between prosthesis conditions for a given terrain condition. † denotes a significant pairwise difference between CCA adapting and locked prosthesis, and § between CCA locked and as prescribed prosthesis. Means for all repeated trials of each individual participant are shown in both plots.

A.6 Recovery Step Lateral Foot Placement - Individual Participant Means:

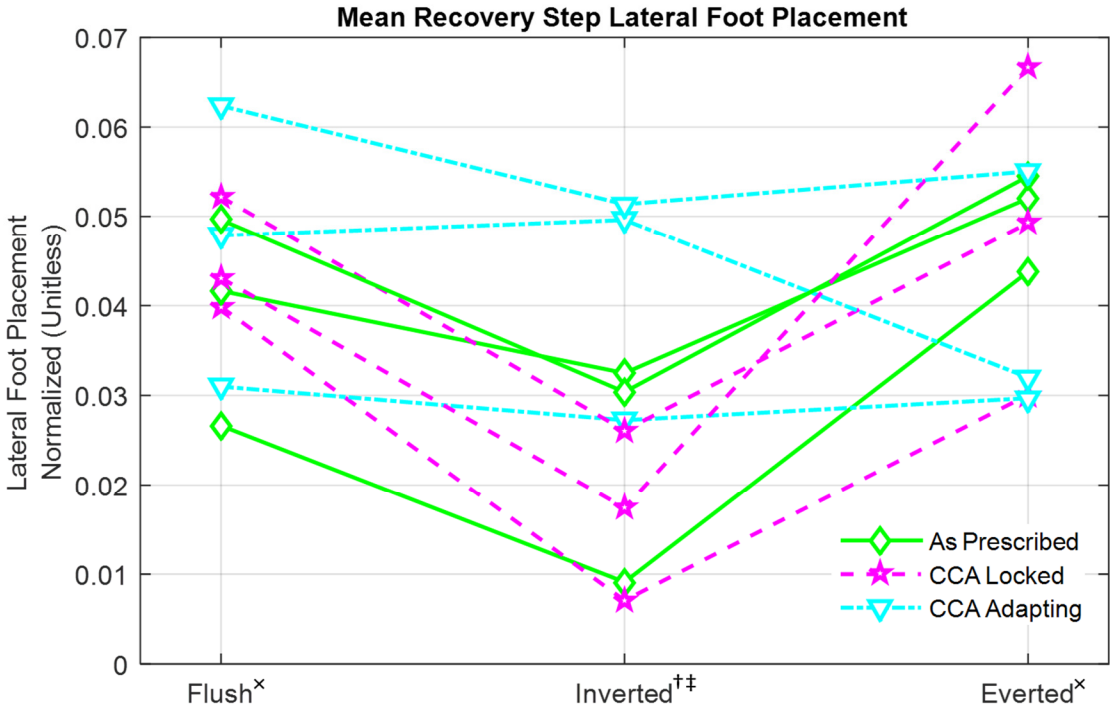

Figure 35: Mean recovery step lateral foot placement for all terrain and prosthesis combinations. × denotes no significant pairwise differences between prosthesis conditions for a given terrain condition. † denotes a significant pairwise difference between CCA adapting and locked prosthesis, and ‡ between CCA adapting and as prescribed prosthesis. Means for all repeated trials of each individual participant are shown.

A.7 Foot Mount Coronal Angle - Individual Participant Means:

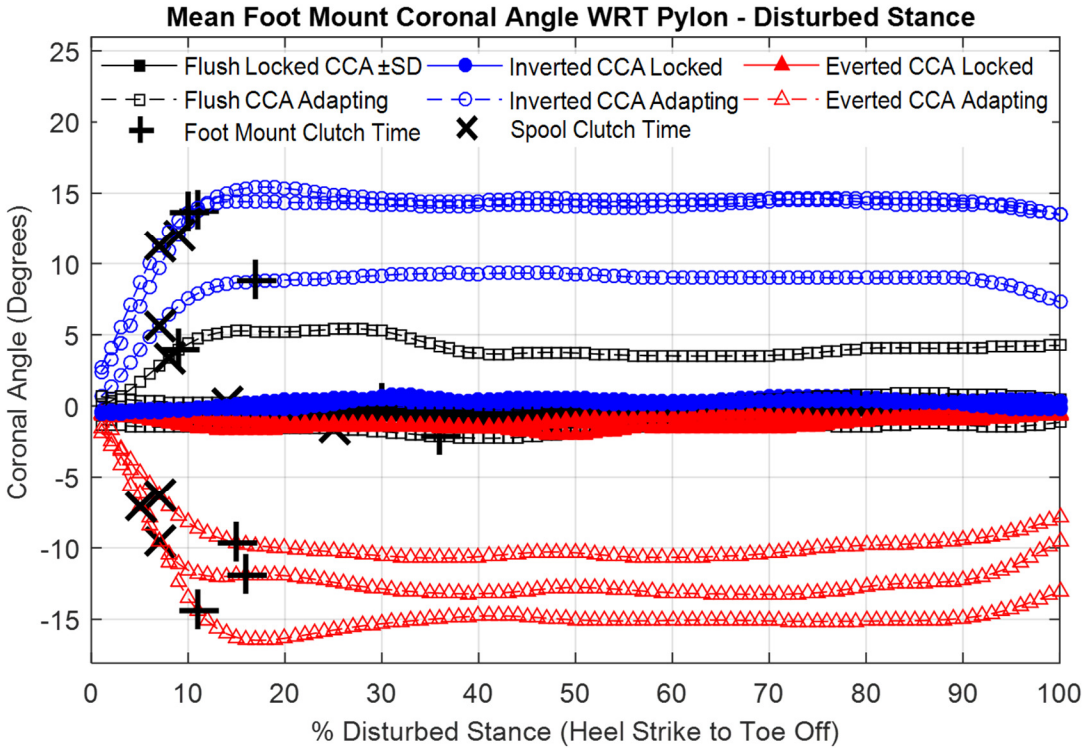

Figure 36: Time series of mean foot mount coronal angle with respect to the CCA pylon over the disturbed stance. Spool clutch time, and foot mount clutch time are shown for reference. Means for all repeated trials of each individual participant are shown.

References:

[1] M. L. Finlayson and E. W. Peterson, "Falls, Aging, and Disability," *Phys. Med. Rehabil. Clin. N. Am.*, vol. 21, no. 2, pp. 357–373, May 2010.

[2] W. C. Miller, A. B. Deathe, M. Speechley, and J. Koval, "The influence of falling, fear of falling, and balance confidence on prosthetic mobility and social activity among individuals with a lower extremity amputation," *Arch. Phys. Med. Rehabil.*, vol. 82, no. 9, pp. 1238–1244, Sep. 2001.

[3] J. Kulkarni, S. Wright, C. Toole, J. Morris, and R. Hirons, "Falls in Patients with Lower Limb Amputations: Prevalence and Contributing Factors," *Physiotherapy*, vol. 82, no. 2, pp. 130–136, Feb. 1996.

[4] W. Li, T. H. M. Keegan, B. Sternfeld, S. Sidney, C. P. Quesenberry, and J. L. Kelsey, "Outdoor Falls Among Middle-Aged and Older Adults: A Neglected Public Health Problem," *Am. J. Public Health*, vol. 96, no. 7, pp. 1192–1200, Jul. 2006.

[5] A. K. Silverman and R. R. Neptune, "Differences in whole-body angular momentum between below-knee amputees and non-amputees across walking speeds," *J. Biomech.*, vol. 44, no. 3, pp. 379–385, Feb. 2011.

[6] C. D. MacKinnon and D. A. Winter, "Control of whole body balance in the frontal plane during human walking," *J. Biomech.*, vol. 26, no. 6, pp. 633–644, Jun. 1993.

[7] S. Standring, *Gray's Anatomy: The Anatomical Basis of Clinical Practice*. Churchill Livingstone/Elsevier, 2008.

[8] A. Lundberg, O. K. Svensson, C. Bylund, I. Goldie, and G. Selvik, "Kinematics of the Ankle/Foot Complex—Part 2: Pronation and Supination," *Foot Ankle Int.*, vol. 9, no. 5, pp. 248–253, Apr. 1989.

[9] S. B. Sepic, M. P. Murray, L. A. Mollinger, G. B. Spurr, and G. M. Gardner, "Strength and range of motion in the ankle in two age groups of men and women," *Am. J. Phys. Med.*, vol. 65, no. 2, pp. 75–84, Apr. 1986.

[10] D. Stefanyshyn and J. Engsberg, "Right to left differences in the ankle joint complex range of motion.," *Med. Sci. Sports Exerc.*, vol. 26, no. 5, pp. 551–555, May 1994.

[11] F. H. Netter, *Atlas of Human Anatomy*. Elsevier Health Sciences, 2010.

[12] K. Yeates, "Gait Effects of Unexpected and Coronally-Uneven Terrain on Healthy Adults," Thesis, 2015.

[13] J. H. J. Allum, A. L. Adkin, M. G. Carpenter, M. Held-Ziolkowska, F. Honegger, and K. Pierchala, "Trunk sway measures of postural stability during clinical balance tests: effects of a unilateral vestibular deficit," *Gait Posture*, vol. 14, no. 3, pp. 227–237, Dec. 2001.

[14] C. R. Nott, F. E. Zajac, R. R. Neptune, and S. A. Kautz, "All joint moments significantly contribute to trunk angular acceleration," *J. Biomech.*, vol. 43, no. 13, pp. 2648–2652, Sep. 2010.

[15] J. A. Raymakers, M. M. Samson, and H. J. J. Verhaar, "The assessment of body sway and the choice of the stability parameter(s)," *Gait Posture*, vol. 21, no. 1, pp. 48–58, Jan. 2005.

[16] C. E. Bauby and A. D. Kuo, "Active control of lateral balance in human walking," *J. Biomech.*, vol. 33, no. 11, pp. 1433–1440, Nov. 2000.

[17] "Inverse Dynamics - Visual3D Wiki Documentation." [Online]. Available: http://www.c-motion.com/v3dwiki/index.php?title=Inverse_Dynamics. [Accessed: 25-Aug-2014].

[18] M. P. Kadaba, H. K. Ramakrishnan, and M. E. Wootten, “Measurement of lower extremity kinematics during level walking,” *J. Orthop. Res.*, vol. 8, no. 3, pp. 383–392, May 1990.
[19] D. A. Winter, *Biomechanics and Motor Control of Human Movement*. John Wiley & Sons, 2009.
[20] R. W. Selles, J. B. J. Bussmann, R. C. Wagenaar, and H. J. Stam, “Effects of prosthetic mass and mass distribution on kinematics and energetics of prosthetic gait: A systematic review,” *Arch. Phys. Med. Rehabil.*, vol. 80, no. 12, pp. 1593–1599, Dec. 1999.
[21] J. J. Gorges, “Controlled Coronal Stiffness Prosthetic Ankle for Improving Balance on Uneven Terrain,” Thesis, 2013.
[22] “AISI 4140 Steel, annealed at 815°C (1500°F) furnace cooled 11°C (20°F)/hour to 665°C (1230°F), air cooled, 25 mm (1 in.) round.” [Online]. Available: http://www.matweb.com/search/DataSheet.aspx?MatGUID=7b75475aa1bc41618788f63c6500d36b. [Accessed: 09-Nov-2015].
[23] “Aluminum 7075-T6; 7075-T651.” [Online]. Available: http://www.matweb.com/search/DataSheet.aspx?MatGUID=4f19a42be94546b686bbf43f79c51b7d. [Accessed: 09-Nov-2015].
[24] K. Dodson, “AOPA Prosthetic Foot Project Report.” American Orthotic and Prosthetic Association, 2010.
[25] E. K. Antonsson and R. W. Mann, “The frequency content of gait,” *J. Biomech.*, vol. 18, no. 1, pp. 39–47, 1985.
[26] A. Sawers and M. E. Hahn, “Gradual training reduces practice difficulty while preserving motor learning of a novel locomotor task,” *Hum. Mov. Sci.*, vol. 32, no. 4, pp. 605–617, Aug. 2013.
[27] A. K. LaPre and F. Sup, “Simulation of a slope adapting ankle prosthesis provided by semi-active damping,” in *2011 Annual International Conference of the IEEE Engineering in Medicine and Biology Society, EMBC*, 2011, pp. 587–590.
[28] R. J. Williams, A. H. Hansen, and S. A. Gard, “Prosthetic Ankle-Foot Mechanism Capable of Automatic Adaptation to the Walking Surface,” *J. Biomech. Eng.*, vol. 131, no. 3, pp. 035002–035002, Jan. 2009.
[29] J. J. Eng and D. A. Winter, “Kinetic analysis of the lower limbs during walking: What information can be gained from a three-dimensional model?,” *J. Biomech.*, vol. 28, no. 6, pp. 753–758, Jun. 1995.
[30] A. L. Hof, R. M. van Bockel, T. Schoppen, and K. Postema, “Control of lateral balance in walking: Experimental findings in normal subjects and above-knee amputees,” *Gait Posture*, vol. 25, no. 2, pp. 250–258, Feb. 2007.
[31] A. Segal and G. Klute, “Lower-limb amputee recovery response to an imposed error in mediolateral foot placement,” *J. Biomech.*, vol. 47, no. 12, pp. 2911–2918, Sep. 2014.
[32] “Chapter 4 - Sidewalk Design Guidelines and Existing Practices - Sidewalks - Publications - Bicycle and Pedestrian Program - Environment - FHWA.” [Online]. Available: http://www.fhwa.dot.gov/environment/bicycle_pedestrian/publications/sidewalks/chap4b.cfm. [Accessed: 09-Feb-2016].